



FEDERAL UNIVERSITY OF AMAZONAS
PRO-RECTORATE OF RESEARCH AND POSTGRADUATE STUDIES
GRADUATE PROGRAM IN PHYSICS



CAMILA DA COSTA PINTO

**Unraveling the Semicrystalline Structure of Different Types of Starch (A, B, C
and V) using X-Ray Diffraction and Structural Refinement**

MANAUS-AM

2025

CAMILA DA COSTA PINTO

Unraveling the Semicrystalline Structure of Different Types of Starch (A, B, C and V) using X-Ray Diffraction and Structural Refinement

Thesis submitted in partial fulfillment of the requirements for the Ph.D. degree in Physics in the Graduate Program in Physics at the Federal University of Amazonas.

Supervisor: Prof. Dr. Sérgio Michielon de Souza

MANAUS-AM

2025

Ficha Catalográfica

Elaborada automaticamente de acordo com os dados fornecidos pelo(a) autor(a).

- P659u Pinto, Camila da Costa
 Unraveling the semicrystalline structure of different types of starch (A, B, C and V) using X-ray Diffraction and structural refinement / Camila da Costa Pinto. - 2025.
 155 f. : il., color. ; 31 cm.
- Orientador(a): Sérgio Michielon de Souza.
 Tese (doutorado) - Universidade Federal do Amazonas, Programa de Pós-Graduação em Física, Manaus, 2025.
1. X-ray Diffraction. 2. Difração de raios X. 3. Structural refinement. 4. Refinamento estrutural. 5. Starch. I. Souza, Sérgio Michielon de. II. Universidade Federal do Amazonas. Programa de Pós-Graduação em Física. III. Título
-

CAMILA DA COSTA PINTO

Unraveling the Semicrystalline Structure of Different Types of Starch (A, B, C and V) using X-Ray Diffraction and Structural Refinement

Tese apresentada como parte dos requisitos para obtenção do título de Doutor em Física no Programa de Pós-Graduação em Física da Universidade Federal do Amazonas.

Aprovado em 07 de março de 2025.

BANCA EXAMINADORA

Prof. Dr. Sérgio Michielon de Souza, Presidente, Universidade Federal do Amazonas – UFAM.

Prof. Dr. Edgar Aparecido Sanches, Membro, Universidade Federal do Amazonas – UFAM.

Prof. Dr. Marcos Marques da Silva Paula, Membro, Universidade Federal do Amazonas – UFAM.

Profa. Dra. Maria Teresa Pedrosa Silva Clerici, Membro, Universidade Estadual de Campinas – Unicamp.

Profa. Dra. Yvonne Mascarenhas, Membro, Universidade de São Paulo – USP.



Documento assinado digitalmente
SERGIO MICHIELON DE SOUZA
Data: 11/03/2025 13:40:14-0300
Verifique em <https://validar.iti.gov.br>

Prof. Dr. Sérgio Michielon de Souza



Documento assinado digitalmente
EDGAR APARECIDO SANCHES
Data: 12/03/2025 19:44:44-0300
Verifique em <https://validar.iti.gov.br>

Prof. Dr. Edgar Aparecido Sanches



Documento assinado digitalmente
MARCOS MARQUES DA SILVA PAULA
Data: 11/03/2025 16:40:01-0300
Verifique em <https://validar.iti.gov.br>

Prof. Dr. Marcos Marques de Silva Paula



Documento assinado digitalmente
MARIA TERESA PEDROSA SILVA CLERICI
Data: 11/03/2025 17:58:33-0300
Verifique em <https://validar.iti.gov.br>

Profa. Dra. Maria Teresa Pedrosa Silva Clerici

Profa. Dra. Yvonne Primerano Mascarenhas



USPAssina - Autenticação digital de documentos da USP

Registro de assinatura(s) eletrônica(s)

Este documento foi assinado de forma eletrônica pelos seguintes participantes e sua autenticidade pode ser verificada através do código TXV4-NH1P-BUR5-3B22 no seguinte link: <https://portalservicos.usp.br/iddigital/TXV4-NH1P-BUR5-3B22>

Yvonne Primerano Mascarenhas

Nº USP: 16196

Data: 16/03/2025 13:50

To my beloved ones, I wanted to share this process with you. Although some of you are no longer with me, your love and support will always remain in my heart. There must be a way to go on.

To my dear niece Letícia, I hope this work inspires you to become whoever you want to be.

Lastly, I owe a debt of gratitude to a few essential elements that were crucial to this work: friendships, caffeine, excitement, and music.

ACKNOWLEDGMENTS

The pursuit of science is not a solitary endeavor; it requires collaboration, support (including financial), and guidance from others. This research was conceived, developed, and supported within the framework of public, free, state-funded, and high-quality federal and state universities, federal institutes, and foundations. These institutions not only provided the financial resources but also the intellectual environment necessary to nurture and accomplish this work, being the place where many stakeholders of this thesis met and worked together. I am grateful for the many individuals who have played a role in my journey, including funding agencies, the Institute I work at (IFAM) and the University where I studied (UFAM), my family, friends, and colleagues.

I would like to thank the Coordination for the Improvement of Higher Education Personnel (CAPES) for funding my research scholarship through PPGFIS, and the Amazonas State Research Support Foundation (FAPEAM) for making this research possible through the projects “Melhoria da qualidade de água em tanques de aquicultura indoor com a aplicação de material filtrante composto com fibra vegetal regional e dopado com nanomateriais” and “Diminuição da perda de frutos produzidos em Presidente Figueiredo com o uso de desidratador de frutas automático de baixo custo”. I would also like to thank National Council for Scientific and Technological Development (CNPq) for the projects “Nano-farinhas de favas peruanas e de carás amazônicos visando aplicações em impressora 3d para produtos de dietas especiais” and “Mineração Urbana, reciclagem de ímãs permanentes de terras-raras”, which contributed, both directly and indirectly, enhancing the relevance of my research. I would also want to thank all those funding agencies and UFAM for the research infrastructure, and the laboratories and its coordinators where measurements were carried out for this work: LabMat (under prof Sérgio Michielon) and Nanopol (under prof Edgar Sanches) at UFAM, Laboratório de Cereais, Raízes e Tubérculos (under profa Maria Teresa Clerici) and my own recently inaugurated laboratory called “AGROBIO - Laboratório de Agricultura e Biomateriais” – IFAM .

I would like to express my deepest gratitude to my loving family - my husband Leonardo, sister Mônica, brother Luciano, cousins Rodrigo and Monick - who have been incredibly patient and supportive throughout this journey. Although my father João Marcos and mother Rosemary Pinto are no longer with me, their memory and unwavering love continue to inspire me every day. I am also grateful to my dear advisor and friend Sérgio Michielon and to all my wonderful friends Edgar Sanches, Maria Teresa, Querem, Ruzo, Hermínio and so many

others. Science is a collaborative effort, and I couldn't have accomplished this work without their guidance and support. Their valuable insights and encouragement have been instrumental in helping me reach this point.

FOREWORD

This scientific endeavor is not "commoditized", but flourishes in hard work and many collaborations. It stands as a testament to Amazonian thought, generating sustainable possibilities rooted in our region's unique perspectives and traditions, and funded by public, free, state-funded, and high-quality federal and state universities, federal institutes, and foundations.

This work calls for the recognition of us, the Amazonian people, as creators and guardians of our own knowledge and sustainable practices, challenging the perception of being mere providers of raw data for external scientific pursuits. It underscores the intrinsic value of local knowledge, asserting the sovereignty of Amazonian science and culture as vital contributors to global understanding. Moreover, this work reflects my personal journey as an emerging scientist, intertwining my heritage with the pursuit of meaningful and impactful researches. A humble root, rediscovered during my research on the structure of raw and modified starches, illuminated this profound possibility and deepened my understanding of the interconnectedness between science, ancestral traditional knowledge and sustainability.

The first time I came across purple cará (cará roxo, or purple yam, *Dioscorea trifida L.*), it was through my grandmother, who would eat it every afternoon alongside her coffee. After her passing, the tradition lingered faintly—my mother would eat purple cará occasionally, though the ritual slowly faded. Over time, I too lost the habit of eating purple cará. However, I unexpectedly rediscovered it through the research I now conduct with my advisor, in collaboration with an incredible group of people in whole Brazil and even in foreign countries. This journey not only brought many tuberous roots from Amazon region back into my life but also rekindled a profound connection to my own Amazonian roots.

For generations, my grandmother, great-grandmother, and countless others Amazonian in my family tree cultivated Amazonian roots, not only as sustenance but as a lifeline. Seeing this humble vegetable again, now as a research sample, carried immense personal significance. It reminded me of the deep ties between agriculture and survival, between heritage and identity. Amazonian tubers, such as cará, are not just roots; they are a testament to the perseverance and ingenuity of Amazonian communities. This ingenuity continues to be reflected in our resourcefulness, agricultural practices, knowledge of plant breeding, and sustainable ways of managing and utilizing the natural resources of the Amazon.

We, Amazonians, know. We know ariá (*Calathea allouia* (Aubl.) Lindl) and cará, we know the people who plant it, and we understand how the sun shines and the rain falls in our region. We know our roots.

Or rather, multiple communities know, because, after all, plant cuttings (such as stems, roots, or leaves for propagation of the best specimens) are exchanged, gifted, sent by boat, or, in the past and even now, carried in baskets on backs and transported by canoes along rivers. These plants were shared because they were especially productive, nutritious, flavorful or even colorful. And now these plants are also precious scientific and technological resources.

An entire community collectively cultivating the living technology embodied by that and many other plants—a reflection of the decoloniality of knowledge. It represents centuries of cultivation, selection, and sharing by those who sought not only to grow food but to improve it for future generations. These “seeds” carry stories, exchanged long before science set its gaze upon them. Our family trees have flourished as communities in this region thanks to our ability to adapt to its complex environment, refine crops over generations, develop and share methods to ensure food security and resilience, often in the face of challenging conditions.

As my mother often said, "When it comes to humankind, behind every number is a person." Years after her passing, this truth still resonates deeply with me: behind every tuber root produced in Amazonas, there is a family engaged in family farming, trying to resist and adapt. What if this work—this investigation of several ancestral crops in hopes it can also help us face other “modern” issues—could somehow improve the lives of the very people who nurtured it? What if the impact of understanding these roots could extend to the communities that have lived symbiotically with them for centuries?

With this thought, I find hope and purpose in my own tiny research. My aspiration is that this small contribution might, in some way, benefit my Amazonian community, honoring the legacy of my family and countless others who have shaped and been shaped by this land.

We are not here merely to serve as data providers for others to study; we have the capacity to be protagonists in our own narratives. By rejecting the paradigm of knowledge extraction by external parties, we assert our role as creators, innovators, and custodians of our cultural and scientific heritage. It is through this lens that we contribute meaningfully to global knowledge, guided by the understanding that our voices and perspectives are integral to shaping the future of sustainable science and equitable collaboration.



"...In my own funny ways I find I learn much more"

Gentle Giant

ABSTRACT

Given the widespread use of carbohydrates in the industry, the complexity of their structures, and the challenges in accurately determining the semicrystalline nature of biopolymers, particularly starches, this work proposes a comprehensive understanding of the main structural characteristics of those important material and the implications of its processing. Specifically, the focus is on analyzing the structural changes in various types of starches (A, B, C and V-type) resulting from different processing techniques, with particular emphasis on nanocrystal production and structural modification. These techniques encompass acid hydrolysis, gamma irradiation and non-thermal processes (High-Intensity Ultrasound and Cold Plasma treatments). By examining the effects of these processing techniques on starch structure, this thesis aims to provide valuable insights into the modifications and transformations at the structural level, which in turn might be useful for “tuning” starches microstructure into a specific application. To overcome these challenges and achieve a more precise and unbiased characterization of starch crystallinity, a combined approach based on X-ray diffraction (XRD) and Rietveld refinement techniques was proposed. The microstructural information derived from Rietveld refinement can be integrated with other techno-functional characterizations commonly utilized in the food industry to enhance the understanding of the potential applications of starch sources. Gamma irradiation demonstrated a reduction in the amorphous fraction, accompanied by increased crystallinity, with B-type starch showing greater structural resilience due to its higher water content. Cold plasma treatment, applied under varying operational parameters, significantly influenced the crystallinity of Ariá (*Calathea allouia* (Aubl.) Lindl) starch, leading to increases in crystallinity by 18% at 200 Hz, as well as reductions of the amorphous content. This study presents the first quantification of phase fractions (A- and B-type) in C-type starches from Amazonian sources such as Ariá and thorn yam (*Dioscorea chondrocarpa* Griseb), revealing its polymorphic complexity and the remarkable potential for structural modulation. This research has far-reaching implications beyond the immediate scope of the study, with potential impacts in multiple industries such as food, packaging, pharmaceuticals, cosmetics and other biomedical sectors. By deepening our understanding of starch's structural properties and its response to different processing methods, this research holds the potential to drive the innovation in product development, processing techniques and new technologies.

Keywords: X-ray diffraction; nanocrystal production; structural refinement; Rietveld method; A-type starch; B-type starch; C-type starch; V-type starch.

RESUMO

Dada a ampla utilização dos carboidratos na indústria, a complexidade de suas estruturas e os desafios na determinação precisa da natureza semicristalina dos biopolímeros — em particular dos amidos — este trabalho propõe uma compreensão abrangente das principais características estruturais desses materiais e das implicações de seu processamento. Especificamente, o foco está na análise das alterações estruturais em diferentes tipos de amido (tipos A, B, C e V) resultantes de distintas técnicas de processamento, com ênfase especial na produção de nanocristais e modificação estrutural. As técnicas avaliadas incluem hidrólise ácida, irradiação gama e processos não térmicos, como ultrassom de alta intensidade e tratamentos com plasma frio. Ao examinar os efeitos dessas técnicas sobre a estrutura do amido, esta tese busca fornecer insights valiosos sobre as modificações e transformações estruturais que ocorrem, permitindo, assim, a "modulação" da microestrutura dos amidos para aplicações específicas. Para superar os desafios de caracterização e obter uma avaliação mais precisa e isenta da cristalinidade dos amidos, propõe-se uma abordagem combinada baseada em difração de raios X (XRD) e no método de refinamento de Rietveld. As informações microestruturais obtidas pelo refinamento de Rietveld podem ser integradas a outras caracterizações tecnofuncionais amplamente utilizadas na indústria alimentícia, contribuindo para a melhor compreensão do potencial de aplicação das fontes de amido. A irradiação gama demonstrou redução da fração amorfa acompanhada de aumento na cristalinidade, sendo que o amido do tipo B apresentou maior resistência estrutural, possivelmente devido ao seu maior teor de água. Já o tratamento com plasma frio, aplicado sob diferentes parâmetros operacionais, influenciou de maneira significativa a cristalinidade do amido de Ariá (*Calathea allouia* (Aubl.) Lindl), promovendo um aumento de até 18% na cristalinidade a 200 Hz, além da redução da fração amorfa. Este estudo apresenta a primeira quantificação das frações de fases (tipos A e B) em amidos tipo C provenientes de fontes amazônicas, como Ariá e cará-de-espinho (*Dioscorea chondrocarpa* Griseb), revelando sua complexidade polimórfica e o notável potencial para modulação estrutural. A pesquisa possui implicações que ultrapassam os limites imediatos do estudo, com impacto potencial em múltiplos setores industriais, como os de alimentos, embalagens, farmacêutico, cosmético e outros segmentos biomédicos. Ao aprofundar a compreensão sobre as propriedades estruturais do amido e sua resposta a diferentes métodos de processamento, esta pesquisa oferece subsídios valiosos para impulsionar a inovação no desenvolvimento de produtos, técnicas de processamento e novas tecnologias.

Keywords: difração de raios X; produção de nanocristais; refinamento estrutural; método de Rietveld; amido tipo A; amido tipo B; amido tipo C; amido tipo V.

LIST OF FIGURES

Figure 1 – The chaining of groups through alpha or beta linkages. Figure from (Nascimento et al., 2021).....	30
Figure 2 – Starch multiscale structure. Figure from (Le Corre; Bras; Dufresne, 2010)	31
Figure 3 – Section of amylopectin indicating the branching pattern of unit (1 - 4)-a-chains (A, B1–B3) joined together by (1 - 6)- a- linkages (branch points). The chaining of groups through alpha or beta linkages. Figure from (Tester; Karkalas; Qi, 2004).....	32
Figure 4 – From granule to lamellae. Figure from (Tester; Karkalas; Qi, 2004)	33
Figure 5 – Lamellar structure of a starch granule. Figure from (Tetlow, 2011).....	33
Figure 6 – A and B-type polymorphs of amylose. Figure from (Tetlow, 2011)	37
Figure 7 – Diffraction patterns from crystalline solids, liquids, amorphous solids, and monatomic gases as well as their mixtures. Figure adapted from (Vitalij K. Pecharsky; Zavalij, 2009).....	49
Figure 8 – Peak-shape functions of a Bragg reflection. Thick arrows indicate the full widths at half maximum (FWHM). Figure from (Vitalij K. Pecharsky; Zavalij, 2009)	52
Figure 9 – Same semicrystalline structure with different FWHM. Detail shows the overlapping of information. Figure made by the author.....	53
Figure 10 – idealized model of a perfect crystalline structure for A-type (left) and B-type (right) starches. Figure made by the author.	55
Figure 11 – Diffraction patterns rice starch nanocrystals, with amorphous regions manually fitted. Figure from (Xie et al., 2014)	58
Figure 12 – Diffraction patterns with amorphous regions fitted with an arbitrary semi-circle. Figure from (Cheetham; Tao, 1998).....	59
Figure 13 – Damaged oriented silicon sample holder. Photo taken by the author.	71

Figure 14 – Adapted sample holder with a fake bottom made of Mylar® film. Photo taken by the author.	71
Figure 15 – Adapted sample holder filled with starch sample. Photo taken by the author.	72
Figure 16 - XRD patterns comparing the Control and US-treated samples. Inset depicts details of the structure Figure from the author, published in (Pinto; Campelo; Michielon de Souza, 2020b).....	78
Figure 17 – Schematic projection of the P6 ₁ structural model, illustrating amylopectin's left-handed double helices arranged in parallel, encapsulating 36 water molecules. Figure reconstructed based in (Okazaki, 2018).	79
Figure 18 – Rietveld refinement of the Control sample. Figure from the author, published in (Pinto; Campelo; Michielon de Souza, 2020b).....	82
Figure 19 – Rietveld refinement of the US-treated sample. Figure from the author, published in (Pinto; Campelo; Michielon de Souza, 2020b).....	83
Figure 20 – Baseline analysis illustrating contributions based on FWHM and varying crystallite sizes. Figure from the author, published in (Pinto; Campelo; Michielon de Souza, 2020b).....	85
Figure 21 – Comparison of XRD patterns for Hydrolyzed and US-Hydrolyzed samples. Figure from the author, published in (Pinto; Campelo; Michielon de Souza, 2020b)	86
Figure 22 – Overlay comparison of XRD patterns for US and US-Hydrolyzed samples, highlighting interhelix peaks. The inset demonstrates the planes (1 0 0) and (0 1 0). Figure from the author, published in (Pinto; Campelo; Michielon de Souza, 2020b).....	87
Figure 23 – Rietveld refinement of the US-Hydrolyzed sample. Figure from the author, published in (Pinto; Campelo; Michielon de Souza, 2020b).....	88
Figure 24 – XRD patterns of Ariá samples before and after 4 doses of radiation.....	94
Figure 25 – The details in the XRD patterns shows the structural changes caused by irradiation of Ariá samples.	95

Figure 26 – XRD patterns of Ariá starch overlapped the theoretical patterns of A-type and B-type starch perfect crystals, in different ranges of 2θ .	96
Figure 27 – Refined XRD patterns of freeze-dried raw Ariá starch.	100
Figure 28 – Refined XRD patterns of Ariá starch sample submitted to 20kGy.	101
Figure 29 – Refined XRD patterns of Ariá starch sample submitted to 50kGy.	101
Figure 30 – The XRD baselines obtained from the Rietveld Refinement of freeze-dried raw Ariá and irradiated starch samples.	102
Figure 31 - XRD patterns of native and cold plasma treated aria starches.	105
Figure 32 - The XRD data Rietveld refinement method was applied to the starch samples treated with cold plasma at 50 Hz.	106
Figure 33 - The XRD data Rietveld refinement method was applied to the starch samples treated with cold plasma at 100 Hz.	106
Figure 34 - The XRD data Rietveld refinement method was applied to the starch samples treated with cold plasma at 200 Hz.	107
Figure 35 - The XRD data Rietveld refinement method was applied to the starch samples treated with cold plasma at 350 Hz.	107
Figure 36 - The XRD data Rietveld refinement method was applied to the starch samples treated with cold plasma at 550 Hz.	108
Figure 37 – XRD patterns of Ariá samples before and after cold plasma treatment with varying voltage.	110
Figure 38 – Normalized XRD patterns of Ariá samples before and after cold plasma treatment with varying voltage.	111
Figure 39 – Refined XRD patterns of the sample treated at 14 kV.	112
Figure 40 – Baselines of freeze-dried samples before and after plasma treatment.	113

Figure 41 – (A) superposition of the normalized X-ray Diffraction Patterns of the starch samples extracted from peruvian beans, peruanite (AFP), quelcão (AFQ) and fava verde (AFV); (B), (C) and (D) correspond to refinements by Rietveld method considering crystallographic information of type A starch and type B starch..... 118

Figure 42 – Experimental XRD patterns of (A) raw starch samples extracted from Chullpi, Cuzco, Piscorunto, Purple, and Sacsa corn varieties; (B) normalized starch samples extracted from Chullpi, Cuzco, Piscorunto, Purple, Sacsa, and standard Sigma Aldrich maize corn starch..... 121

Figure 43 – XRD patterns of (A) starch samples extracted from Chullpi, Cuzco, Piscorunto, Purple, and Sacsa corn varieties overlapped with idealized XRD patterns obtained from the CIF information for A and V-type; Refined X-ray diffraction patterns of starch samples extracted from (B) Chullpi, (C) Purple, (D) Piscorunto (E) Sacsa, (F) Cuzco..... 123

Figure 44 - Experimental diffractogram of yam starch (highlighted in black). In red, there is the diffractogram calculated using the Rietveld method, derived from the structural refinements of type A (represented in blue) and type B (indicated in magenta) starches. The difference between the experimental and calculated diffractogram is represented in gray.... 127

Summary

ABSTRACT	12
RESUMO	13
LIST OF FIGURES	14
Summary.....	18
Introduction	21
Objectives	26
CHAPTER 1 - STATE OF THE ART	27
The Quest for crystallinity in semicrystalline biopolymers.....	27
1.1. A brief consideration on the chemistry and structure of polysaccharides.....	29
1.2. Starch Polymorphs.....	35
1.3. Applications and Modifications of starch structures	38
1.3.1. Acid hydrolysis.....	40
1.3.2. Ultrasound-Assisted Processing	41
1.3.3. Gamma Radiation	42
1.3.4. Cold Plasma.....	43
1.4. Crystallography – X Ray Diffraction for microstructure	46
1.4.1. Analyzing Semi-Crystalline Nanocrystals in XRD Patterns	51
1.5. Starch Crystallography	54
1.6. How the reported literature discusses crystallinity of biopolymers using XRD?	55
1.7. The quest for crystallinity remains	59

CHAPTER 2 – METHODOLOGY	60
X-ray Diffraction and Rietveld Refinement for Unraveling the Semicrystalline Structure of Starches.....	60
2.1. Crystallinity: Quantifying Order through Structural Refinement	61
2.2. XRD characterization	69
CHAPTER 3 – RESULTS I: Proof of concept.....	74
Potato Starch Nanocrystals: physicochemical modifications investigated through Rietveld Refinement.....	74
3.1 Experimental procedures	76
3.2 X-Ray Diffraction Analysis of Starch Samples with Ultrasonic Preprocessing	77
3.3 Repercussion of our work:.....	90
3.4 Other questions remain.....	90
CHAPTER 4 – RESULTS II.....	91
Modifying exotic Amazon starch from Ariá (<i>Goeppertia allouia</i>) with unconventional processing techniques	91
4.1 γ -radiation of Ariá starch	92
4.1 Cold plasma treatment of Ariá starch	103
4.1.1 Variation of Cold plasma excitation frequency	104
4.1.2 Variation of Cold plasma generation voltage	110
CHAPTER 5 – RESULTS III.....	115
Science Strengthened Through Collaboration: Investigating alternative Starch Sources from Amazon Biome.....	115
5.1 Andean Fava beans	116

5.2 Peruvian Andean Maize.....	120
5.3 Thorny Cará or Thorn-yam (<i>Dioscorea chondrocarpa Griseb.</i>).....	125
CONCLUSIONS	130
Challenges and Opportunities for Future Investigations	132
REFERENCES	133

Introduction

Biopolymers, such as starch and cellulose, are versatile materials with adjustable properties, well-established supply chains, biocompatibility, and renewable sources (Odeku, 2013). These polysaccharides have been widely utilized by humans in various forms and applications even before mankind came to be, and understanding its structure is critical for exploring even more opportunities and applications in different industries such as agriculture, filtration, hygiene, protective clothing, food applications, pharmaceutical and medical industries, administration of medicine, regenerative medicine, production of natural, biodegradable, or even edible packaging, and petroleum recovery (Rus; Sulong, 2013). Starch, in particular, plays a significant role in nutrition, as well as in the pharmaceutical and cosmetics industries (Odeku, 2013).

As a result, there is a rising interest in the development of innovative products that integrate starch as a vital component across diverse sectors, and the continuous exploration of new sources and varieties of starch is strategic for the ongoing progress of these industries (Chisenga et al., 2019). The Amazon region, renowned for its abundant biodiversity, provides a wealth of options in terms of roots and cereals that can be effectively harnessed by the industry (Barros et al., 2020; Bueno; Weigel, 1981; Da Costa Pinto et al., 2023).

While naturally occurring polymers have long been extensively utilized and their agricultural aspects well-understood (Hafezi, 2022; Ilyas et al., 2019a; Prabhu et al., 2019), the comprehensive understanding of their microstructure has emerged relatively recently with the discovery and advancements in light scattering characterization techniques (Lopez-Rubio et al., 2008). These techniques can be integrated with other techno-functional characterizations commonly utilized in the food industry, enabling the assessment of various information and the establishment of correlations between the microstructure and macroscopic properties of these polymers, enhancing the understanding of the potential applications of many yet unexplored starch sources (Horstmann; Lynch; Arendt, 2017; Versino et al., 2016). For instance, gaining insights into the organization of atoms within macromolecules of starch or cellulose, especially in terms of short-term organization or quantifying the degree of disorganization, and understanding how this organization influences their properties, holds immense potential for

unlocking a myriad of applications for these carbohydrates (Da Costa Pinto et al., 2023; Pinto; Campelo; Michielon de Souza, 2020; Pinto et al., 2021a).

In this thesis, the main goal was to investigate and analyze the semicrystalline structure of different types of biopolymers (including starches) through the combined use of X-ray diffraction (XRD) and structural refinement techniques. By employing these methods, our findings allowed a comprehensive understanding of the structural characteristics of raw starch sources and how different modifications might impact its organization, particularly in relation to nanocrystal modification induced by well-known mechanochemical processes, but not neglecting emerging processing techniques. The initial focus was on potato starch, chosen for its accessibility and commercial availability, as well as the utilization of commonly employed and straightforward processing techniques such as acid hydrolysis and ultrasound-assisted process. Furthermore, other starch sources, including Ariá and Cará roots, as well as exotic Andine corn and bean varieties, were investigated using a range of processing techniques such as gamma irradiation, cold plasma, gelation-retrogradation and extrusion.

This research was driven by in the significant scientific and technological relevance of biopolymers, specifically starches, and their broad potential for modification and application (Da Costa Pinto et al., 2023; Martins; Gutkoski; Martins, 2018). The structural analysis of nanostructured polymers presents unique challenges, particularly in distinguishing and characterizing the semicrystalline regions amidst the complexity of amorphous components in diffraction patterns (Driemeier; Calligaris, 2011). The current methods employed for cellulose analysis may not directly correspond to the diffraction patterns of semicrystalline starches (French; Santiago Cintrón, 2013; Pinto; Campelo; Michielon de Souza, 2020), especially in the nanometric scale where the behavior of nanocrystals and the amorphous portion interact. This research bridges this gap by combining information from structural parameters obtained by X-Ray Diffraction (XRD) and refined using the Rietveld Method (RM) (Manzato et al., 2017; Pinto; Campelo; Michielon de Souza, 2020), (Dave et al., 2015).

XRD data-combined RM techniques allowed a deeper understanding of the structural modifications induced by mechanochemical processing of starches and their impact on their nanocrystal structure (Pinto; Campelo; Michielon de Souza, 2020). This thesis was only the first step toward a comprehensive analysis of starches focused on crystallographic analyses, encompassing various types and sources of starches, expanding knowledge in Materials and Food Engineering of this important biomaterial. The findings of this research have the potential

to bolster new products and applications that harness the unique properties of starches, thereby benefiting industries such as food, packaging, and biomedical sectors (Dave et al., 2015). Ultimately, this thesis aimed to expand the frontier of knowledge on the semicrystalline structure of starches, as well as improve the scientific community's comprehension of this versatile biopolymer (Pinto; Campelo; Michielon de Souza, 2020). Many compelling outcomes (including new research topics for our research group, national and international collaborations, and large-scale projects) have already been generated from this research, which remains in full development.

Thus, this work presented a methodology for analyzing diffractograms where the X-ray scattering pattern obtained for the non-crystalline phase considers the effects of microstructure and crystallite size on the peaks widening (Pinto; Campelo; Michielon de Souza, 2020), even allowing the quantification of each phase in the sample (Carvalho et al., 2021; Da Costa Pinto et al., 2021, 2023). Last but not least, the crystallographic information provided by the Rietveld Method has minimal influence of the researcher in obtaining these quantities (De Figueiredo; Ferreira, 2014).

Chapter 1 begins with a state-of-the-art description of the structure of biopolymers and the organization of these macromolecules into semicrystalline arrangements and some methods those materials might be processed to enhance specific characteristics. The challenges associated with analyzing biopolymeric nanostructures are then discussed in the context of X-ray diffraction technique, highlighting the limitations of traditional methodologies for determining crystallinity in biopolymers. The chapter illustrates various methods employed to assess crystallinity, offering a critical reflection on the difficulties of obtaining precise and accurate information using conventional approaches. These methods prove to be limited in their ability to extract unbiased reliable data from nanometric semicrystalline materials. The discussion then shifts to the particularly complex structure of starch, identifying a significant scientific gap: What are the best approaches to exploring the microstructure of starches and quantifying their crystallinity under a systematic and unbiased manner?

In Chapter 2, the focus shifts to the methodology proposed by using the XRD technique) combined with structural refinement techniques, particularly the Rietveld (RM), to extract and quantify microstructural information in nanometric semi-crystalline materials. The chapter begins with a concise comparison between Le Bail and Rietveld refinement methods , highlighting their respective applications and differences. Following this, the theoretical

framework and equations underlying the Rietveld refinement are comprehensively presented. The Scherrer equation (Langford; Wilson, 1978), used for estimating the mean crystallite size, is also introduced as an additional tool to quantify the non-crystalline component and calculate crystallinity. Additionally, a section of the chapter is dedicated to the experimental setup, emphasizing the critical role of sample preparation in ensuring the quality and reliability of the data obtained. This comprehensive discussion lays the foundation for the practical application of the methodology in subsequent analyses, demonstrating its robustness in characterizing semi-crystalline materials.

In Chapter 3, as a proof of concept of the proposed method, potato starch—a widely recognized and extensively exploited polysaccharide—was analyzed employing XRD and the Rietveld Method to investigate possible crystal modifications under physicochemical processes. (Pinto; Campelo; Michielon de Souza, 2020). This marked the first application of the method to such hydrocolloids, and the study has garnered interest within the scientific community, reaching 18 citations as of December 2024. The section concludes by highlighting that XRD-combined RM represents a promising approach for detailed analysis of the semi-crystalline structure of biopolymers, and our focus now shifts to new and unexplored starch sources and innovative processing techniques.

After demonstrating the potential of this method, Chapter 4 discusses more results of this work: how an exotic source of starch, derived from Amazon root Ariá (*Goepertia allouia*), was subjected to non-conventional modification (gamma irradiation and cold plasma) (Carvalho et al., 2021; Pinto et al., 2021a, 2023). This more complex structure was successfully dissected: Rietveld Method proved an efficient path for deconvolution of both crystalline phases (A and B-type) and noncrystalline portion of the starch. Additionally, the microstructure information derived from the structural refinement was correlated with other characterization technique, such as FTIR and rheology, corroborating the findings and inspiring further investigations. These three works generated significant interest within the scientific community, achieving together a total of 112 citations as of December 2024.

Chapter 5 highlights ongoing and already investigations conducted in collaboration with food scientists at both national and international levels. These studies successfully demonstrated the effectiveness of combining XRD and Rietveld Refinement to extract valuable insights into starch microstructure. Other starch sources from Amazon Biome were analyzed: Peruvian Maize (*Zea mays sp.*), Peruvian Fava Beans (*Vicia faba L.*) and Thorn-yam

(*Dioscorea chondrocarpa* Griseb). This emphasizes the significance of this work in promoting the use of local resources for food production and adding value to previously underexplored starch sources of Amazon biodiversity.

The concluding chapter provided valuable insights by comparing the discussions on the combined use of XRD and RM, highlighting how processing influences the structure and techno-functional properties of both raw and processed starches. This experience enhanced the understanding of the significance of this work as a means to better appreciate the biodiversity of local resources and potentially reduce dependence on external starch sources. Moreover, this research could serve as inspiration for exploring diverse processing mechanisms capable of modifying crystallinity or even transforming one structural type of starch polymorph into another, opening up a broad spectrum of potential applications that benefit from this deeper understanding. This work also opens pathways for the broader scientific community to adopt and expand the use of more robust and complementary techniques—such as X-ray diffraction (XRD) combined with Rietveld refinement (RM)—for accessing complex and detailed structural information of semicrystalline biopolymer nanocrystals. Furthermore, it encourages the investigation of how various processing methods can modulate these semicrystalline regions, providing structural insights that are critical for advancing the understanding and targeted application of these materials.

Objectives

General Objective

Investigate starches employing X Ray Diffraction technique and Structural Refinement.

Specific Objectives

- Develop a solution to accurately investigate the crystallinity of various starches in the light of X Ray Diffraction technique.
- Apply the developed methodology to comprehensively investigate different starches, including various types of unexplored amazonian sources.
- Conduct physicochemical modifications (such as hydrolysis, ultrasound, gamma irradiation, cold plasma) on starches and evaluate their effects on microstructure using the proposed methodology.
- Combine X-ray diffraction analysis with other techno-functional characterizations commonly utilized in the food industry to achieve a comprehensive understanding of the potential applications of those starches.

CHAPTER 1 - STATE OF THE ART

The Quest for crystallinity in semicrystalline biopolymers

This chapter explores the challenges of analyzing biopolymer structures, particularly their semicrystalline nature, with an emphasis on starch nanocrystals and their role in evaluating molecular order. It discusses complexities in quantifying microstructural information from XRD patterns, highlighting that the methodologies applied so far to biopolymers are not entirely robust for assessing their crystallinity, often lacking impartial and improved approaches.

Starch and cellulose are biopolymers that have versatile properties, established supply chains, biocompatibility, and renewable sources, making them useful materials in various industries such as pharmaceuticals, cosmetics, food, and health industries (De Souza; E Magalhães, 2010; Farrán et al., 2015). The pursuit of new sources and varieties of starch remains vital for advancing these many industries, particularly as a means to discover alternative food sources to combat hunger and malnutrition. It also serves to enhance the understanding of nutritious and sustainable regional crops, ensuring food security, reducing vulnerability, and improving the dietary quality of populations (Salvador-Reyes et al., 2024; Salvador-Reyes; Clerici, 2020). The Amazon biodiversity has a number of different possibilities of roots and cereals that might as well be employed by the industry (De Souza; E Magalhães, 2010).

Starch, the second most abundant natural polymer after cellulose, serves as a vital energy storage molecule found in a diverse range of renewable resources such as cereals, tubers, roots, fruits, and seeds (Bertoft, 2017). Its ubiquity and versatility underscore its importance as a sustainable material for numerous industries (Dai et al., 2018). Beyond its conventional applications as food, the study of starch crystals offers innovative opportunities for enhancing its functionality. The modification of starch is a key approach for tailoring its structural and functional properties, driven by the demands of specific applications (Toraya-Avilés et al.,

2017). Starches also play an important part in the sustainability of the industry of consumer goods: as carbohydrates, starches serve as a vital feedstock for fermentation processes in the production of polylactic acid (PLA), a biodegradable thermoplastic that is transforming the materials industry (Suwanmanee; Leejarkpai; Mungcharoen, 2012). PLA combines durability with compostability, making it a sustainable alternative to petroleum-based thermoplastics. As the need to reduce pollution from traditional plastics intensifies, the role of starch-derived PLA is expected to become increasingly significant in addressing global environmental challenges (Inkinen et al., 2011). These advancements not only highlight the potential of starch as a renewable and sustainable resource but also contribute to reducing reliance on non-renewable materials in food, packaging, and other industrial applications (Marco-Aurelio De Paoli, 2008).

This material is highly sensitive to structural modifications, and several applications might be derived from making it critical to understand not only its chemical composition but also the intricate architecture of its carbohydrate arrangements (Imberty et al., 1991). Crystallinity, a key structural property of all materials including starches, serves as a valuable parameter for interpreting structural information and its correlation with functional properties (Pinto et al., 2021a). It is frequently employed to evaluate processes such as the formation of starch films (Abral et al., 2019), thermoplastics (Halimatul et al., 2019a), hybrid composites (Ilyas et al., 2019b, 2020), bionanocomposites of starch and nanocellulose (Abral et al., 2019; Da Silva et al., 2021; Halimatul et al., 2019b; Ilyas et al., 2018a, 2019c; Ilyas; Sapuan; Ishak, 2018) and starch nanocrystals (highly ordered crystalline structures derived from the selective erosion of the amorphous regions in starch granules) (Pinto et al., 2024). By examining crystallinity, we researchers may gain deeper insights into the structural evolution of starch and its impact on material properties, enabling the development of advanced applications and even increasing yield in engineering applications and manufacturing processes.

This chapter not only examines the challenges inherent in analyzing the structure of biopolymers, particularly their semicrystalline nature, but also reflects on my own journey of recognizing starches as more than just a food source. It highlights how starches, like other semicrystalline materials, offer a fascinating platform for structural studies. This chapter also provides a detailed definition of crystallinity of biopolymers, its chemical foundation, and its relevance to the functional properties of biopolymers. The structural characteristics of starch are explored with a focus on the semicrystalline nature of its nanocrystals and their pivotal role in evaluating structural changes during processing, and how that might be influenced by water content.

Additionally, this section addresses the complexities of quantifying microstructural information derived from X-ray Diffraction (XRD) patterns, highlighting the inherent difficulties in deconvoluting overlapping peaks and separating contributions from crystalline and amorphous phases. While various strategies have been developed to address these challenges, they often overlook key aspects of conducting an unbiased study for accurately quantifying crystallinity. Consequently, this persistent issue underscores the need for improved methodologies that ensure precision and reliability in the structural analysis of biopolymers.

1.1. A brief consideration on the chemistry and structure of polysaccharides

Polysaccharides play three main functions in animals and plants: they serve as energy sources (such as glucose in plants and glycogen in animals), structural components (such as cellulose), and water binders (such as agar, pectin, and alginate) (Frazier, 2015b; Nascimento et al., 2021). The molecular structure of polysaccharides can vary, with some being linear (such as amylose and cellulose), branched (such as amylopectin and glycogen), interrupted (such as pectin), block-like (such as alginates), or having alternate repetition (such as agar and carrageenan) (Andréa Bertolini, 2010; Nascimento et al., 2021). Depending on the geometry of the glycosidic linkages, the chains of polysaccharides can form disordered regions, extended strands, entangled structures, or helices (Frazier, 2015b; Nascimento et al., 2021).

Natural polysaccharides are usually named according to their chemical structure, including whether those are homopolymers or copolymers, whether they are linear or branched, the dominant sugars (oses), and whether the hemiacetal linkages are alpha or beta (Frazier, 2015b; Nascimento et al., 2021). Starch and cellulose are examples of homopolymers of glucose and are referred to as glucans for this reason (Nascimento et al., 2021).

The classification of plant polysaccharides is mostly based on the main organic functions present in their composition (Nascimento et al., 2021). Polysaccharides are predominantly composed of repeated hemiacetal groups separated by pyranose ring segments, and the linkages between the groups occur through alpha and beta acetal linkages (Nascimento et al., 2021), demonstrated in Figure 1.

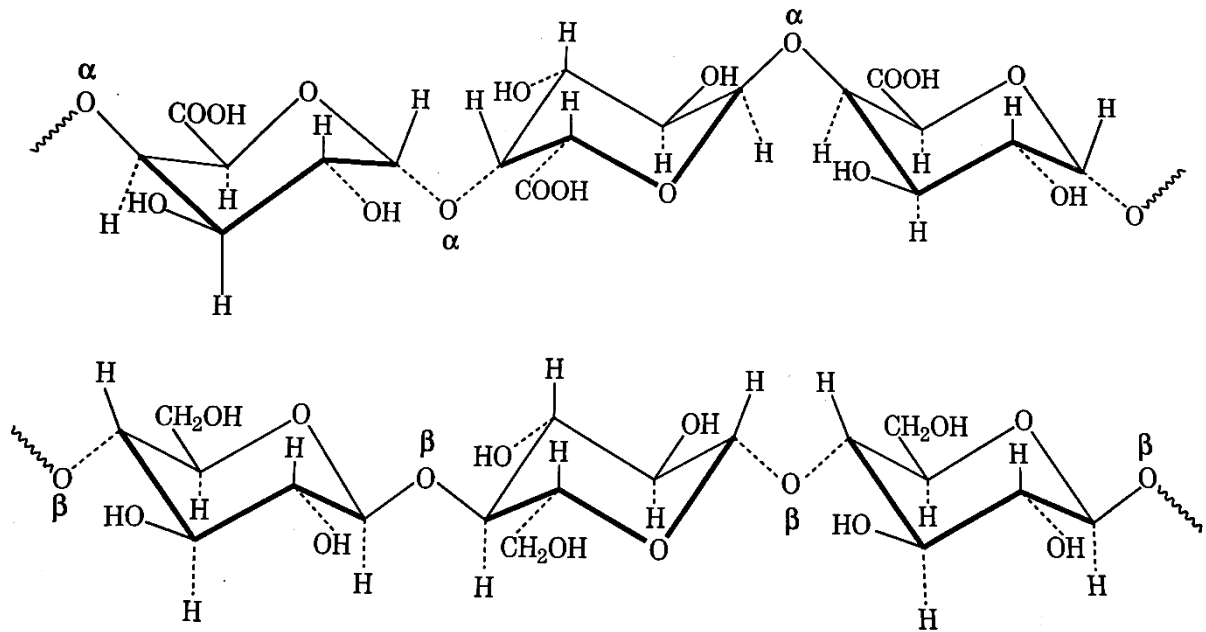


Figure 1 – The chaining of groups through alpha or beta linkages. Figure from (Nascimento et al., 2021)

Polysaccharides from microorganisms, such as algae and bacteria, can contain both alpha and beta linkages, resulting in gums such as agar, sodium alginate, carrageenan, gelatin gum, and xanthan gum (Frazier, 2015b; Nascimento et al., 2021).

Starch is a mixture of amylose and amylopectin, and its proportion varies according to the botanical source and cultivation conditions (Jane, 2006). It is synthesized in the chloroplasts of plants, where chlorophyll facilitates the conversion of water and carbon dioxide into starch under the influence of sunlight. I find it to be particularly beautiful to think of starch as crystallized light—a tangible manifestation of the Sun's energy, made accessible for plants and animals as a vital energy source. As a storage material, starch is stored in different parts of plants, such as fruits, seeds, bulbs, and tubers (Andréa Bertolini, 2010). Figure 2 represents the multiscale structure of starch granules.

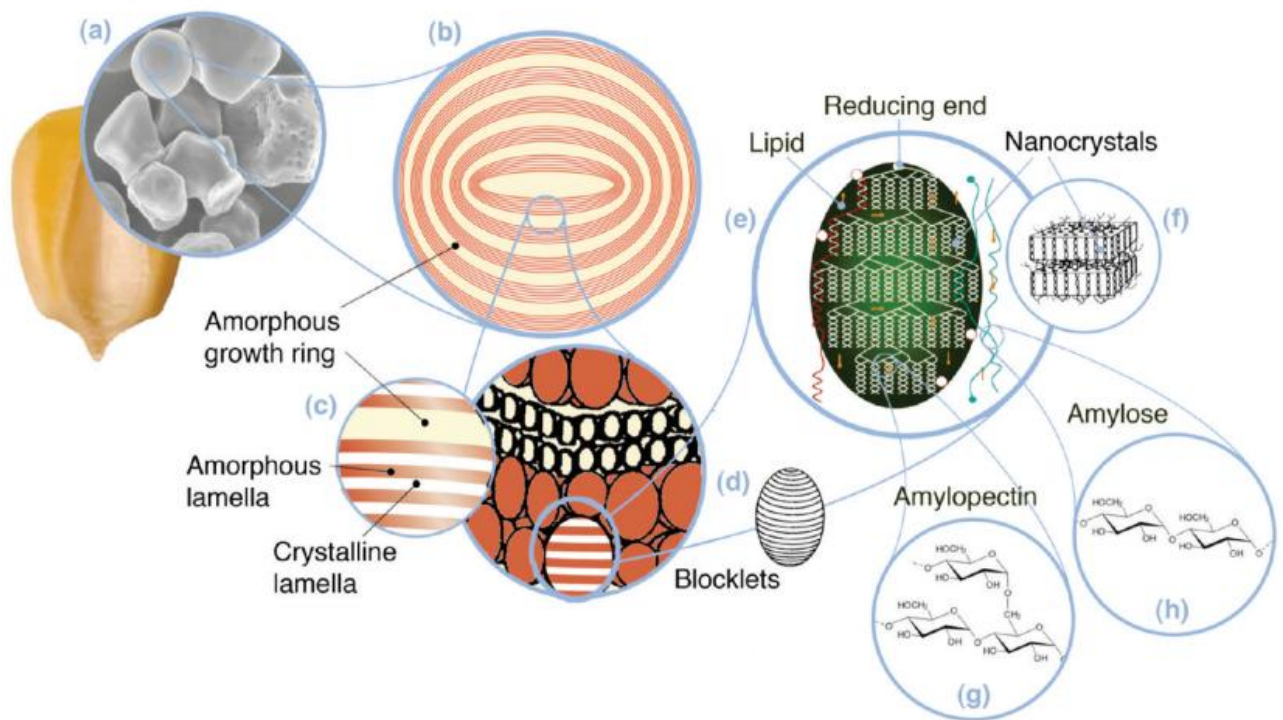


Figure 2 – Starch multiscale structure. Figure from (Le Corre; Bras; Dufresne, 2010)

In this nearly complete schematic, many details of the starch granule are represented, as extracted from (Le Corre; Bras; Dufresne, 2010):

- (a) Starch granules derived from normal maize (30 μm)
- (b) Amorphous and semicrystalline growth rings (120-500 nm)
- (c) Amorphous and crystalline lamellae (9 nm), with magnified details of the semicrystalline growth ring
- (d) Blocklets (20-50 nm) that constitute a unit of the growth rings
- (e) Amylopectin double helices forming the crystalline lamellae within the blocklets
- (f) Nanocrystals, an alternative representation of the crystalline lamellae known as starch nanocrystals when isolated through acid hydrolysis
- (g) Molecular structure of amylopectin
- (h) Molecular structure of amylose (0.1-1 nm)

Amylose is a linear chain of poly(anhydroglucopyranose), with polycondensation occurring at the 1,4- α positions. On the other hand, amylopectin is a branched chain with a much higher molecular weight, and its branches occur at the 1,6- α positions every 15-30 glucosidic units of the main chain, forming dendritic structures. Amylopectin can be explained by the cluster model, where A chains are non-branched and located at the ends of dendritic formations with α (1-4) linkages. B chains have α (1-4) and (1-6) linkages, while C chains, in addition to these linkages, have a reducing group at the end (Tester; Karkalas; Qi, 2004). The regions of A chains generate crystalline clusters, while the B regions form non-crystalline regions (Nascimento et al., 2021). This classification should not be confused with the structural type formed by the condensation of amylose and amylopectin (Bertoft, 2017; Imberty et al., 1991; Pinto et al., 2021a; Rodriguez-Garcia et al., 2021) and is represented in Figure 3.

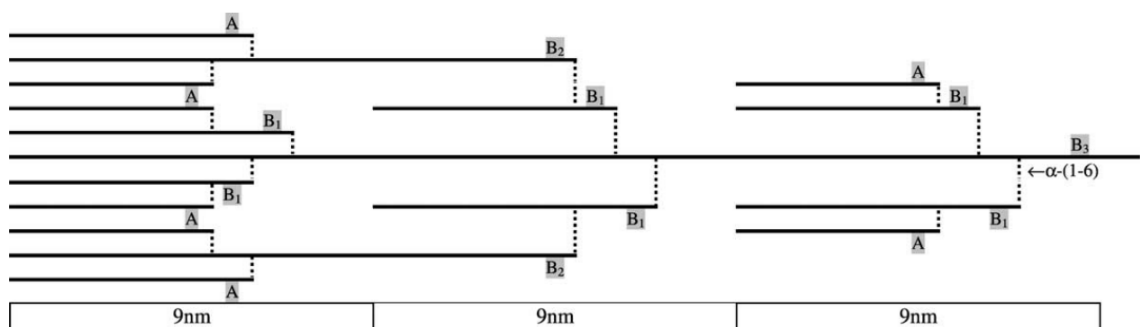


Figure 3 – Section of amylopectin indicating the branching pattern of unit (1 - 4)- α -chains (A, B₁–B₃) joined together by (1 - 6)- α - linkages (branch points). The chaining of groups through alpha or beta linkages. Figure from (Tester; Karkalas; Qi, 2004)

Starch grows in lamellae, forming concentric layers that result in spherulitic structures. However, starch granules have an ellipsoidal shape due to the deposition of incomplete layers (Nascimento et al., 2021). This alternation of crystalline and non-crystalline layers contributes to the semicrystalline structure of starch (Jane, 2006). Figure 4 depicts a simplified version of the starch granule and the crystalline clusters.

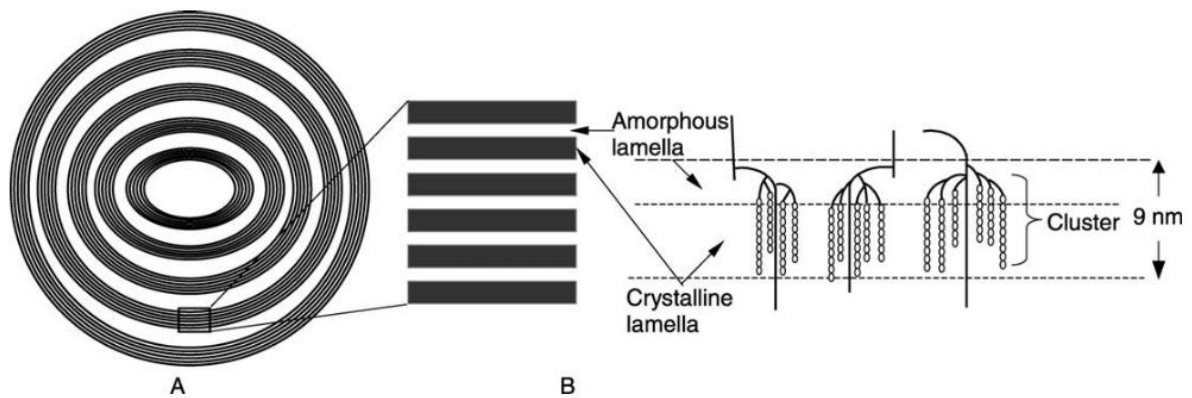


Figure 4 – From granule to lamellae. Figure from (Tester; Karkalas; Qi, 2004)

In the structure of a starch granule, (A) depicts microcrystalline lamellae arranged in stacks, separated by amorphous growth rings. A closer look at (B) reveals the distinct amorphous and crystalline regions. The crystalline lamellae shown are formed by double helical structures, which result from the interaction of adjacent chains of amylopectin. In contrast, the amorphous regions consist of branching points.

In a closer look at the cluster region, in Figure 5, the mean size of those chains can be accounted for.

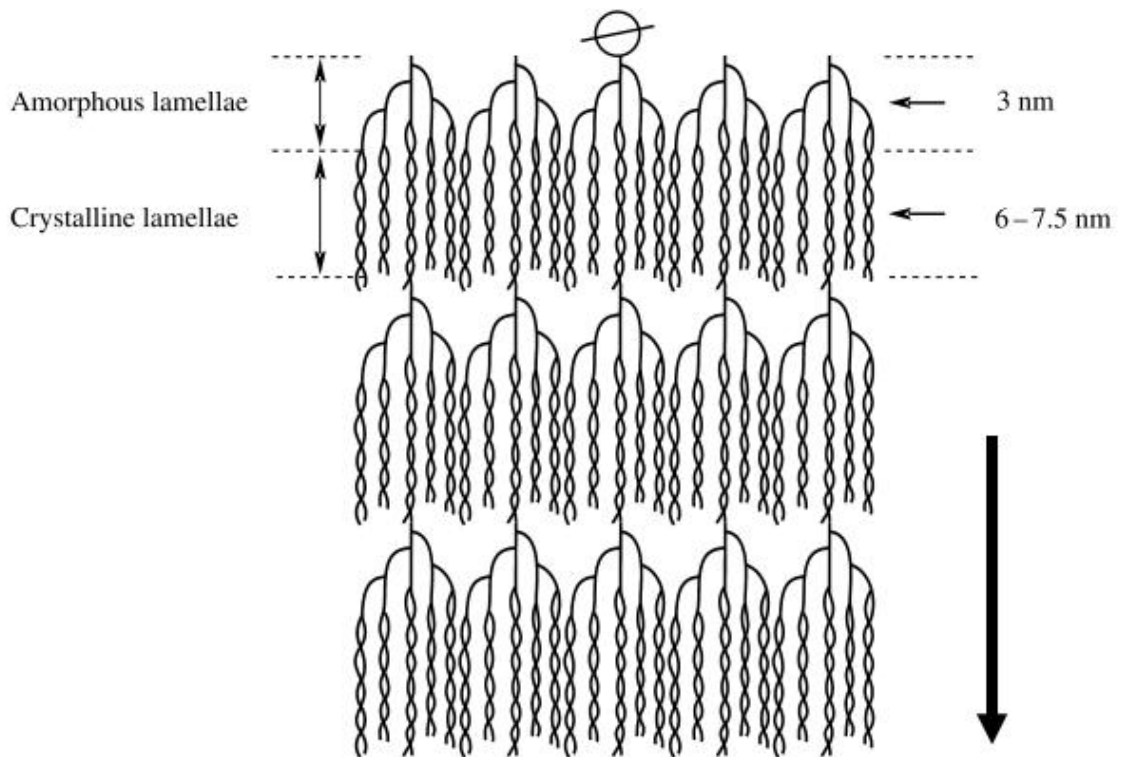


Figure 5 – Lamellar structure of a starch granule. Figure from (Tetlow, 2011)

The starch granule, which can reach lengths of up to 50mm, consists of numerous regions comprising alternating amorphous and semicrystalline zones (Tetlow, 2011). These regions, with widths of several hundred nanometers, are organized into pairs, forming a single growth ring (Tester; Karkalas; Qi, 2004). The growth rings, along with other well-structured elements within the granule, are embedded in an amorphous background containing amylopectin in a less ordered state. Amylose is interspersed between the amorphous zones and the clusters of amylopectin (Malin Sjöö; Lars Nilsson, 2009; Tetlow, 2011).

In the shown tandem-linked glucan clusters, parallel chains of α -(1 - 4)-O-linked glucan, composed of short to intermediate-length glycosyl units (degree of polymerization (DP)), assemble to form double helices (Tetlow, 2011). Polymer growth occurs from the non-reducing end in the direction indicated by the arrow. These double helices contribute to the water-insoluble properties of the polymer (Tester; Karkalas; Qi, 2004). The amorphous lamellae are characterized by clustered α -(1 - 6)-linked glucosidic linkages (branch-points), while longer glucan chains connect the crystalline lamellae (Tetlow, 2011). Notably, the length of the crystalline and amorphous regions, approximately 9-10 nm, appears to be highly conserved regardless of the starch source (Tester; Karkalas; Qi, 2004).

These structures are organized in such a manner that optimizes their packing within the plant while also facilitating the storage of water. Water plays a very important role in the structure and functionality of all carbohydrates (no wonder those molecules are, themselves, “hydrates”), both as intrinsic water and as adsorbed water (BeMiller; Whistler, 2009; Wang, 2020). Intrinsic water refers to water molecules that are structurally bound within the starch granule, often forming part of the crystalline lattice or tightly associated with amylose and amylopectin molecules. This water contributes to the stabilization of the granule’s semicrystalline structure by facilitating hydrogen bonding between polymer chains (Malin Sjöö; Lars Nilsson, 2009). In contrast, adsorbed water exists on the surface or within the amorphous regions of the granule, interacting loosely with the polymer matrix. Adsorbed water affects the mobility of starch molecules and influences gelatinization and retrogradation processes, as water availability dictates the degree of granule swelling and subsequent structural changes (Buléon et al., 1998). The interplay between these water types is critical for techno-functional properties of starches much valued by the industry, such as viscosity, gelation, and crystallinity, influencing its behavior in food and industrial applications, and thus understanding the role of intrinsic and adsorbed water is therefore essential for optimizing starch-based materials for specific uses (Castillo et al., 2019; Frazier, 2015; Huang; Perdon, 2020).

Intrinsic water occupies specific crystallographic sites within starch, influencing the structural organization of starch polymorphs and the arrangement of these macromolecules within the plant. A deeper investigation into these structural differences provides a vital foundation for understanding the role of water in starch architecture.

1.2. Starch Polymorphs

In pure starches (without fat or cellulose), amylose and amylopectin form a complex matrix that can be understood in terms of two main components: (i) a disordered portion formed by helix branches and molecular fragments, and (ii) a highly organized semicrystalline component with a short-range periodic order in a helical conformation (Buléon et al., 1998). These two components intertwine to form alternating amorphous and crystalline lamellae, ultimately resulting in the formation of a starch granule (Domene-López et al., 2019). According to Takahashi et al. (Takahashi; Kumano; Nishikawa, 2004), the positions occupied by water molecules within the amylose structure exhibit different statistical probabilities, often surrounded by up to six double-strand helices. On the other hand, the disordered component (amylose) is comprised of helix branches and molecular fragments (Sreenivasulu, 2019).

The semicrystalline fraction can organize itself naturally in three different polymorphs : A-type (commonly found in cereals, is highly packed and has a comparatively high molar proportion of short to long chains), B-type (may be found in tubers, stems, and fruits, contains larger amount of water molecules stored between the chains, with lower ratio of short to long chains), and C-type (usually found in beans (Wild; Blanshard, 1986), and described as a combination of A and B types) (Malin Sjöö; Lars Nilsson, 2009). Although the geometry of double helices is identical in both the A- and B-forms, the two structures differ in their water content and crystalline arrangements (Andréa Bertolini, 2010). How, then, can one distinguish

between different polymorphs¹? The answer lies in the very definition of the term: "morph," in this context, refers to the arrangement of atoms and molecules, and "poly" give us a hint of how many different ways the arrangement of such molecules might occur. The discipline dedicated to uncovering and analyzing these arrangements is crystallography, a scientific field that provides detailed insights into the structural organization of materials at the atomic and molecular levels.

The polymorphism and crystallinity can directly impact the physicochemical characteristics and techno-functional properties of starches (Schwall et al., 2000), making this classification valuable for studying the mechanisms behind a number of processing techniques such as enzymatic digestion (Blazek; Gilbert, 2010), gelatinization (Le Corre; Angellier-Coussy, 2014), plasticization (Domene-López et al., 2019) and structural modifications studies in general.

The structural differences between A-type and B-type starches are primarily attributed to their packing density and water content within the starch granules, which in turn influences their physicochemical properties, such as gelatinization temperature and digestibility, and make it possible to convert to one polymorph to the other according to moisture and temperature, both in manmade processing and by the own vegetable (Imberty; Chanzy; Perez, 1988; Le Bail et al., 1999). The crystallographic studies by Imberty and Pérez (Imberty et al., 1991) play important part in advancing our understanding of the role of intrinsic water in starch structures, particularly concerning the A- and B-type polymorphs. In both cases, starch molecules organize into double helices that are arranged in parallel arrays, but the distinction between both starches

¹ Although the literature often distinguishes between the terms polymorph and allomorph—typically reserving polymorph for simpler compounds and allomorph for more complex compounds and macromolecules—this work adopts the term polymorph exclusively. This choice aligns with its frequent usage in related studies and ensures consistency with the terminology employed by other researchers in the field (Fawcett et al., 2013; French, 2014; French; Santiago Cintrón, 2013; Kong et al., 2014; Le et al., 2018, 2021; Science; Bonington, 1986; Shama; Bianco-Peled; Shimoni, 2003; Wild; Blanshard, 1986; Xu et al., 2020).

polymorphs primarily arises from their water content and the specific packing of these double helices within the crystalline lattice. (Imberty; Perez, 1988)

A simplified model is represented in Figure 6.

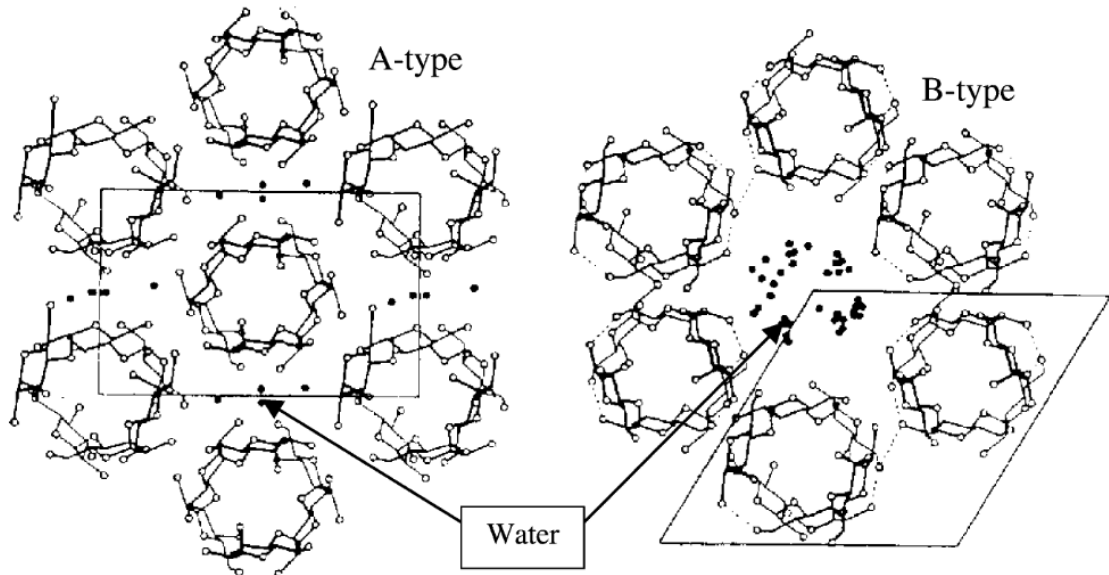


Figure 6 – A and B-type polymorphs of amylose. Figure from (Tetlow, 2011)

A-type starches, typically found in cereals, exhibit tightly packed structures with low water content, making them less permeable to water and more thermally stable, but less drought resistant (BeMiller; Whistler, 2009; Imberty et al., 1991; T.L. Barsby; A.M. Donald; P.J. Frazier, 2001; Wang, 2020). Its monoclinic crystalline arrangement, with variations in water content and double helix packing compared to B-type starch, has only four water molecules in its structure (Imberty; Chanzy; Perez, 1988).

In contrast, B-type starches, commonly found in tubers and roots, have looser packing arrangements, allowing for higher water retention within the granules (Imberty et al., 1991; Pinto; Campelo; Michielon de Souza, 2020; Rodriguez-Garcia et al., 2021). The hexagonal unit cell contains 12 glucose residues organized into two left-handed, parallel-stranded double helices (Imberty; Perez, 1988; Takahashi; Kumano; Nishikawa, 2004). These helices are stabilized by 36 water molecules situated between them, contributing to the overall stability and specific packing arrangement of the crystalline structure (Takahashi; Kumano; Nishikawa,

2004). The retained water within B-type starches plays a vital role in the plant's water storage mechanisms, contributing to increased drought resistance. (Imberly; Perez, 1988)

The V-type polymorph, unlike other starch polymorphs, is not naturally occurring and is primarily formed through the complexation of amylose with various compounds such as iodine, alcohols, or lipids (Le Bail et al., 1999). This polymorph exhibits several subtypes, each characterized by specific structural arrangements (Adamu, 2001; Le Bail et al., 1999; Shu et al., 2006). Advancing the understanding and optimization of amylose–lipid complex formation is crucial for enhancing the functional applications of starch in both food and non-food industries (Le Bail et al., 1999).

These differences play an important part in the techno-functional applications of starches, such as their suitability for thickening, gelling, and film formation in various industrial and food processes (Salvador-Reyes et al., 2024). Furthermore, these structural variations also dictate how semicrystalline regions in C-type starches, which combine characteristics of both A- and B-type polymorphs, respond to processing. The way each polymorph interacts with processing conditions, such as heat, enzymatic treatments, or mechanical stress, can alter their functional properties and broaden their potential applications in tailored formulations (Carvalho et al., 2021; Pinto et al., 2021a, 2023, 2024; Salvador-Reyes et al., 2024).

Understanding these modifications stems from the needs of industry. A comprehensive understanding of the structural modifications induced by various processing techniques on starch requires a more detailed examination of the methodologies employed for modifying it.

1.3. Applications and Modifications of starch structures

Starch is a widely used renewable biopolymer that finds applications in both the food and non-food industries, and the exact application will be influenced by its structure (De Souza; E Magalhães, 2010), (Vamadevan; Bertoft, 2015). Starches with lower crystallinity are valued primarily as a carbohydrate energy source but also for their gelling and water interaction (absorption, retention) properties, which are extensively utilized to control texture and physical characteristics of a number of products (Schmitz et al., 2006).

The interaction between water and heat creates the most fundamental modification of starches: gelation-retrogradation process. When starch is heated in the presence of water, it does

not dissolve but absorbs the water and hydrates (Frazier, 2015). Starch granules swell until they burst, losing their organized structure (Frazier, 2015). This results in the formation of a starch paste, whose consistency varies depending on process factors such as heating, stirring, and water content. When chemical agents like acids and enzymes are present, starch molecules can be degraded, resulting in low viscosity starches, dextrans, syrups, and sugars (Da Costa Pinto et al., 2023).

Upon cooling, the starch paste forms a gel due to the formation of hydrogen bonds between amylose and amylopectin. This gel can undergo a process called retrogradation when stored for an extended period (Martins; Gutkoski; Martins, 2018). Retrogradation involves the separation of water from the gel, resulting in syneresis, where water accumulates on the gel's surface (Frazier, 2015). Additionally, amylose molecules join together to form crystalline clusters (Vamadevan; Bertoft, 2015). This effect may be undesirable in food products but can be desirable in various packaging manufacturing (Chisenga et al., 2019).

More advanced starch processing methods have increasingly focused on modified starches, which have garnered significant attention for their potential in materials applications. These modifications are particularly valued for enhancing sustainability, biocompatibility, and safety in food packaging solutions (Khalil; Hashem; Hebeish, 1990). Moreover, biodegradable edible films derived from starch have emerged as important materials in food packaging research due to their environmentally friendly nature (Molavi et al., 2015). To meet the requirements of these diverse applications, starch often undergoes processing, and the particular production of starch nanocrystals has gained considerable interest (Dai et al., 2018; Dufresne, 2014; Mohammad Amini; Razavi, 2016; Pinto et al., 2024).

The production of starch nanocrystals primarily involves two main methods: chemical and mechanical. Chemical methods focus on corroding the amorphous phase of starch through the use of eroding agents like enzymes (Tomasik; Horton, 2012) and strong acids (Angellier et al., 2004; Asiri; Ulbrich; Flöter, 2018; Le Corre; Angellier-Coussy, 2014). On the other hand, mechanical methods aim to break the polymer chains using high-energy techniques such as milling (Vertuccio et al., 2009) and ultrasound (Bel Haaj et al., 2013; Chang et al., 2017). Combining physical and chemical methods offers advantages such as reduced processing time (compared to solely chemical methods that can take up to 5 days) and minimized damage from heat (as highly energetic physical methods can increase starch temperature, leading to phase changes and thermal degradation). Some combined methods involve acid hydrolysis with

thermo-sonication (Mohammad Amini; Razavi, 2016; Pinto; Campelo; Michielon de Souza, 2020b) or milling (Dai et al., 2018).

Investigating the specific processing methods selected for the studies described in this thesis provides critical insights into their influence on the molecular and crystalline structure of starch. By analyzing these techniques in greater depth, it becomes possible to elucidate the underlying mechanisms driving structural changes, such as depolymerization, crystallinity alterations, and modifications in water-starch interactions.

1.3.1. Acid hydrolysis

Acid hydrolysis is a widely employed technique that modifies the structural and functional properties of starch granules into nanocrystals, making it an essential process in both food and material sciences. This method involves the use of mineral acids, such as hydrochloric acid or sulfuric acid, to cleave the glycosidic bonds within the starch molecules, resulting in the breakdown of the polymer into smaller oligosaccharides or even glucose (Bismark et al., 2021). The process begins with the penetration of the acid into the starch granules, preferentially attacking the amorphous regions, which leads to the erosion of these areas and the degradation of the starch molecules (Liu et al., 2023). As a result, acid hydrolysis can produce starch nanoparticles, which have gained attention for their unique properties and potential applications in various fields, including drug delivery and biodegradable materials (Anand et al., 2018).

The extent of hydrolysis can be controlled by adjusting parameters such as acid concentration, temperature, and reaction time. For instance, higher acid concentrations can accelerate the erosion of amorphous regions, leading to the rapid formation of nanoparticles (Baruah; Singha; Uppaluri, 2023). However, prolonged hydrolysis may also result in undesirable effects, such as excessive degradation of the crystalline regions, which can negatively impact the quality and stability of the final product (Li et al., 2022). Studies have shown that the structural changes induced by acid hydrolysis can enhance the solubility and swelling power of starch, making it more suitable for various applications (Sumardiono et al., 2022). Additionally, the process can influence the retrogradation behavior of starch, a very interesting property of starches that add functionality in food products (Ghalambor et al., 2022).

1.3.2. Ultrasound-Assisted Processing

Ultrasound refers to high-frequency sound waves exceeding the human auditory threshold (~20 kHz). Its functional mechanism is grounded in the propagation of alternating high and low-pressure regions through a medium, with acoustic pressure variations directly proportional to the energy input (Chemat; Zill-e-Huma; Khan, 2011). Ultrasound applications are broadly categorized by intensity and frequency: low-intensity ultrasound (1 W cm^{-2} , 5–10 MHz) is typically used for non-destructive testing, while high-intensity ultrasound ($10\text{--}1000 \text{ W cm}^{-2}$, 20–100 kHz) is employed for processing and modification of materials (Justino et al., 2024).

The key mechanism behind ultrasound processing is cavitation, a phenomenon where high-energy waves create microscopic bubbles in the medium. These bubbles collapse violently, generating localized regions of high temperature and pressure (Mohammad Amini; Razavi, 2016). This process facilitates numerous physical and chemical effects, such as enhancing mass and heat transfer, promoting emulsification, and improving the extraction of bioactive compounds from food matrices (Su & Cavaco-Paulo, 2021). For example, Jiang et al. (2021) demonstrated that ultrasound accelerates heat and mass transfer, producing stable emulsions through homogenization of the colloid. Similarly, Kernou et al. (2021) observed that sonication increased the concentration of bioactive compounds in orange juice while also influencing its texture.

Ultrasound technology is extensively applied in the food industry for enhancing efficiency, reducing processing time, and preserving the nutritional and functional qualities of food products. Some applications are microbial inactivation (Piyasena; Mohareb; McKellar, 2003), enzymatic deactivation (Islam; Zhang; Adhikari, 2014), bioactive compound extraction (Esclapez et al., 2011), pre-treatment for drying (Musielak; Mierzwa; Kroehnke, 2016), and the modification of biopolymers such as carbohydrates (Bera et al., 2015) and proteins (Su; Cavaco-Paulo, 2021).

In the polymer industry, ultrasound is also a transformative technology for blending, modifying, synthesizing or recycling polymers: the cavitation effects generated by ultrasound enhance the dispersion of fillers within polymer matrices, resulting in improved mechanical and thermal properties (Sun et al., 2023). This capability is particularly important for the development of nanocomposites, where uniform distribution of nanoparticles during synthesis

is essential for optimizing material performance (Boro; Kashyap; Moholkar, 2022; Zhu et al., 2019).

Chemat et al (2011) also brings another interesting mechanism of ultrasound processing: depolymerization. The depolymerization process is driven by the effects of cavitation and can proceed via two distinct mechanisms: either the mechanical degradation of the polymer, resulting from the intense localized forces generated by the collapse of cavitation bubbles, or the chemical degradation occurring due to reactions between the polymer and high-energy species, such as hydroxyl radicals, formed during the cavitation process (Chemat; Zill-e-Huma; Khan, 2011). This process may interact differently within the polymer matrix and similarly exhibit distinct effects on the structural organization of starches.

As for the end of the life-cycle, the depolymerization and degradation mechanisms are particularly beneficial as a pre-treatment step before conventional acid hydrolysis, effectively reducing polymer chain length and improving the efficiency of subsequent processing steps (Sun et al., 2023). This idea inspires the combination of techniques for processing starches (Pinto; Campelo; Michielon de Souza, 2020; Pinto et al., 2024)

1.3.3. Gamma Radiation

Gamma radiation has emerged as a pivotal technology in the food industry, particularly for the treatment and enhancement of starch-based materials (Verma et al., 2018). This method employs high-energy electromagnetic waves to induce physicochemical modifications in starch, improving its functionality and extending the shelf life of food products (Sudheesh et al., 2019). The application of gamma radiation in food processing serves two primary purposes: microbial decontamination (thereby improving food safety and extending shelf life) and structural modification of food components, with a focus on techno-functional properties of starches.

Studies have demonstrated that gamma irradiation effectively reduces microbial loads in various starchy food products, including rice, ensuring sanitary quality and prolonging storage periods (Biomy, 2021; Wang et al., 2018). The high penetration capacity of gamma rays allows for effective treatment even in packaged foods, making it a practical and hygienic solution for food preservation (Biomy, 2021).

Moreover, gamma radiation can enhance the nutritional profile of starchy foods. Research indicates that low doses of irradiation increase the concentration of phenolic compounds, which are associated with antioxidant activity (Popović et al., 2013; Taheri et al., 2014). This dual effect—improving the physicochemical properties of starch and boosting the antioxidant potential—further underscores its value in food processing (Bao; Ao; Jane, 2005; Kiran, 2023).

Additionally, gamma radiation induces structural and functional changes in starch (Pinto et al., 2021a). Doses below 2 kGy have been shown to modify critical starch properties such as gelatinization temperature and moisture content, enhancing its suitability for diverse food applications (Sunder; Mumbrekar; Mazumder, 2022; Tran; Nguyen; Tran, 2022). This modification occurs through the generation of free radicals, which initiate molecular rearrangements in the starch matrix. These changes have been observed to improve the pasting properties of starches derived from sources like potatoes and corn, rendering them more versatile for culinary and industrial uses (Sunder; Mumbrekar; Mazumder, 2022). Gamma irradiation also influences the crystallinity and morphology of starch granules, enhancing functional attributes such as solubility and viscosity (Bao; Ao; Jane, 2005; Tran; Nguyen; Tran, 2022). These improvements are particularly noteworthy for the food industry, where texture and consistency are critical for consumer satisfaction, and was the motivation for the starch modification made in this thesis.

1.3.4. Cold Plasma

Plasma, often referred to as the fourth state of matter after solids, liquids, and gases, is a partially or fully ionized gaseous state characterized by its ability to conduct electricity. First described by Irving Langmuir in 1928, plasma is visually represented as a fluorescent light discharge or arc and contains a mixture of activated molecules, free radicals, ions, and neutral atoms (Harikrishna et al., 2023). Plasma is generated by subjecting gases (e.g., H₂, O₂, N₂, Ar) to external energy sources such as alternating or direct currents, microwave or radiofrequency fields, or magnetic fields, resulting in the formation of plasma particles with high kinetic energy. The transition to the plasma state occurs when the energy input exceeds a critical threshold, ionizing the gaseous molecules (Thirumdas; Sarangapani; Annapure, 2015).

Plasma can be categorized into thermal (equilibrium) and non-thermal (non-equilibrium) types. Thermal plasma, operating at temperatures of approximately 20,000 K, maintains thermodynamic equilibrium between its components (Banura et al., 2018; Thirumdas et al., 2017). In contrast, non-thermal plasma, often referred to as atmospheric cold plasma (ACP) or cold plasma (CP), operates at much lower temperatures (30–50 °C) due to localized energy input primarily affecting electrons rather than the entire gas flow. This localized energy distribution makes non-thermal plasma particularly suitable for applications requiring minimal heat impact, such as food processing (Sarangapani et al., 2016).

One of the prominent systems used for generating atmospheric plasma is the dielectric barrier discharge (DBD) method (Dong et al., 2017; Yan et al., 2020). This approach was chosen as a processing technique in our work, and involves a dielectric material between two electrodes to prevent spark formation while ionizing a neutral gas to create plasma. Operating at pressures of 10^4 – 10^6 Pa and frequencies ranging from 0.05 to 500 kHz, DBD systems are energy-efficient, requiring 10–100 W for operation. The efficiency of DBD depends on parameters such as gas composition, electrode spacing, and applied voltage, making it ideal for treating large surfaces (Harikrishna et al., 2023).

Cold plasma technology has garnered attention in the food industry due to its energy efficiency, eco-friendliness, and versatility. It is employed in surface modification, sterilization, and structural alterations of food components without compromising bulk properties. One of the primary applications of cold plasma in food processing is its antimicrobial capability. Cold plasma has been shown to effectively inactivate foodborne pathogens such as *Escherichia coli* and *Salmonella* species on food surfaces and within food matrices (Niemira; Boyd; Sites, 2018; Punia Bangar et al., 2022; Varilla; Marcone; Annor, 2020). This makes it particularly beneficial for starchy foods, which are often prone to microbial contamination. By reducing microbial loads, cold plasma not only enhances food safety but also extends shelf life (Karkhanis; Singh, 2024; Nwabor et al., 2022). Additionally, it can be used on food contact surfaces, minimizing cross-contamination risks during processing (Niemira; Boyd; Sites, 2014; Punia Bangar et al., 2022).

Techniques such as etching and plasma sputtering selectively enhance the techno-functional and surface properties of granular and powdered food products, maintaining their overall structure (Harikrishna et al., 2023). Cold plasma treatment is increasingly recognized for its ability to modify the physicochemical properties of starches, such as solubility,

gelatinization behavior, and viscosity. These modifications are essential for enhancing the performance of starches as thickening agents, stabilizers, or texturizers in various food applications (Li et al., 2024; Rao et al., 2023). The treatment primarily affects the surface of starch granules, leading to improved water absorption and swelling capacity (Carvalho et al., 2021; Pinto et al., 2023). Molecular changes such as depolymerization or cross-linking of polymer chains contribute to enhanced gel formation and structural stability (Birania et al., 2022; Dong et al., 2017).

The effectiveness of cold plasma in modifying starch properties is highly influenced by operational parameters, particularly voltage and excitation frequency (Carvalho et al., 2021; Pinto et al., 2023). Higher voltages and specific frequency adjustments generate varying levels of ionization and reactive species, directly impacting the antimicrobial and functional modification effects (Ganesan et al., 2021; Sun; Wang, 2022). For instance, studies show that optimizing excitation frequency can maximize the generation of reactive species, improving the effectiveness of microbial inactivation and starch modification (Noriega et al., 2011; Varilla; Marcone; Annor, 2020). These parameters can be tailored to achieve desired outcomes, offering flexibility and precision in food processing.

The technology is also widely recognized for its environmental and energy-saving benefits, leading to the development of various plasma sources for food and non-food industrial applications. It is considered an environmentally sustainable technology due to its minimal energy requirements and the absence of harmful chemical residues (Venkataratnam et al., 2020; C, 2023). This aligns with the growing demand for green technologies in food processing, where reducing environmental impact is increasingly prioritized. By enhancing food safety and modifying food components without compromising quality, cold plasma provides a promising alternative to traditional processing methods (Punniyamorthy, 2024).

Cold plasma has been used to modify a variety of starches, including banana (Yan et al., 2020), rice (Thirumdas et al., 2017), maize and cassava (Banura et al., 2018), among others. These treatments have been shown to improve properties such as solubility, gel formation, and textural behavior, making them suitable for diverse applications (Mir; Shah; Mir, 2016; Muhammad et al., 2018). However, studies on processing time (Bie et al., 2016) and plasma potency (Banura et al., 2018) have highlighted the importance of optimizing treatment conditions to achieve the desired effects.

Both plasma tension and excitation frequency influence the behavior of electrons and plasma ions, determining the type and abundance of reactive species in the plasma environment (Noriega et al., 2011). While fixed frequencies have been applied to starch modification in some studies (Banura et al., 2018), the effects of varying excitation frequencies on the physicochemical properties of starches remain largely unexplored, which will be vastly discussed in this work.

The many possibilities of innovative processing techniques represent an exciting avenue for further research, particularly for enhancing the functional and physicochemical properties of unconventional starches such as Amazon tuberous roots, and this thesis all but scratches the surface. Cold plasma, as a green technology, holds immense potential for revolutionizing food processing by improving the sustainability and quality of food products, especially starch-based materials.

To effectively utilize these innovative processing methods, it is vital to emphasize that starches, as materials, are sensitive to structural modifications. In addition to understanding their chemical composition and polymorphic classification, a comprehensive understanding of the complex structure underlying the intricate arrangements of carbohydrates is also essential (Imberty et al., 1991). Crystallinity, as an important structural property of starch, can be employed as means to evaluate processes and the formation of starch films (Abral et al., 2019), thermoplastics (Halimatul et al., 2019a), hybrid composites (Atiqah et al., 2019) and bionanocomposites of starch and nanocellulose (Halimatul et al., 2019b; Ilyas et al., 2018a, 2019c, 2020; Ilyas Rushdana et al., 2017). Additional microstructural information can be utilized to predict the macroscopic properties of starch; however, understanding its complex semi-crystalline structure remains a challenging endeavor. The intricate interplay between crystalline and amorphous regions in starch complicates efforts to fully characterize its structural organization. Nevertheless, crystallographic techniques offer valuable insights, providing critical data that can aid in unraveling the complexities of starch structure and its relationship to functional properties.

1.4. Crystallography – X Ray Diffraction for microstructure

Crystallography is the scientific study of the arrangement of atoms and molecules within crystalline materials (Eric Lifshin, 1999). It seeks to elucidate the structural organization and

periodicity of atoms in a crystal lattice, providing critical insights into the physical and chemical properties of materials. Crystallography is integral to understanding the symmetry, bonding, and spatial organization of atoms, which influence the behavior and functionality of an organized substance (Brandon; Kaplan, 2008; Elton K Kaufmann, 2003).

A fundamental tool in crystallography is X-ray Diffraction (referred to as XRD in this work), a technique that exploits the interaction of X-rays with the electron clouds of atoms in a crystal (Eric Lifshin, 1999). When X-rays are directed at a crystalline sample, those are scattered in specific directions depending on the arrangement and spacing of the atomic planes. This scattering produces a diffraction pattern, which serves as a fingerprint of the crystal's structure. By analyzing the positions and intensities of the diffracted beams, crystallographers can determine key structural parameters, such as lattice dimensions, atomic positions, and the degree of crystallinity (B.E. Warren, 1990). XRD is thus a cornerstone of modern crystallography, enabling precise characterization of both natural and synthetic crystalline materials (Cullity; Stock, 2014; Pecharsky; Zavalij, 2005).

Whenever the analysis and quantification of a material's structure are desired, particularly for those exhibiting short-range atomic order, the most widely used non-destructive technique for this purpose is XRD (Cullity; Stock, 2014). Understanding this essential technique empowers materials scientists to explore their materials' structure and its correlation with macroscopic properties in novel ways (Ashcroft, Neil W, Mermin, 1976). Simultaneously, materials engineers can leverage this knowledge to tune the material's microstructure, emphasizing desirable properties and mitigating undesirable ones (Farrán et al., 2015). Consequently, possessing knowledge of a material's structure opens up avenues for seeking improved applications and enables deliberate structural modifications to develop new products and diverse industrial applications (Brandon; Kaplan, 2008).

The most commonly utilized technique for structural analysis is powder diffraction using reflected beams. Crystals in this method are analyzed based on the diffraction patterns produced when X-rays interact with their atomic arrangement, which consists in a set of points represented by the diffracted intensity versus the scanning angle of the 2θ goniometer with an increment step of $\Delta 2\theta$. Whenever $2\theta = 2\theta_{hkl}$ Bragg's law is satisfied, it results in the maximum intensity. The geometric nature of Bragg's law establishes a broad range of symmetry group theories (B.E. Warren, 1990; Eric Lifshin, 1999; Vitalij K. Pecharsky; Zavalij, 2009),

mathematically defining all possible periodic symmetries. Thus, the mathematical structure of crystallography is wider than the crystals observed in nature (Cullity; Stock, 2014).

Although XRD can be applied in various forms, such as transmission diffraction, powder diffraction in reflection mode stands out as the most widely employed method due to its feasibility in laboratories using relatively simple and accessible equipment (Dinnebier; Billinge, 2008). X-ray Diffraction by powder method (Dinnebier; Billinge, 2008) is a highly comprehensive technique utilized for the characterization of crystalline, semicrystalline, and amorphous materials, playing a vital role in studying phase formation and transition mechanisms (Ashcroft, Neil W, Mermin, 1976). During XRD powder experiments, a monochromatic X-ray beam interacts with the sample, resulting in interference patterns that exhibit high sensitivity to the atomic arrangement within the material (Vitalij K. Pecharsky; Zavalij, 2009). Disordered atomic arrangements scatter X-rays diffusely, forming halos, while ordered arrangements form symmetric structures that can be described using crystallographic planes or Miller indices (hkl) (Cullity; Stock, 2014). In the case of crystals, the incident light beams undergo successive refractions, producing peaks (or rings in the case of 2D XRD) in accordance with Bragg's law. This law establishes a relationship between the interplanar distance (d), the half-angle of diffraction (θ), the wavelength of the incident beam (λ), and an integer value (n) as represented by the equation below:

$$2d_{hkl}\sin\theta_{hkl} = n\lambda \quad \text{Equation 1}$$

By capturing the intensity of diffracted beams at various goniometer angles, an X-ray diffractometer registers a characteristic diffraction pattern as a curve of intensities versus 2θ diffraction angles, facilitating the determination of interplanar distances (d_{hkl}) and the identification of the diffraction-causing planes. However, many factors can cause peak broadening in diffraction patterns, such as crystal imperfections, average size of the crystallites and lattice microstrains distributions (B.E. Warren, 1990; Vitalij K. Pecharsky; Zavalij, 2009).

The analysis of diffraction patterns in semicrystalline materials is challenging due to the coexistence of organized and disorganized components (Cullity; Stock, 2014; Ossi, 2006). The disordered component introduces diffuse scattering, resulting in elevations in the diffraction baseline known as halos that poses difficulties in accurately determining the crystallinity due to the overlapping with diffraction peaks from crystalline region: the most elementary definition

of crystallinity is the percentage of crystalline component compared to non-crystalline region (Cullity; Stock, 2014; Ossi, 2006; Pecharsky; Zavalij, 2005).

The Figure 7 presented below (adapted from (Pecharsky; Zavalij, 2005)) illustrates the convolution of a diffraction pattern produced by a well-formed crystal that exhibits consistent diffraction behavior.

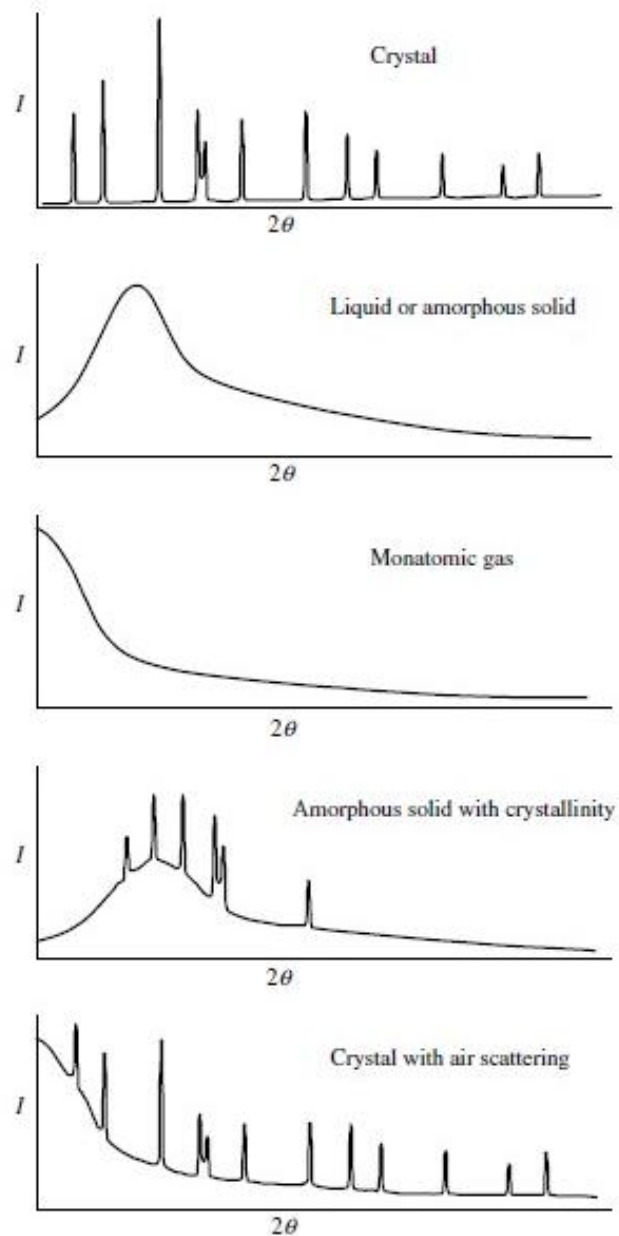


Figure 7 – Diffraction patterns from crystalline solids, liquids, amorphous solids, and monatomic gases as well as their mixtures. Figure adapted from (Vitalij K. Pecharsky; Zavalij, 2009)

Assuming an ideal crystal, the X-ray diffraction (XRD) pattern consists of narrow and well-defined peaks. However, when an amorphous material is added, the presence of a disordered component introduces additional diffuse scattering, which is visible in the XRD patterns as a curved profile (referred to as halos), resulting in salient elevations in the diffractogram baseline. The background halo in the diffraction pattern, then, includes contributions from inelastic scattering processes and disorganized regions, further complicating data interpretation (Eric Lifshin, 1999). Some researchers represent the amorphous component using a semi-circle beneath the crystalline pattern, but this is a simplified approximation. In reality, the amorphous halo has a more complex and enlarged shape (Guinier et al., 1963; Ossi, 2006).

Measuring the incoherent radiation within the background halo is experimentally challenging as it is weak and superimposed on other forms of diffuse scattering, such as Compton modified scattering (also known as temperature-diffuse scattering) shape (Guinier et al., 1963). The presence of Compton modified scattering darkens the diffraction pattern's background, potentially causing issues for characterization techniques like fluorescence (Cullity; Stock, 2014). Diffuse scattering arises from various sources, including disorder, defects, and fluctuations in the atomic positions, as well as from inelastic scattering processes. It provides valuable information about the structural characteristics and dynamics of disordered materials, amorphous substances, and materials with imperfect crystal structures. Although it is not possible to eliminate Compton modified scattering, this undesired effect must be taken into account in diffraction analysis (B.E. Warren, 1990; Ossi, 2006).

The analysis of the diffuse scattering dependence is a critical issue as it can lead to false quantifications of the amorphous component. It should be noted that the microstructure effect of the crystalline component significantly influences the profile, especially in the case of small, nanometric crystals. When two nearby broad peaks overlap, they contribute to an increased intensity in the diffuse halo region, further complicating the interpretation of the diffraction pattern (B.E. Warren, 1990). With the contribution of diffuse scattering, this background becomes even more complicated, and only a polynomial with a certain number of variables is able to describe this baseline, making it very difficult, if not impossible, to correctly deconvolute manually any diffraction pattern of semicrystalline samples (Guinier et al., 1963).

Moreover, dealing with nanoscale crystallites presents its own challenges. As the crystal size decreases, the peaks tend to broaden due to microstructure effects (measured by FWHM,

the Full Width at Half Maximum explained in the next section (Elton K Kaufmann, 2003; Guinier et al., 1963)). The inelastic scattering from the amorphous component can overlap with the peak broadening caused by tiny nanocrystals, resulting in merged curves that are difficult to separate in terms of shape. Many scientists employ different methods for trying to deconvolute these components, but this is no easy task, as shall now be discussed.

1.4.1. Analyzing Semi-Crystalline Nanocrystals in XRD Patterns

In nature, crystals are never perfect, meaning that no crystal exhibits infinite narrowness (B.E. Warren, 1990; Cullity; Stock, 2014). Bragg reflections ideally occur as sharp, well-defined peaks at the precise Bragg diffraction angle. However, in crystals of finite size, such as those approximately 1000 Å in dimension, the limited number of atomic planes disrupts the constructive and destructive interference required for precise scattering cancellation. This results in the diffraction peak broadening over a range of angles, with intensity extending below and beyond the ideal Bragg angle. This effect, known as "particle size broadening" (B.E. Warren, 1990) highlights the influence of reduced crystal dimensions on the coherence of X-ray scattering and the resulting diffraction patterns. The broadening of diffracted peaks can arise from various factors, making the study of peak broadening a complex and multifaceted area of investigation. Distinguishing between non-crystalline background and the influence of small crystallite size on diffraction patterns is a hard task (Laven, 2010).

To address this complexity, mathematical functions and some models (such as Scherrer's) are often employed to describe the individual contributions of these factors to the overall peak shape, enabling a more detailed and accurate analysis of the diffraction patterns (Eric Lifshin, 1999; Vitalij K. Pecharsky; Zavalij, 2009). Thus, the intensity of the powder diffraction pattern has the summed contribution of the background and the overlapped individual Bragg peaks, that can be better represented as the mixture of peak-shapes functions: Lorentzian, Gaussian, and/or their convolution profiles (Voigt and pseudo-Voigt) (B.E. Warren, 1990; Vitalij K. Pecharsky; Zavalij, 2009).

Represented in the Figure 8 below, shape of XRD peaks, Full Width at Half Maximum (FWHM), and positions ($2\theta_{hkl}$) carry a wide variety information about the microstructure of the investigated sample (Cullity; Stock, 2014).

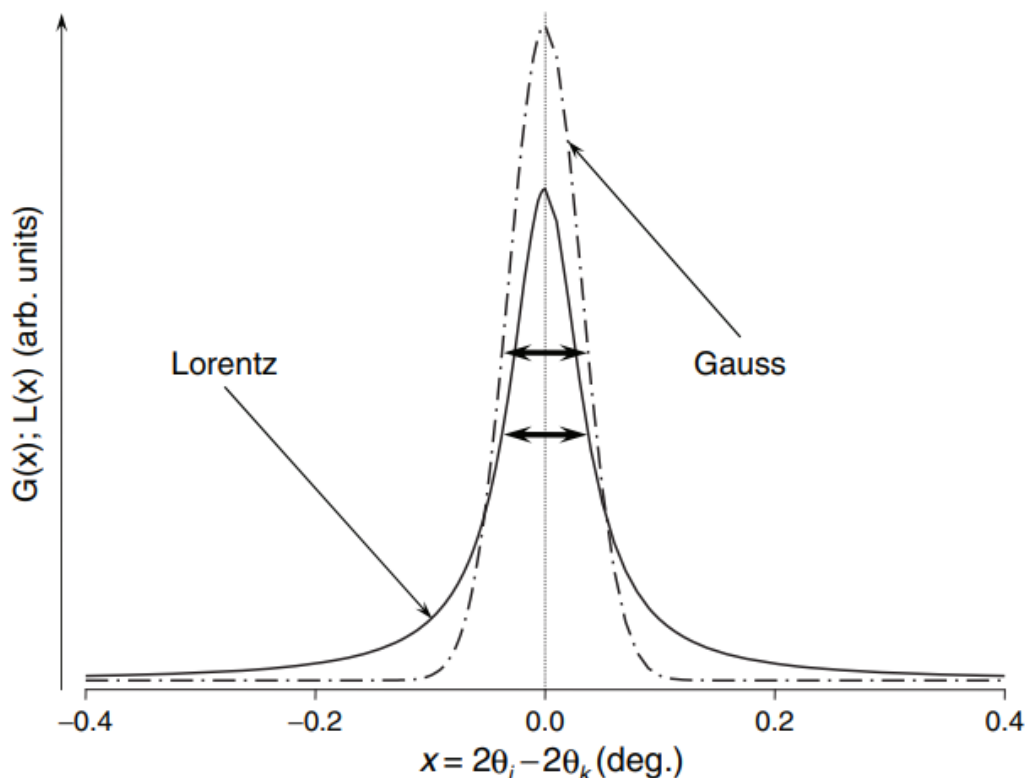


Figure 8 – Peak-shape functions of a Bragg reflection. Thick arrows indicate the full widths at half maximum (FWHM). Figure from (Vitalij K. Pecharsky; Zavalij, 2009)

This figure discusses the shape of the Bragg reflections, and also that the presence of a “tail” in the shape is predicted (which in turn can overlap with another closer “tail” in a near peak). Thus, the shape of the Bragg reflections can be better understood if a modified pseudo-Voigt function is used for the separation of FWHM shape (Guinier et al., 1963; Vitalij K. Pecharsky; Zavalij, 2009), and the contribution of FWHM to the crystallite size can then be better understood: bigger the index, smaller are the crystals. Even with all this considered, imperfections inherent in crystals lead to peak broadening, which becomes even more pronounced when the crystallites are on a nanoscale (Vitalij K. Pecharsky; Zavalij, 2009). In general, the overlapping of the extended tails of neighboring reflections can lead to an overestimation of the background level. Consequently, this may result in an underestimation of the peak areas, thereby introducing inaccuracies in the analysis (B.E. Warren, 1990). Thus, the effect of the FWHM might be simulated using a model crystal of B amylose as demonstrated in Figure 9, and the effect of crystallite size are demonstrated.

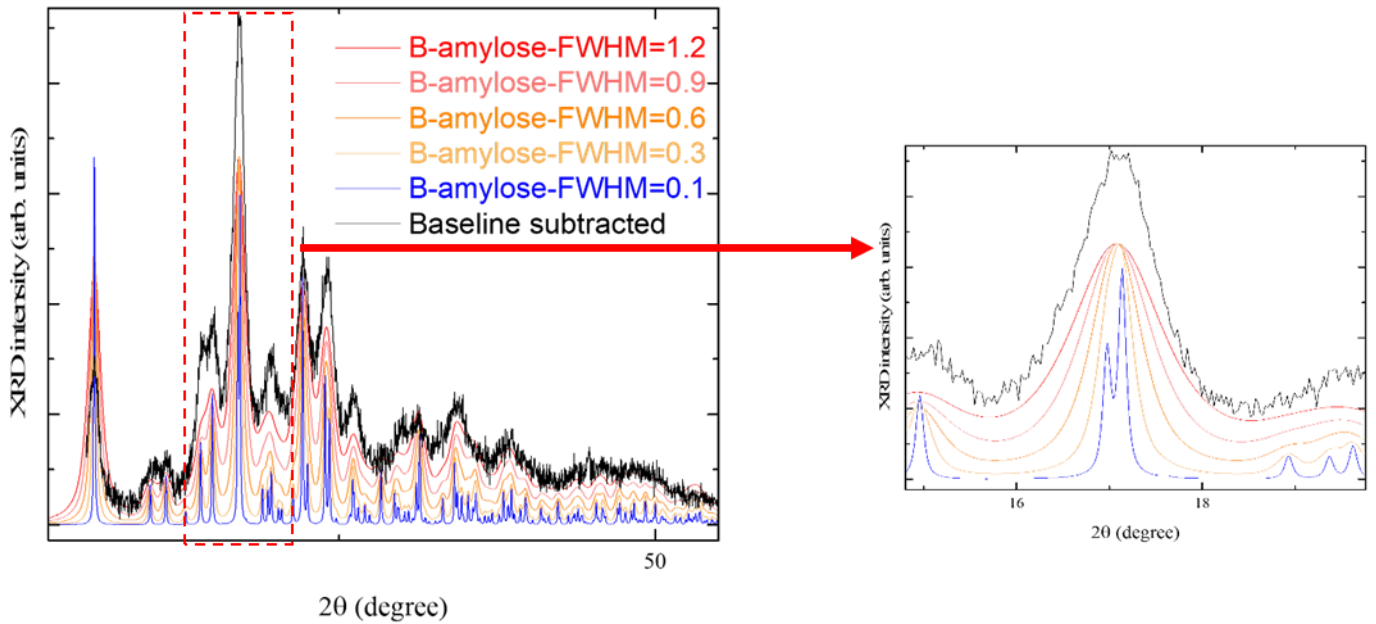


Figure 9 – Same semicrystalline structure with different FWHM. Detail shows the overlapping of information.

Figure made by the author.

In the detail of the figure, it is perceptible that the shape of the semicrystalline XRD pattern becomes even more complicated with the reduction of crystallite sizes (Pinto; Campelo; Michielon de Souza, 2020). The complexity of the effect of enlargement of diffracted peaks caused by increment in FWHM is further amplified in semicrystalline nanocrystals, such as the biopolymers examined in this study. It significantly complicates the analysis of microstructure, as the peak shapes become considerably broadened to the extent that adjacent peaks can overlap, making it nearly impossible to distinguish between them. When studying samples composed of multiple phases, achieving accurate deconvolution becomes highly challenging without employing a suitable algorithm for structural refinement (Dinnebier; Leineweber; Evans, 2018). Consequently, for the assessment of parameters like crystallite size, phase fraction, or crystallinity, a more sophisticated solution is required, surpassing the limitations of manual pattern deconvolution.

1.5. Starch Crystallography

Going back to biopolymers, the starch crystallography itself has many interesting questions remaining² (Bertoft, 2017; Hamaker, 2021; Rodriguez-Garcia et al., 2021; Wang, 2020).

The A-type polymorph is well-documented in the literature as a monoclinic system with space group B2, having unit cell parameters $a = 20.83(6) \text{ \AA}$, $b = 11.45(4) \text{ \AA}$, $c = 10.58(3) \text{ \AA}$ (chain axis and monoclinic axis), and $\gamma = 122.0(2)^\circ$ (Popov et al., 2009).

On the other hand, B-type starch is composed of hexagonal clusters with space group P 61 (No. 169), and its lattice parameters are $a = b = 18.5 \text{ \AA}$, $c = 10.4 \text{ \AA}$, $\gamma = 120^\circ 120^\circ$ (Imberty et al., 1991; Imberty; Perez, 1988). This polymorph can trap 36 water molecules within the structure's cavities (Imberty; Perez, 1988; Takahashi; Kumano; Nishikawa, 2004), and this has an important influence in its structure. The interhelix peak around $2\theta = 5.6^\circ$ (Blazek; Gilbert, 2010), corresponding to the (1 0 0) and (0 1 0) crystallographic planes, is composed of regularly arranged water molecules, resulting in a regular lamellar spacing. The lamellar peak occurs due to the separation of the double helices from the polymer backbone and the alignment of the lamellar layers in the presence of water (Blazek; Gilbert, 2010). Therefore, a decrease in the relative intensity of this peak might indicate the removal of water molecules from the structural cavities (Pinto; Campelo; Michielon de Souza, 2020), reducing the trapped water in amylopectin and potentially decreasing the inherent hydrophilic behavior of starches (Ilyas et al., 2018a). Although not the focus of the current study, further investigation into this mechanism could provide valuable insights into enhancing the water resistance of starch-based packaging (Atiqah

² Currently, there is ongoing debate regarding the precise space group assignments for both A- and B-type starches (Rodriguez-Garcia et al., 2021). However, the present study provides robust experimental evidence supporting the adoption of the proposed symmetries, contributing valuable clarity to this area of structural characterization.

et al., 2019; Castillo et al., 2019; Halimatul et al., 2019a). Such advancements are key for promoting the broader adoption of this sustainable alternative to synthetic thermoplastics.

To summarize this section, the following graphs on illustrate the characteristic features of A and B polymorphisms commonly observed in raw starches. These visual representations provide a clear comparison of their distinct structural properties and behavior. Figure 10 illustrates A-type and B-type starches, representing an idealized model of a perfect crystalline structure.

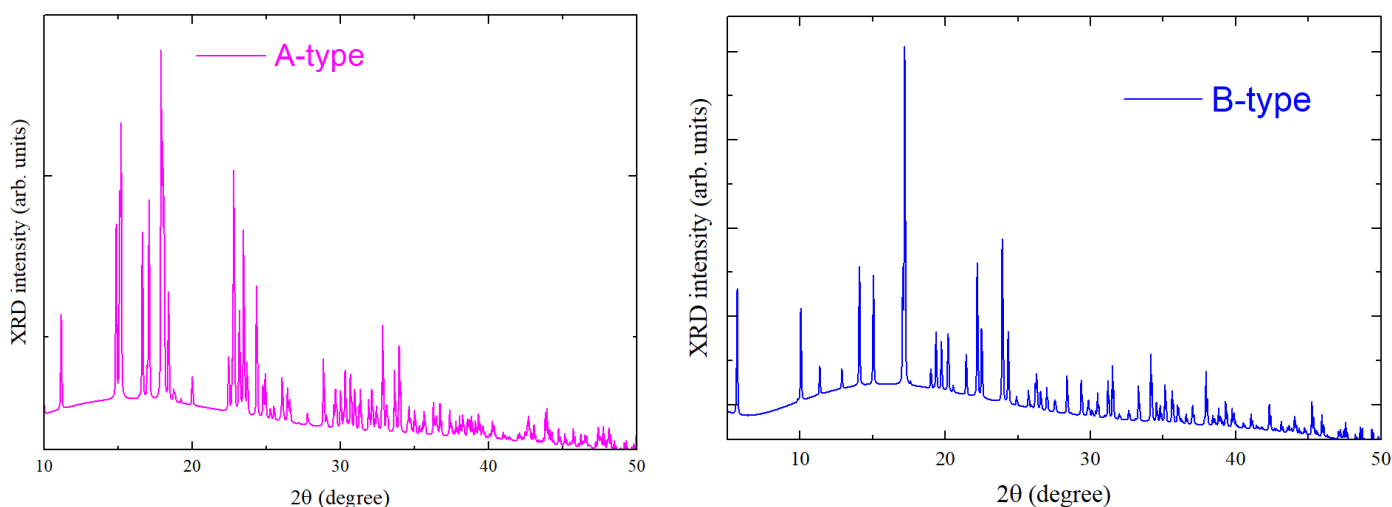


Figure 10 – idealized model of a perfect crystalline structure for A-type (left) and B-type (right) starches. Figure made by the author.

This highlights the inherent complexity of the semi-crystalline structure of starch, making the extraction of accurate structural information a challenging endeavor. To address this, researchers have proposed various methodologies to analyze and interpret the intricate patterns of starch crystallinity.

1.6. How the reported literature discusses crystallinity of biopolymers using XRD?

i. Cellulose

Cellulose, as one of the most commonly utilized nanostructured polysaccharides in the industry, has been extensively studied, and various researchers have proposed methods for

quantifying its crystallinity and exploring parameters related to its microstructure (French, 2014). The crystallites of cellulose have a number of organization profiles, presenting different diffraction patterns, with crystallites in nanometric sizes (Leonarski et al., 2022). With so many important applications, there is a well-established literature on the structural refinement of cellulose. (Leonarski et al., 2022)

An easier, straightforward and well-discussed methodology is Segal's method (Ahvenainen; Kontro; Svedström, 2016; French; Santiago Cintrón, 2013; Nam et al., 2016; Segal et al., 1959), an empirical Crystallinity Index (CI) technique. It is based on the results of a powder diffractometer X-ray experiment, which offers a rapid means of determining the relative crystallinity of different samples (French; Santiago Cintrón, 2013). This method operates on the premise that cellulose material consists of two components: crystalline and non-crystalline or amorphous. The height of the highest diffraction peak represents the amount of crystalline material, while the height of the minimum intensity between the major peaks represents the amount of amorphous material (Ahvenainen; Kontro; Svedström, 2016; Segal et al., 1959). The Crystallinity Index (CI) is calculated by taking the difference between these two intensities and dividing it by the intensity of the highest peak (French; Santiago Cintrón, 2013).

Some authors already found fault in this method (Agarwal; Reiner; Ralph, 2010; Park et al., 2010; Thygesen et al., 2005), but it was Driemeier and Calligaris (Driemeier; Calligaris, 2011) that meticulously discussed the results from Segal's method and Rietveld Refinement Method. This work encompassed the investigation of cellulose crystallinity, considering factors like preferred orientation, incoherent scattering, and moisture, and to ensure accurate results the authors employed Rietveld refining of X-ray data obtained with a digital area detector, enabling them to determine integrated peak areas. By comparing the area under the peaks to the total corrected integrated intensity, they quantified the absolute fraction of crystalline material. Notably, they pointed out that while the Segal method associates peak height with the degree of crystallinity, the more representative measure is the peak area, which indicates the fraction of the material that is crystalline, and that the background information has still much more data that can be extracted with structural refinement (Driemeier; Calligaris, 2011; French, 2014).

ii. Starches

Apart from the publications by the research group to which the author of this thesis belongs (which are included in this work such as (Carvalho et al., 2021; Da Costa Pinto et al., 2021, 2023; Pinto; Campelo; Michielon de Souza, 2020)), there is no existing literature that reports the use of the proposed combination of XRD and Rietveld Refinement Method for starches. Still, a number of carbohydrate polymers are vastly studied using XRD, such as polysaccharides (Alonso-Gomez et al., 2016; Cheetham; Tao, 1998; Pinto; Campelo; Michielon de Souza, 2020), cellulose (Da Silva et al., 2021; De Figueiredo; Ferreira, 2014; Leonarski et al., 2022; Manzato et al., 2017) and rubber (Takahashi; Kumano, 2004). This is mainly due to the significance of crystallinity (determined after XRD patterns) for discussing structural information for starches and predicting macroscopic properties, thus guiding processing parameters of a number of products derived from biopolymers such as starch films (Molavi et al., 2015), thermoplastics (Halimatul et al., 2019a), hybrid composites (Atiqah et al., 2019) and bio-nanocomposites of starch and nanocellulose (Halimatul et al., 2019b; Ilyas et al., 2018b, 2019c, 2020; Ilyas Rushdana et al., 2017).

As mentioned in the previous section of this thesis, working with nanoscale crystallites presents challenges. As the size decreases, the peaks tend to broaden due to microstructure effects on the line width, and the inelastic behavior of the amorphous portion overlaps with the peak broadening caused by small nanocrystals, resulting in merged curves that are difficult to distinguish in terms of shape (French, 2014; Manzato et al., 2017), (Da Costa Pinto et al., 2021). Nevertheless, some researchers (as shown in Figure 11, from (Xie et al., 2014)) have studied the diffraction patterns of nanometric crystallites using empirical methods designed for cellulose (such as Segal's method (Segal et al., 1959)) or by fitting lines after subtracting the estimated amorphous portion.

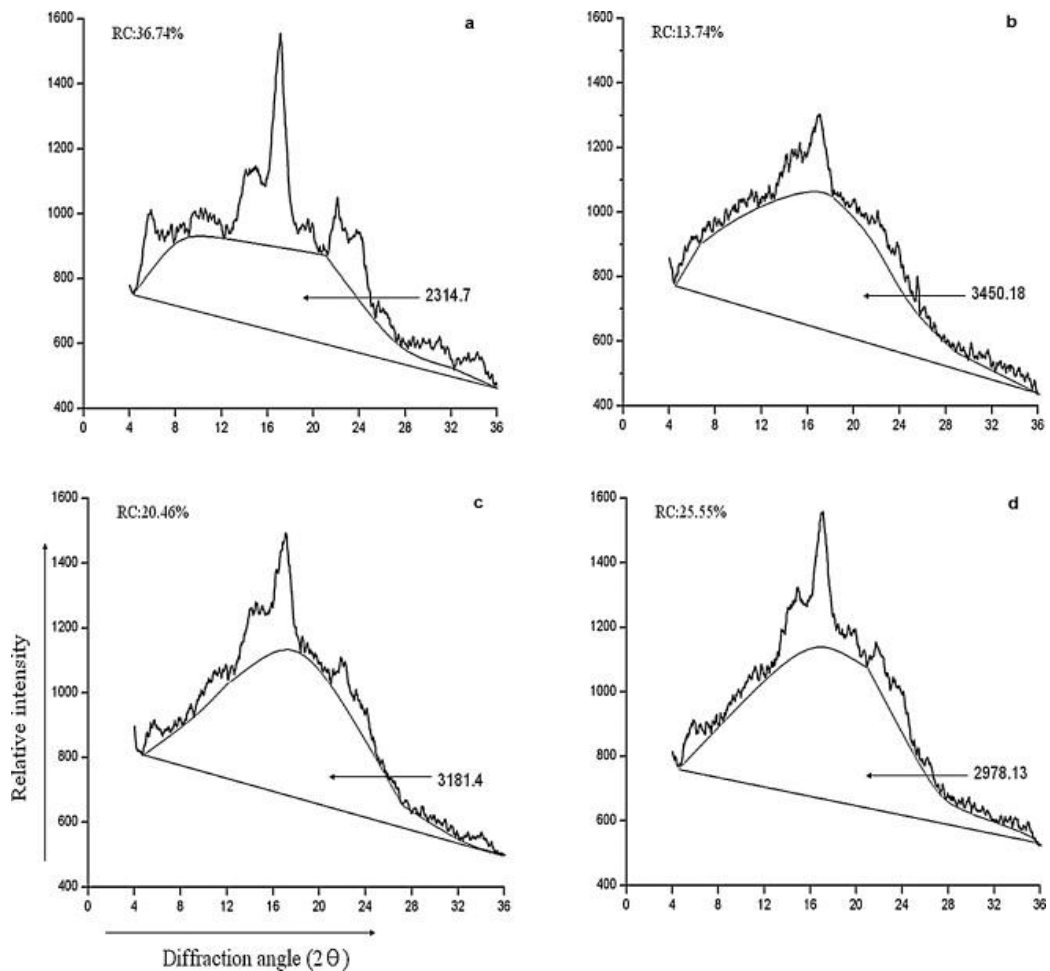


Figure 11 – Diffraction patterns rice starch nanocrystals, with amorphous regions manually fitted. Figure from (Xie et al., 2014)

Even though comparison of the same sample subjected to different treatments can be made to a certain extent, it should be noted that such mathematical fits are sometimes made in an arbitrary way by the researcher, and results may depend on the chosen functions for the fitting process. Moreover, the line broadening will be influenced by both intrinsic and extrinsic factors, that can only be deeply analyzed with proper deconvolution (Ning; Flemming, 2005). The use of structural refinement can subtract the major part of those factors, and deconvolute the contribution of measuring instrument, crystallite size and amorphous component (De Figueiredo; Ferreira, 2014).

Additionally, the estimation of the amorphous component also involves a certain level of arbitrariness, as illustrated in the figures below taken from other authors. Some authors

roughly reproduce the elastic scattering, ignoring important structural factors (Cheetham; Tao, 1998), as shown in Figure 12.



Figure 12 – Diffraction patterns with amorphous regions fitted with an arbitrary semi-circle. Figure from (Cheetham; Tao, 1998)

How, then to lessen the bias from the analysis and have a more reliable way to study the structure of such materials?

1.7. The quest for crystallinity remains

Thus, recognizing the sensitivity of XRD to structural information and the inherent limitations of existing methods, the accurate quantification of crystallinity remains an open question. This challenge underscores the importance of employing Rietveld refinement, which offers a robust and detailed approach to extracting meaningful insights from diffraction data. The application of this method will be proposed and explored in greater detail in the following chapter.

CHAPTER 2 – METHODOLOGY

X-ray Diffraction and Rietveld Refinement for Unraveling the Semicrystalline Structure of Starches

In this chapter, the proposed and previously published approach for estimating the crystallinity of starches, which involves the combination of X-ray Diffraction and Rietveld Refinement, will be presented. The Rietveld Refinement Method offers a more reliable approach to discuss and separate the elastic and inelastic scattering observed in the XRD analysis of semicrystalline nanocrystals. While this method has been widely utilized for cellulose, it represents an initial exploration of the microstructure of starches.

Structural refinement methods applied to X-ray diffraction (XRD) data are widely utilized for investigating the microstructure of various materials, including semicrystalline substances such as polymers (Zhao et al., 2018). These methods are indispensable for the comprehensive analysis of semicrystalline materials, as they enable the extraction of critical microstructural information that advances both fundamental scientific understanding and practical applications (McCusker et al., 1999). By incorporating rigorous physical principles into the interpretation of XRD patterns, structural refinement minimizes subjectivity and ensures a more objective analysis compared to curve-fitting approaches that may be influenced by researcher bias (Leineweber, 2011). This methodological robustness makes structural refinement a powerful tool for accurately characterizing the intricate interplay between crystalline and amorphous domains in semicrystalline materials (Flores Cano et al., 2021).

Thus, as the methodology of this work, the current chapter introduces the well-established methodology of integrating X-ray diffraction (XRD) with Rietveld refinement, but his time for estimating the crystallinity and other microstructure parameters of starch. This approach seeks to overcome the limitations of traditional crystallinity determination methods, which often struggle to separate and quantify the contributions of elastic and inelastic scattering

in the diffraction patterns of semicrystalline materials, especially when those are in nanometric scale, exhibiting a delicate interplay between crystalline and amorphous regions (R E Dinnebier; S J L Billinge, 2008). The proposed methodology builds on the versatility of Rietveld refinement in deconvoluting overlapped diffraction peaks, accurately modeling background contributions, and quantifying phase compositions. While Rietveld refinement has been widely utilized in the structural characterization of cellulose, its application to starch represents a pioneering effort to probe the microstructural features of these biopolymers at a refined level (Leonarski et al., 2022).

The methodology introduced in this chapter forms the foundational framework for the entire thesis. By combining X-ray diffraction (XRD) with Rietveld refinement (RM), this work represents the first documented application of Rietveld structural refinement to analyze the microstructure of starches using experimental data. This approach has proven effective in detecting subtle structural variations, refining lattice parameters, and offering detailed insights into the microstructural organization of starch. By bridging the disciplines of Physics and Food Sciences, this methodology provides a novel lens through which the structural properties of starch can be understood and discussed against other characterizations.

To ensure reproducibility and facilitate future applications, this chapter wraps up with details regarding the sample preparation for XRD data acquisition employed in this study. These procedures are integral to the accurate implementation of the proposed method, highlighting its robustness and versatility for studying semi-crystalline biopolymers.

2.1. Crystallinity: Quantifying Order through Structural Refinement

There is a number of factors that may contribute to modify the XRD pattern of a biopolymeric sample, especially those that went through any degree of processing. In order to separate these influences and advance the analysis of XRD patterns, various structural refinement methods can be successfully employed, leveraging the underlying mathematical principles and accounting for the influence of inelastic scattering caused by other factors (Young, 1993). Structural refinement methods for X-ray diffraction, such as LeBail's and Rietveld's refinement methods, have been widely used in various fields, including crystallography, materials science, and pharmaceuticals (Pinto; Campelo; Michielon de Souza, 2020).

i. Which to choose: LeBail's or Rietveld Refinement Method?

An inherent limitation in extracting information from a powder diffraction pattern arises from the potential overlap of Bragg peaks with different (hkl) values, making the independent determination of their intensities unfeasible (Cullity; Stock, 2014; Elton K Kaufmann, 2003). This overlap can be exact or exhibit a degree of separation, such as in the case of two peaks differing in their angular positions by a fraction of their widths. This problem is mainly solved in the Rietveld method, as the XRD pattern is adjusted as a whole, considering models for microstructure, microstrains, homogeneities, isotropies, etc (Rietveld, 1967). Thus, XRD indexing of a structure is only complete when structural refinement (notably Rietveld Refinement) analysis is performed (Vitalij K. Pecharsky; Zavalij, 2009).

Still, Le Bail's method is also widely used to refine the crystal structures of various materials, from lithium-doped titanates (fairly simple crystals) (Stramare; Weppner, 1999) and cellulose (Manzato et al., 2017). Le Bail himself was the first author to study the *in situ* changes of common raw starch to resistant starch (polymorphic change from B-type to V-type) using synchrotron radiation (Le Bail et al., 1999), and it has indeed a number of interesting applications (Silva et al., 2014).

Both Rietveld and Le Bail methods are widely utilized in various applications involving powder diffraction data and different levels of complexity of the analyzed material. However, these methods differ significantly in their analytical approaches and the depth of structural information they can extract.

Le Bail refinement is a more straightforward technique focused on extracting unit cell parameters and the overall diffraction peak shapes without requiring a detailed structural model. It is particularly advantageous when the crystal structure is unknown or when dealing with samples containing multiple phases (Le Bail et al., 1999; Sanches et al., 2013). Le Bail refinement employs a profile-fitting strategy to decompose the observed diffraction pattern into individual peak shapes, allowing for the extraction of unit cell dimensions and related parameters.

However, it does not provide information about atomic arrangements within the unit cell, limiting its utility for detailed structural analysis, and a number of authors might even

combine refinement techniques to extract microstructure information, with the preliminary step to derive initial structural parameters from Le Bail's before applying a more detailed structural refinement with Rietveld method (Adamski; Albrecht; Moszyński, 2023; Gallyamov et al., 2023).

In contrast, Rietveld refinement Method (RM) is a more advanced approach that fits the entire diffraction pattern to a proposed structural model, enabling the determination of atomic positions, thermal parameters, and other intricate structural details (Evans; Evans, 2021; McCusker et al., 1999; Rietveld, 2014; Young, 1993). RM utilizes a least-squares fitting procedure to minimize the difference between observed and calculated diffraction patterns. This method incorporates the entire information content of the powder pattern, including peak overlap, and allows for a comprehensive analysis of the crystal structure, together with atomic coordinates, occupancy factors, and thermal vibrations (McCusker et al., 1999; Rietveld, 2014; Young, 1993; Zhao et al., 2018).

Furthermore, Rietveld refinement is particularly effective for analyzing complex structures and offers robust statistical metrics, such as the R-factor and reduced chi-squared values, to assess the quality of the fit (Toby, 2006; Wu et al., 2013). This capability makes it well-suited for materials with intricate microstructures or significant disorder (Baerlocher, 1993; Santos, 2001). Thus, for a deeper discussion of microstructure information, the Rietveld refinement method (Rietveld, 2014) is a notable approach that offers a valuable technique for precisely quantifying the parameters obtained from X-ray diffraction experiments, extracting background information caused by the sum of inelastic scattering and diffraction from non-crystalline portions of the material (Rietveld, 1967).

In summary, while Le Bail refinement is an efficient tool for initial structural assessments and simpler analyses, Rietveld refinement provides a comprehensive framework for detailed structural characterization of crystalline materials, making it indispensable for advanced crystallographic studies. Even though Rietveld Refinement Method is prioritized in this work, there are numerous models available for the quantitative analysis of events and characteristics in a sample using structural refinement methods.

As computer processing capabilities continue to advance, more sophisticated and detailed models are constantly being proposed and applied (Mittemeijer; Welzel, 2008). In the process of structural refinement, these models' parameters, including structural values,

background coefficients, and profile parameters, are iteratively adjusted through least-squares minimization until the calculated powder pattern achieves the best fit and convergence with the experimental XRD pattern (De Keijser et al., 1982; Leineweber; Mittemeijer, 2004). Consequently, many of the widely used models aim to explain the line broadening phenomenon and can be described by a series of mathematical relationships extensively discussed by experts (Mittemeijer, 2011), which this work will focus strictly in the models used for Rietveld Refinement. The model employed in this study are among the most well-established mathematically and have a significant presence in the existing literature (Flores Cano et al., 2021; Pinto; Campelo; Michielon de Souza, 2020; Pinto et al., 2021b; Zhao et al., 2018).

ii. Diving deeper in the Rietveld Refinement Method

Rietveld Refinement method poses as an alternative for simple line fitting with manual entries of the baseline. This method was employed in (Manzato et al., 2017), in which authors compared both Segal's and Rietveld Refinement method for crystallinity quantification, stating that the variation in crystallinity percentage between the two approaches can be attributed to the omission of broad peaks resulting from nanocrystal diffraction in the first method. In particular, the I_{bckg} point is influenced by the combination of peak bases $(-1\ 1\ 0)$ and $(1\ 1\ 0)$, as well as the diffuse scattering originating from the non-crystalline phase (Manzato et al., 2017).

In the Rietveld method, the intensities are calculated by taking into account the scattering factor of each element in the incident radiation (λ), which satisfies Bragg's law and, consequently, the entire crystallographic formalism, including instrumental aberrations (Toby, 2006). The study of peaks broadening caused either by i) crystallite size broadening or ii) strain broadening has been a subject of continuous improvement, both in terms of theoretical approaches and experimental techniques (Delhez; De Keijser; Mittemeijer, 1982; Mittemeijer; Welzel, 2008; Van Berkum et al., 1996). By considering instrumental errors (refining a stable NIST reference material of large crystallinity such as LaB_6 (Ning; Flemming, 2005)), it becomes possible to quantify the phases, investigate variations in lattice parameters, and estimate the average size of crystallites through the analysis of the peak profiles using different models (such as Line Profile Analysis) (He, 2009; Oliveira et al., 2020).

As explained in Chapter 1, the peak broadening in crystallographic patterns can be elucidated by two distinct effects in the microstructure: the Lorentzian component of the profile

is linked to the small size of the crystallites, while the Gaussian component is attributed to microstrains (Leineweber; Mittemeijer, 2004; Mittemeijer, 2011). Thus, for the peak profile analysis (also called peak-shape functions (R E Dinnebier; S J L Billinge, 2008; Vitalij K. Pecharsky; Zavalij, 2009)), the study was carried out using the modified Thompson-Cox-Hasting pseudo-Voigt profile function (De Keijser et al., 1982). In this profile function, the full width at half maximum (Γ) is given by (Rodríguez-Carvajal, 1993):

$$\Gamma = \sqrt[5]{\Gamma_G^5 + 2.69269\Gamma_G^4\Gamma_L + 2.42843\Gamma_G^3\Gamma_L^2 + 4.47163\Gamma_G^2\Gamma_L^3 + 0.07842\Gamma_G\Gamma_L^4 + \Gamma_L^5}$$

Equation 2

Where the Gaussian (Γ_G) and Lorentzian (Γ_L) parts are expressed as follows:

$$\Gamma_G = \left[(U - U_{LaB6}) + (1 - \eta)^2 d_{hkl}^4 \Gamma_S^2(hkl) \tan^2 \theta + V \tan \theta + W + \frac{P}{\cos^2 \theta} \right]^{1/2}$$

Equation 3

$$\Gamma_L = \eta d_{hkl}^2 \Gamma_S(hkl) \tan \theta + \frac{X + X_e \cos \phi}{\cos \theta}$$

Equation 4

The parameters V and W depend on the instrument. In this work, the instrumental broadening was analyzed by a certified LaB₆ powder (NIST 660b) and the obtained values of $U_{LaB6} = 0.0$, $V = -0.0036$, $W = 0.0023$ were kept unaltered.

The parameters P and the term $X + X_e \cos \phi$ describe the Gaussian and Lorentzian contributions to size broadening, respectively. The parameters P and X correspond to isotropic crystallite-size broadening while X_e expresses anisotropic crystallite-size effects, ϕ is the angle between a reflection vector and its respective broadening axis (De Keijser et al., 1982; Leineweber, 2007; Scardi; Leoni; Delhez, 2004; Stephens, 1999).

The isotropic strain parameter, U and the anisotropic strain parameter, $\Gamma_S(hkl)$ are a hkl -dependent line broadening function that vary according to the symmetry of the crystals

(Stephens, 1999). The parameter η is a ‘mixing coefficient’ which determines the contributions of the Gaussian ($\eta = 0$) and the Lorentzian ($\eta = 1$) broadening. All these parameters can be adjusted for yielding the best fit. In this work, good refinements were achieved with $\eta = 0.75$, $X_e = 0$, $P = 0$, and the mean crystallite size (D) and microstrains ε were obtained from X and U from equations below refined by the Rietveld method (Soediono, 1989):

$$D = \frac{18000K\lambda}{\pi X} \quad \text{Equation 5}$$

$$\varepsilon = \frac{\pi}{180} \sqrt{U 8 \ln 2} \quad \text{Equation 6}$$

where $K = 0.91$ is the constant of Scherrer (Langford; Wilson, 1978). In this method all peaks have been considered. So, in order to ponder only the well-defined peaks hkl , we applied the single peak method (Melquiádes et al., 2019) considering the full width at half maximum (Γ) separating a Lorentzian (β_L) and Gaussian (β_G) integral widths weighted by the mixture coefficient η parameter in Equation 7 and Equation 8:

$$\beta_G = \frac{\Gamma}{2} \sqrt{\frac{\pi(1 - 0.74417\eta - 0.24781\eta^2 - 0.00810\eta^3)}{\ln 2}} \quad \text{Equation 7}$$

$$\beta_L = \frac{\pi\Gamma}{2} (0.72928\eta + 0.19289\eta^2 + 0.07783\eta^3) \quad \text{Equation 8}$$

So, the mean crystallite size $D_{(hkl)}$ and microstrain $\varepsilon_{(hkl)}$ were calculated using the Scherrer’s equation (Langford; Wilson, 1978), using Equation 9 and Equation 10 below:

$$D_{(hkl)} = \frac{K\lambda}{\beta_L \cos\theta} \quad \text{Equation 9}$$

$$\varepsilon_{(hkl)} = \beta_G / 4 \tan \theta \quad \text{Equation 10}$$

where Γ is obtained from the best-fitted peaks (Delhez; De Keijser; Mittemeijer, 1982).

The disordered component and the background due to inelastic scattering can be then fitted by varying the number of terms of the Chebyshev polynomial. The selection criterion was based on choosing the fewest number of polynomial terms that provided the smallest convergence factors and residual lines (Toby, 2006). This criterion is typically satisfied using 11-term Chebyshev polynomials (I_{BG}) for the starches described in this thesis, which have rather similar baselines.

Assuming that the diffuse scattering I_{BG} simulated by Chebyshev functions describes the amorphous phase where the inelastic scattering is negligible, the total integrated intensity I_{total} can be expressed as the sum of the intensity from the crystalline phase ($I_{crystal}$) and the intensity from the amorphous phase (I_{BG}). The weight fraction of the amorphous component (x_A) was determined from the analysis in Equation 11:

$$x_A(\%) = 100 (1 - x_c) \quad \text{Equation 11}$$

where x_c is crystallinity value in Equation 12 obtained from (He, 2009):

$$x_c(\%) = 100 \frac{I_{crystal}}{I_{crystal} + I_{amorphous}} \quad \text{Equation 12}$$

where $I_{crystal}$ and $I_{amorphous}$ correspond to the integrated intensity of all the crystalline peaks and of the amorphous scattering, respectively.

The crystallinity percentage is calculated by Equation 13:

$$x_c(\%) = 100 \frac{I_{total} - I_{BG}}{I_{total}} \quad \text{Equation 13}$$

Rietveld refinement is also an important model for deconvolution of phases that coexist in a sample, so it might be used to determine the relative weight fractions of all crystalline phases present in a multiphase sample (Toraya, 2016). In this method, the relationship below (Madsen; Scarlett, 2008) calculates the weight fractions of A-type (W_A Equation 14) and B-type (W_B Equation 15) phases in a mixture can be given by

$$W_A = \frac{S_A(ZMV)_A}{S_A(ZMV)_A + S_B(ZMV)_B}$$

Equation 14

and

$$W_B = \frac{S_B(ZMV)_A}{S_A(ZMV)_A + S_B(ZMV)_B}$$

Equation 15

where $Z = 4$ represents the number of formula units per unit cell for both starch polymorphs, M is the molecular mass of the formula unit) and V is the unit cell volume.

Considering that crystalline weight fractions (crystallinity) correspond to the total crystalline weight then total crystallinity weight fraction can be described in Equation 16

$$W_A + W_B = x_c$$

Equation 16

To simplify the application of these mathematical models, there are several software options available for implementing the Rietveld method. These include open-source software like GSAS (Toby, 2001; Von Dreele; Larson, 1994), DBWS (Bleicher; Sasaki; Paiva Santos, 2000) (and its derivative Fullprof (Rodríguez-Carvajal, 1993)), as well as the numerical method MAUD (Lutterotti et al., 1997). Additionally, there are proprietary software programs such as TOPAS (Dinnebier; Leineweber; Evans, 2018), among others.

While all of these programs follow the basic principles of the Rietveld method with minor algorithmic differences, their main distinctions lie in the available models for microstructure, crystallite size, microstrains, texture effects, preferred orientation, isotropic and anisotropic atomic displacement, and more. In this study, the choice was GSAS with the EXPGUI interface (Toby, 2001; Von Dreele; Larson, 1994), primarily select for its appropriate models tailored for nanomaterials, such as the CW4 function with pseudo-Voigt profiles and the Stephens model (Stephens, 1999).

The X-ray diffraction data is compared with metadata in CIF (Crystallographic Information File (Brown; McMahon, 2006)) format using the Mercury software, provided by The Cambridge Crystallographic Data Centre (CCDC) (Macrae et al., 2008) (Macrae et al., 2006), for the identification of crystalline phases present in the sample. The databases utilized include ICSD (Inorganic Crystal Structure Database) (Hellenbrandt, 2004), accessed through the network of the Federal University of Amazonas and made available by CAPES, as well as COD (Crystallography Open Database), which is publicly accessible (Quirós et al., 2018) (Merkys et al., 2016).

2.2. XRD characterization

This study encompasses a variety of processing techniques, each of which is described in detail as they are introduced throughout the text. The main focus, though, is in the XRD data acquisition for further studies with Rietveld refinement.

A cornerstone of the sample preparation process, and a foundation for the entire thesis, is the acquisition of X-ray diffraction (XRD) data. This begins with meticulous attention to the

preparation and configuration of the sample holder, as it directly influences the quality and reliability of the resulting diffraction patterns. The choice of sample holder, its material properties, and how the sample is mounted are all pivotal considerations to minimize artifacts, enhance data accuracy, and ensure reproducibility across experiments. This systematic approach to XRD data acquisition underpins the methodology and contributes significantly to the robustness of the analytical framework presented in this work.

The powdered starch samples were placed in metallic sample holders for X-ray diffraction (XRD) analysis. However, due to the low atomic number of the elements comprising starch (carbons, hydrogens and oxygens), the material has limited X-ray scattering efficiency (Harold P Klug; Leroy E Alexander, 1974; R E Dinnebier; S J L Billinge, 2008). Consequently, the samples can exhibit partial transparency to X-rays, particularly at high diffraction angles ($2\theta \sim 90^\circ$). This can result in unwanted diffraction peaks in the obtained patterns (convoluted with the sample's), arising from the metallic components of the sample holder, primarily composed of stainless-steel alloys. Such interference is undesirable as it compromises the accuracy of the diffraction results.

Although the use of an oriented silicon sample holder is a viable option for XRD analysis, this model has limitations that make it less ideal for certain applications. One significant drawback is its limited capacity, as it can accommodate only a small quantity of the sample. This reduced sample volume leads to lower diffraction signal intensity, primarily because the scattering efficiency is proportional to the amount of material available for X-ray interaction. Also, as highlighted, the reduced intensity of the diffraction patterns can compromise the accuracy and resolution of structural analysis, particularly for semi-crystalline materials like starch, which already exhibit relatively low scattering efficiency due to their composition of light elements.

Another limitation encountered was the inadvertent damage to the oriented silicon sample holder, caused by a fellow researcher who accidentally dropped and fractured the device, as shown in Figure 13.



Figure 13 – Damaged oriented silicon sample holder. Photo taken by the author.

These limitations highlighted the need for an alternative sample holder design capable of handling larger sample volumes to optimize scattering and ensure high-quality diffraction data. This consideration was vital for robust and reliable microstructural characterization in the context of this study.

To mitigate this issue and out of necessity and ingenuity, the author developed and adapted a modified sample holder device for the powder diffraction technique using a custom-designed sample holder with a false bottom made of a specialized polyester film known as Mylar®, depicted in below in Figure 14.



Figure 14 – Adapted sample holder with a fake bottom made of Mylar® film. Photo taken by the author.

Commonly used as sample holding medium for transmission-mode XRD, Mylar® offers several advantages: it is relatively inexpensive and, more importantly, exhibits transparency to X-rays, effectively minimizing background interference from the sample

holder. Additionally, the use of a non-metallic transparent bottom enables the holder to accommodate a greater quantity of powdered sample, as shown in Figure 15 below.



Figure 15 – Adapted sample holder filled with starch sample. Photo taken by the author.

This larger volume improves the scattering efficiency of the starch sample, enhancing the quality and intensity of the diffraction data detected by the instrument (Elton K Kaufmann, 2003; Eric Lifshin, 1999). This methodological adaptation not only reduces metallic interference but also facilitates more accurate analysis of lightweight biopolymers like starch, optimizing the XRD technique for materials with low X-ray scattering efficiency. Finally, it is crucial to emphasize that the sample must be carefully leveled to prevent distortions in the obtained XRD patterns. Ensuring a flat and uniform sample surface is essential for maintaining the accuracy and reliability of diffraction data (Harold P Klug; Leroy E Alexander, 1974; R E Dinnebier; S J L Billinge, 2008).

For the XRD measurements, the sample was prepared in the sample holder and data was collected for all samples in this work using the same diffractometer configuration. X-ray powder diffraction data were collected using an Empyrean diffractometer (Panalytical, Holland) in reflection mode with $\text{CuK}\alpha$ radiation ($\lambda = 1.54056 \text{ \AA}$). The instrument operated at 40 kV and 40 mA and was equipped with a Bragg-Brentano HD mirror, a 0.02 rad soller slit, a 1° anti-scattering slit, and a $1/4^\circ$ divergence slit on the incident beam side. The diffracted beam path included a 0.04 rad soller slit and a 9 mm anti-scattering slit, with photons detected using a PIXcel3D-Medipix3 1x1 area detector. Data acquisition was conducted over a 2θ range of

10° to 100° with a step size of 0.01313° and a dwell time of 60 seconds per step. As demonstrated, special sample holders adapted by the author were used during the measurements.

The collected data were analyzed according to the method described in this chapter, using the Rietveld Refinement method (McCusker et al., 1999; Rietveld, 2014) to separate and quantify the crystalline and amorphous components. The cell parameters for both A and B-type starches were obtained from the literature (Imberty et al., 1991; Takahashi; Kumano; Nishikawa, 2004), and used for refining the experimental data. Other software and online tools were used to later check the consistency of the refined crystallography information obtained, such as the abandonware software FindSym and the database Bilbao (Kroumova et al., 2003).

Driven by the desire to explore and validate this method, we selected potato starch as a readily available and widely studied source for structural analysis. As a proof of concept, both mechanical and chemical processing methods were applied to alter its native structure, and the resulting changes were analyzed using X-ray diffraction (XRD) combined with Rietveld refinement. This approach allowed us to evaluate the efficacy of the methodology, which was then published as the first-reported approach to that matter (Pinto; Campelo; Michielon de Souza, 2020).

CHAPTER 3 – RESULTS I: Proof of concept

Potato Starch Nanocrystals: physicochemical modifications investigated through Rietveld Refinement

This chapter demonstrates the proposed methodology's capability to discern subtle structural changes induced by processing treatments. As a proof of concept, potato starch subjected to ultrasonic pre-treatment and acid hydrolysis was processed and analyzed using X-ray diffraction (XRD) combined with Rietveld refinement. The analysis quantified variations in crystallinity, alterations to unit cell parameters, and the arrangement of water molecules within the crystalline lattice. These findings validate the methodology's robustness and utility, demonstrating its effectiveness, as evidenced by the interest already gathered within the scientific community with its publication.

Starch nanocrystals are crystalline structures derived from starch granules, formed by selectively eroding the amorphous regions while preserving the crystalline domains (Pinto et al., 2024). The modification of starch is a widely utilized process aimed at tailoring its properties to meet specific structural and functional requirements for various applications (Mohammad Amini; Razavi, 2016). Potato starch, along with maize starch, is among the most extensively utilized carbohydrate sources, with its widespread availability and established applications serving as primary factors influencing its selection (Martins; Gutkoski; Martins, 2018).

The primary methods usually employed for producing starch nanocrystals are categorized into chemical and mechanical approaches. Chemical methods primarily target the amorphous phase, utilizing agents such as enzymes or strong acids to degrade the amorphous regions (Angellier et al., 2004b; Asiri; Ulbrich; Flöter, 2018; Le Corre; Bras; Dufresne, 2010). In contrast, mechanical methods focus on physically breaking polymer chains through high-

energy processes, such as milling and ultrasound treatment (Vertuccio et al., 2009). The combination of physical and chemical methods may offer several advantages, including a significant reduction in processing time, as chemical methods alone can take up to five days (Le Corre; Bras; Dufresne, 2010). Additionally, this combined approach minimizes thermal damage, which can occur when highly energetic physical methods elevate the temperature of starch, potentially leading to phase transitions and thermal degradation. For instance, some hybrid techniques integrate acid hydrolysis with thermosonication to enhance efficiency and product quality (Dai et al., 2018; Mohammad Amini; Razavi, 2016).

In this proof of concept, powder X-ray diffraction (XRD) combined with Rietveld refinement (RM) was employed to quantify the crystallinity and crystallite sizes of B-type starch. Food-grade potato starch, rich in B-type amylose, was selected as the model material. Samples were subjected to hydrolysis with HCl, and one batch was pre-processed using ultrasound prior to hydrolysis. These processing methods were chosen for their simplicity and effectiveness in producing high-quality starch nanocrystals. After drying, the resulting powders were analyzed using XRD, with diffractograms simulated via RM to separate crystalline and amorphous components. Apparent crystallite sizes were calculated using the Scherrer equation, and crystallographic parameters were further refined to enhance the precision of the analysis.

Intriguing hypotheses emerge regarding the role of structural water in influencing the diffraction patterns of B-type starch. Structural water, occupying specific crystallographic sites within the starch lattice, may contribute to the observed diffraction intensities and peak shapes. These insights not only deepen our understanding of the semi-crystalline organization of starch but also open new avenues for exploring how intrinsic water impacts the stability, functionality, and processing behavior of starch-based materials.

Such findings underscore the potential externalities and broader implications of this study, offering valuable perspectives that may inform future research in fields ranging from food science to materials engineering. The interplay between water distribution and starch crystallinity, as revealed by this analysis, highlights the interconnected nature of structural and functional properties, emphasizing the importance of integrating crystallographic techniques to uncover these complex relationships.

This approach demonstrates the utility of combining XRD and RM to explore the crystallinity changes in starch resulting from diverse processing techniques.

3.1 Experimental procedures

i. Materials:

Commercial food-grade powdered potato starch was procured from Metachem Group, São Paulo, Brazil. The chemical reagent used for the study was hydrochloric acid (HCl, 37%) sourced from Nuclear, Brazil.

ii. Sample Preparation:

The powdered potato starch was divided into four distinct treatment groups based on the processing procedures:

- Control: Untreated raw potato starch.
- US: Potato starch subjected to high-energy ultrasound processing, followed by oven drying.
- Hydrolyzed: Starch processed via acid hydrolysis using HCl.
- US-Hydrolyzed: Starch pre-treated with high-energy ultrasound before undergoing acid hydrolysis.

iii. Ultrasound-Assisted Processing:

For this proof of concept, the ultrasound treatment for the US and US-Hydrolyzed samples was performed based on a modified version of the methodology described by (Yang et al., 2019). To manage the temperature during sonication, the process was fractionated. Starch samples were dissolved in distilled water at a ratio of 1:10 (gram to milliliter) and continuously agitated using a magnetic stirrer. High-intensity ultrasound processing was conducted with a VibraCell VCX 750 W (20 kHz, USA) operating at 600 W for 15 minutes. The samples were placed in an ice bath to prevent temperature increases during sonication. After processing, the solutions were centrifuged to separate the precipitate from the supernatant. The precipitate was oven-dried in an air-circulated oven at 40 °C for 24 hours before undergoing XRD analysis.

iv. Acid hydrolysis:

In this work, the ultrasound-treated and raw starch samples were processed following a modified protocol based on the method described in the literature (Mohammad Amini; Razavi, 2016). For both the Hydrolyzed and US-Hydrolyzed samples, starch was dissolved in a 3.14 M HCl solution at a ratio of 3 grams of starch to 17 mL of solution. The mixtures were subjected to acid hydrolysis in an ultrasonic bath (40 kHz frequency, model USC-3300, Unique, Brazil) at a controlled temperature of 40 °C for 45 minutes. Following hydrolysis, the solutions were centrifuged to separate the precipitate from the supernatant. The precipitates were then washed multiple times with distilled water until the pH of the starch was approximately neutral. Subsequently, the starch samples were dried in an air-circulated oven at 40 °C for 24 hours.

v. Moisture Content Measurement:

Since the starch structure might be influenced by the water content, determining moisture content is necessary for reproducibility of the experiment. In this work, it was determined using a methodology adapted from (Ilyas et al., 2020). The dried starch samples were oven-dried overnight at 105 °C. The initial and final weights of the samples were measured using a moisture analyzer (I-THERMO 163L, Bel Engineering). The average moisture content across all samples was found to be 15.75%.

3.2 X-Ray Diffraction Analysis of Starch Samples with Ultrasonic Preprocessing

i. Unhydrolyzed samples

Figure 16 presents the X-ray diffraction (XRD) patterns of the Control and US samples prior to hydrolysis. Ultrasonication is known to break covalent bonds in polysaccharides, leading to the depolymerization of amylose and amylopectin components, which can improve properties relevant to industrial applications (Gernat et al., 1990; Radosta et al., 2016).

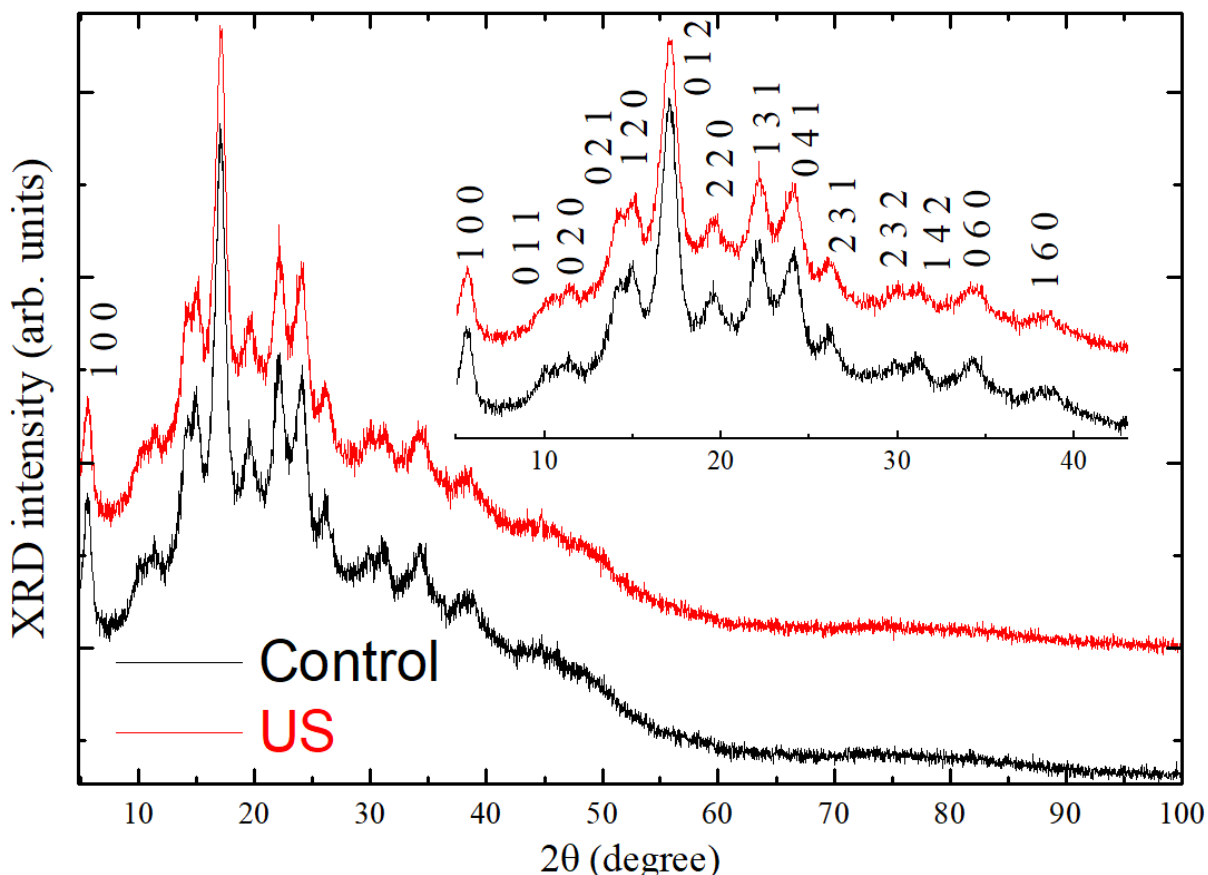


Figure 16 - XRD patterns comparing the Control and US-treated samples. Inset depicts details of the structure Figure from the author, published in (Pinto; Campelo; Michielon de Souza, 2020)

Thus, this pre-treatment was expected to make a measurable difference. Still, as seen in the diffraction patterns exhibited, just slight changes succeeded ultrasonic treatment, suggesting minor structural alterations while maintaining overall stability. The interhelix peak near $2\theta = 5.6^\circ$ corresponds to the (1 0 0) and (0 1 0) crystallographic planes, representing the periodic arrangement of water molecules and the lamellar spacing (Blazek; Gilbert, 2010). This lamellar peak arises from the decoupling of double helices from the polymer backbone and their alignment in the presence of water (Takahashi; Kumano; Nishikawa, 2004). A decrease in the relative intensity of this peak in the US sample indicates the removal of water molecules from structural cavities due to ultrasonic treatment, reducing trapped water in amylopectin and decreasing the hydrophilicity of the starch (Ilyas; Sapuan; Ishak, 2018).

The refinement process assumes that water molecules occupy defined positions within the unit cell, consistent with earlier models (Imberty; Perez, 1988; Takahashi; Kumano; Nishikawa, 2004), and demonstrated in Figure 17. This assumption aligns with the hexagonal

$P6_1$ space group symmetry characteristic of B-type starch, where the precise arrangement of water molecules contributes to the stability of the crystalline lattice.

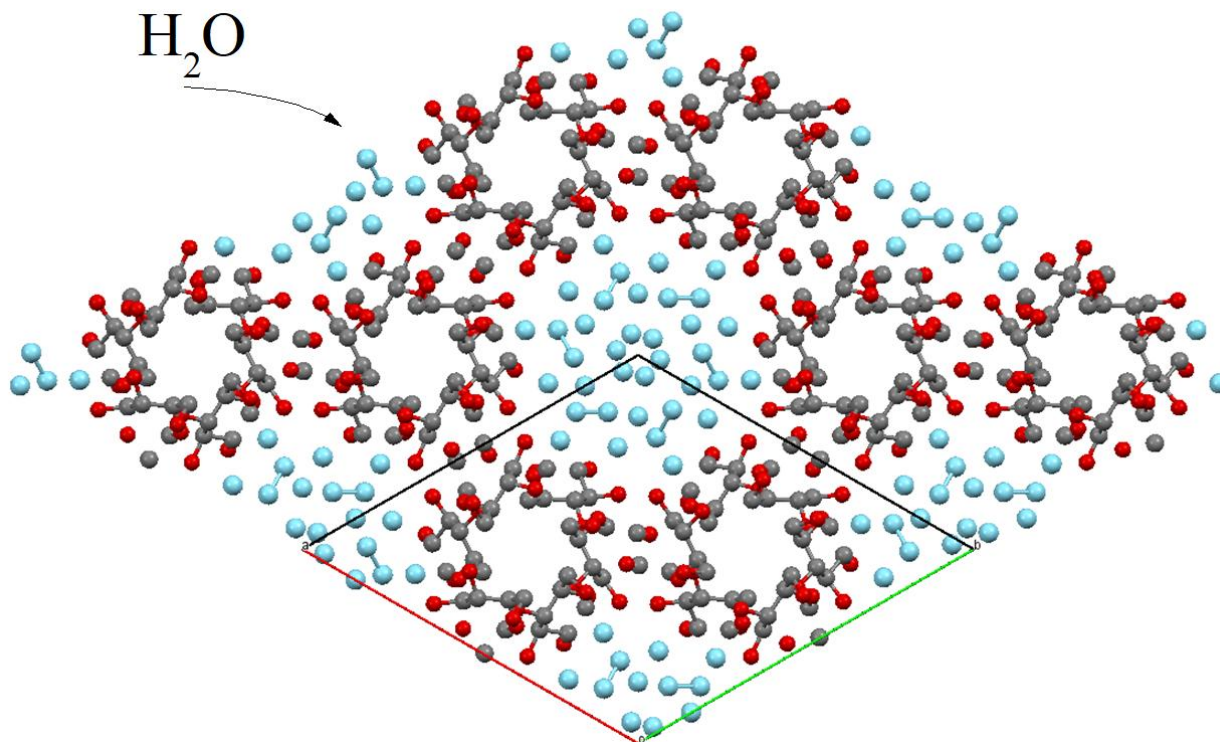


Figure 17 – Schematic projection of the $P6_1$ structural model, illustrating amylopectin's left-handed double helices arranged in parallel, encapsulating 36 water molecules. Figure reconstructed based in (Okazaki, 2018).

These water molecules are strategically located in discrete pockets within the unit cell, interacting with the starch double helices through hydrogen bonding. This structural organization plays a critical role in maintaining the semi-crystalline nature of B-type starch, influencing its physicochemical properties, including hydration behavior and thermal stability (Imberty; Perez, 1988; Takahashi; Kumano; Nishikawa, 2004).

Since this way each crystallographic site was supposed to accommodate a molecule instead of a single atom, it was assumed that the same site accommodates two hydrogen atoms and one oxygen atom, being oxygen the element that has larger scattering efficiency. The fractional coordinates used for this refinement are presented in **Table 1** and **Table 2**, allowing for reproducibility of this refinement.

Table 1 - Fractional coordinates for water molecules in the B-type starch structure.

Water	x	y	z
H ₂ O (1)	-0.191(3)	-0.090(2)	0.367(3)
H ₂ O (2)	-0.239(4)	-0.185(3)	0.457(5)
H ₂ O (3)	0.232(3)	-0.104(2)	-0.167(4)
H ₂ O (4)	-0.001(2)	-0.158(2)	0.169(5)
H ₂ O (5)	0.020(3)	0.0647(3)	0.598(7)
H ₂ O (6)	0.268(2)	0.061(2)	0.179(4)

Table 2 - Fractional atomic coordinates of B-type starch.

Atom	x	y	z
C1	0.4902	0.0955	0.2504
C2	0.5428	0.5400	0.2600
C3	0.6271	0.1071	0.1855
C4	0.6134	0.1348	0.0545
C5	0.5622	0.1775	0.0651
C6	0.5430	0.2031	-0.0625
C7	0.4285	0.2721	-0.5828
C8	0.3870	0.1781	0.5926
C9	0.4401	0.1467	0.5186
C10	0.4680	0.1880	0.3875
C11	0.5107	0.2820	0.3979
C12	0.5365	0.3266	0.2702
O1	0.5255	0.1653	0.3333
O2	0.5556	0.0345	0.3768
O3	0.6632	0.0552	0.1715
O4	0.6933	0.1918	0.0000
O5	0.4824	0.1202	0.1235
O6	0.5073	0.1353	-0.1528
O7	0.4982	0.3067	0.6658
O8	0.3674	0.1459	0.7095
O9	0.3883	0.0588	0.5048
O10	0.4533	0.3045	0.4559
O11	0.4659	0.3111	0.1926

Figure 18 illustrate the XRD intensities for the Control sample (unaltered raw starch sample) refined by the Rietveld method. Rwp and χ^2 factors obtained can be considered acceptable results, and original crystallinity was then found to be 26%.

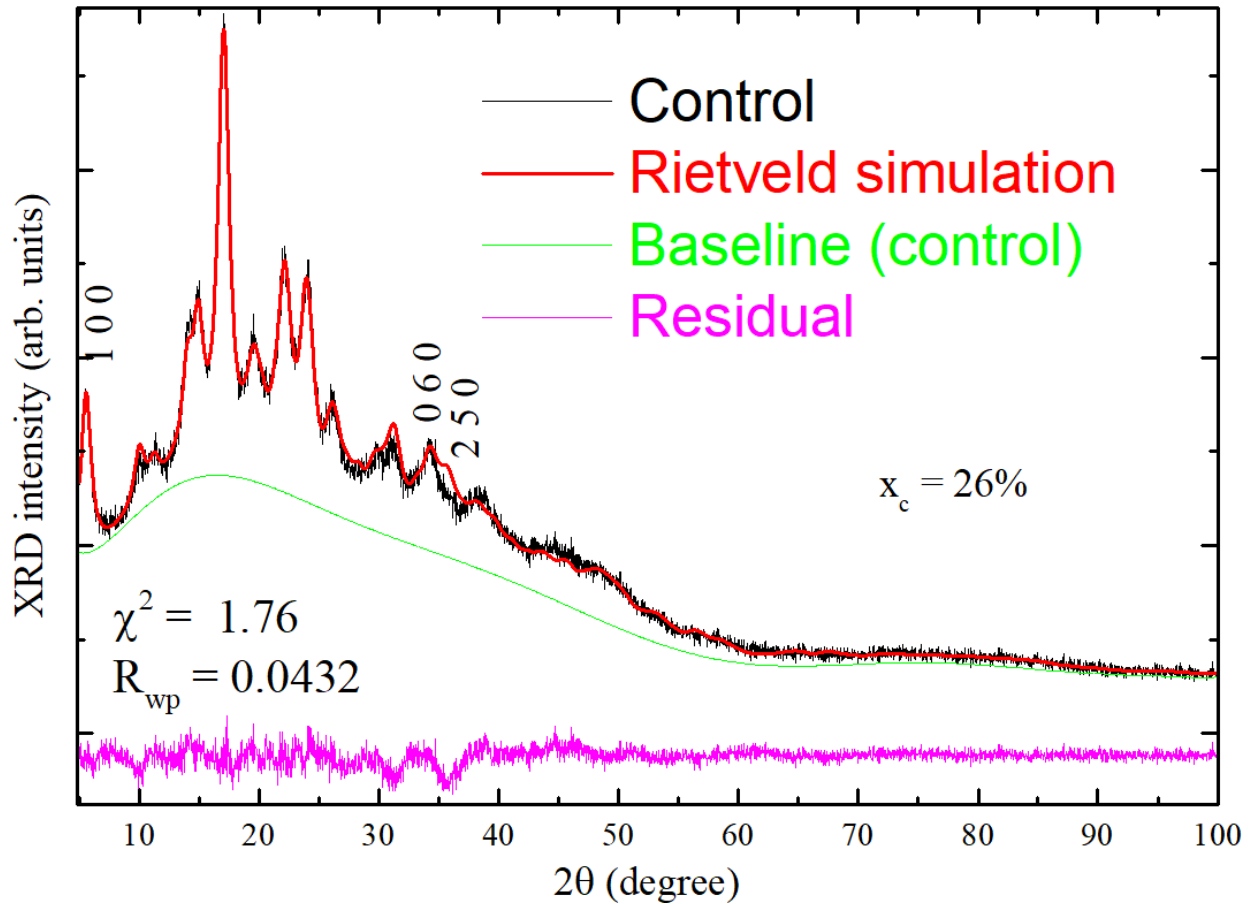


Figure 18 – Rietveld refinement of the Control sample. Figure from the author, published in (Pinto; Campelo; Michielon de Souza, 2020)

Figure 19 shows the US sample (just underwent ultrasound treatment), Rietveld refinement parameters considered acceptable, and both refined using the Rietveld method. Excellent agreement between the experimental data and the refined model is evident in the residual curves and the convergence factors Rwp and χ^2 (Toby, 2006).

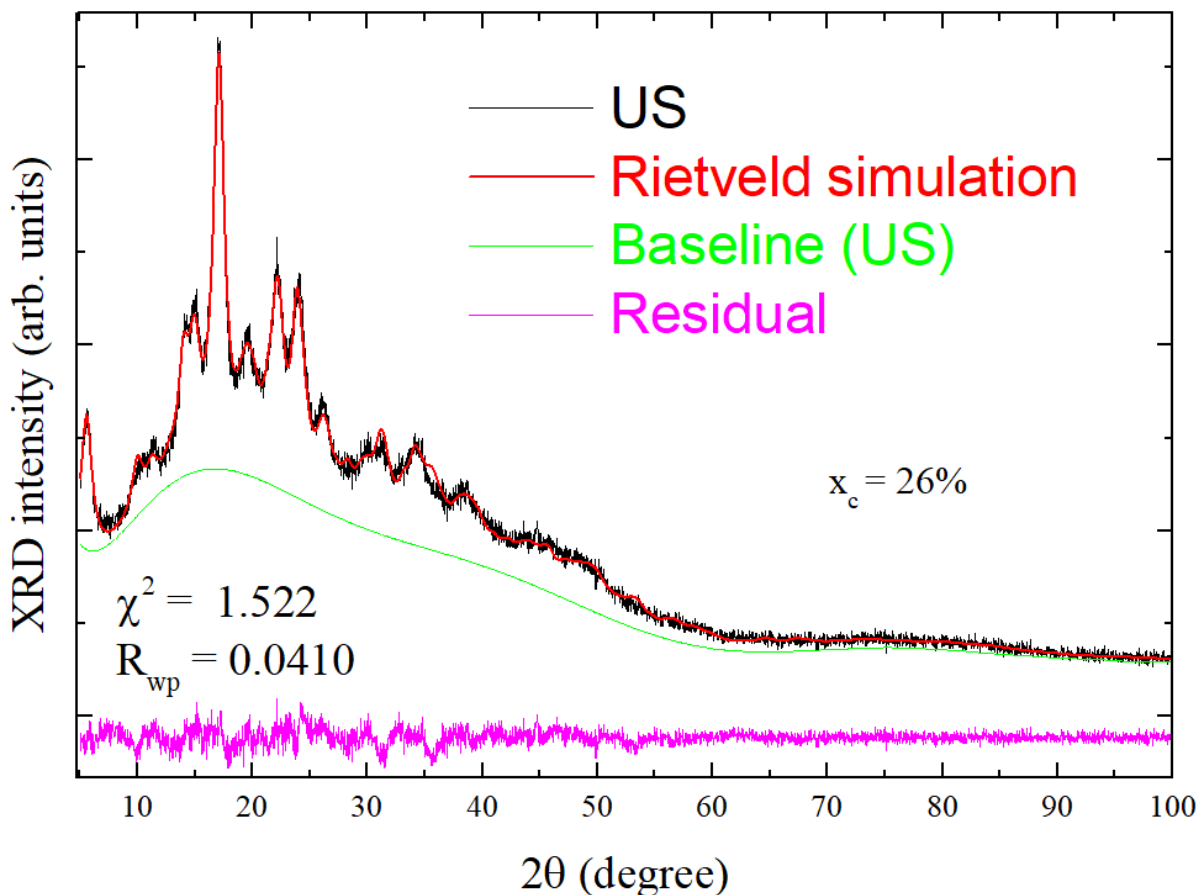


Figure 19 – Rietveld refinement of the US-treated sample. Figure from the author, published in (Pinto; Campelo; Michielon de Souza, 2020)

Table 3 presents the refined unit cell parameters, indicating that the hydrolysis process preserved the original structure with a slight expansion compared to the initial parameters of the Control and US samples.

We extensively defined, in Chapter 1, the mechanism in which the diffuse scattering pattern reflects the microstructural effects of the crystalline component, which can influence amorphous phase quantifications. It can be summarized as follows: Nanometric crystals generate broad peaks, and the overlap of two nearby peaks at 2θ contributes to increased intensity in the diffuse halo region.

Table 3 - Lattice parameters of B-type starch (hexagonal symmetry, space group $P6_1$) derived from Rietveld refinement and comparison with literature data. Published in (Pinto; Campelo; Michielon de Souza, 2020)

B – Type Starch	a (Å)	c (Å)	$V(\text{Å}^3)$
Control	18.169(5)	10.703(8)	3059.8(2)
US	18.080(6)	10.62(1)	3006.4(5)
Hidrolyzed	18.110(1)	10.95(2)	3110.6(5)
US-Hidrolyzed	18.115(7)	10.76(1)	3057.9(6)
(Imberty; Perez, 1988)	18.5	10.4	3082.5
(Takahashi; Kumano; Nishikawa, 2004)	18.52	10.57	3139.7

Using

Equation 3 and Equation 4 for line widths of crystalline peaks, the apparent crystallite sizes were calculated with both Equation 5 and Equation 9. Crystallites in the well-fitted region ($2\theta \sim 5^\circ\text{--}24^\circ$) averaged ~ 50 Å, whereas the entire pattern yielded sizes around ~ 80 Å. These results align with established crystallite sizes for B-type starch in the literature (40–80 Å), corresponding to 10–20 glucosyl units (Bertoft, 2017). However, the apparent crystallite size calculated with

Equation 3 may be overestimated due to lower resolution in some peaks, as it considers peaks that are not well fitted or have a lower resolution in the experimental diffractograms.

Crystallinity (X_c) was determined using Equation 12, resulting in approximately 26% crystallinity and 74% amorphous content for both analyzed samples. This calculation aligns with established values in the literature, reflecting the semi-crystalline nature of starch. In comparison, Lopez-Rubio et al. (2008) proposed an alternative manual fitting approach utilizing Gaussian functions, which yielded a slightly higher crystallinity value of approximately 30% for potato starch. This discrepancy underscores the sensitivity of crystallinity measurements to the mathematical models employed for fitting diffraction peaks.

The choice of fitting function—whether Gaussian, Lorentzian, or pseudo-Voigt—significantly affects the derived crystallinity values, and it is vital to stress the importance of selecting appropriate fitting functions and methodologies to minimize systematic errors in crystallinity calculations, emphasizing the need for standardized protocols when comparing results across studies, ensuring that differences in fitting approaches do not compromise the

reliability and reproducibility of crystallinity measurements. Among these, pseudo-Voigt functions are generally recognized for their superior ability to represent diffraction peak shapes, as they combine Gaussian and Lorentzian components to accommodate variations in peak broadening mechanisms (B.E. Warren, 1990). This flexibility makes pseudo-Voigt functions more suitable for accurately modeling diffraction patterns, particularly for materials like starch that exhibit complex structural features due to their semi-crystalline nature.

Figure 20 shows the XRD pattern of the US sample after baseline subtraction using a simulated Chebyshev curve. Each curve represents a distinct Full Width at Half Maximum (FWHM) parameter, corresponding to a potential variation in crystallite size. These variations in crystallite size influence the degree of interaction with the baseline, which must be accounted for during extraction.

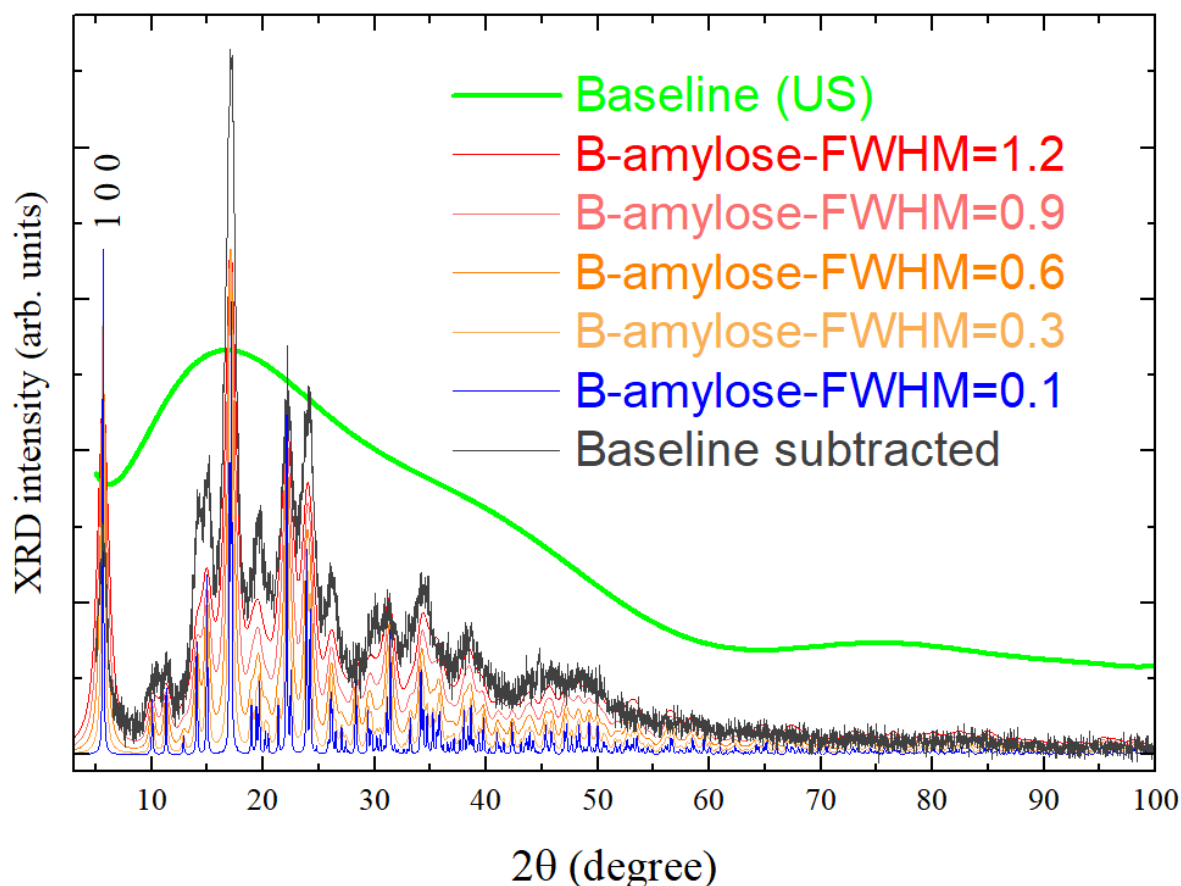


Figure 20 – Baseline analysis illustrating contributions based on FWHM and varying crystallite sizes. Figure from the author, published in (Pinto; Campelo; Michielon de Souza, 2020)

The idealized diffractograms, generated with the Mercury software (Macrae et al., 2006, 2008) based on the refined crystallographic data (**Table 2**, **Table 1** and **Table 3**), demonstrate the impact of FWHM variations on peak overlap, as extensively defined in Chapter 1 of this work. The simulated patterns closely match the experimental data, indicating that the baselines effectively represent the diffuse scattering contribution. These results highlight that the baseline increase accounts not only for the amorphous phase but also for overlapping broadened peaks.

i. Hydrolyzed samples

As established in this chapter, to produce starch nanocrystals both pre-treated and non-treated samples underwent hydrolysis under identical conditions for 45 minutes. Figure 21 presents the overlapping XRD patterns of hydrolyzed samples, with and without ultrasonic pre-treatment (referred to as Hydrolyzed and US-Hydrolyzed, respectively).

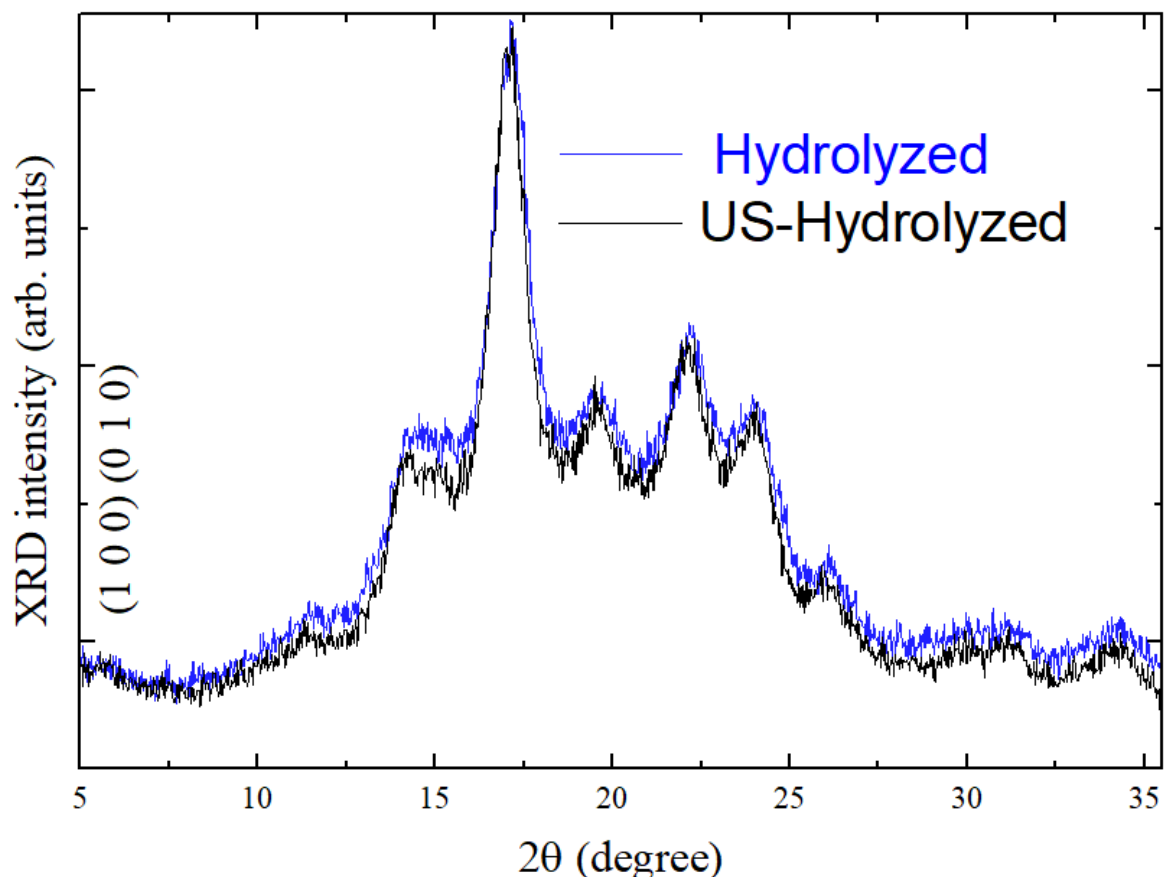


Figure 21 – Comparison of XRD patterns for Hydrolyzed and US-Hydrolyzed samples. Figure from the author, published in (Pinto; Campelo; Michielon de Souza, 2020)

The observed similarity between the diffraction patterns suggests that the hydrolysis process is not suggestively influenced by ultrasonic pre-treatment (at least not in the setup used for this work). This indicates that ultrasonic processing with the chosen parameters for this work, while potentially altering certain structural features of the starch prior to hydrolysis, does not substantially affect the subsequent hydrolytic reaction or the resulting structural properties of the starch.

Figure 22 compares the diffractograms of samples before and after ultrasonic pre-treatment and hydrolysis (US and US-Hydrolyzed).

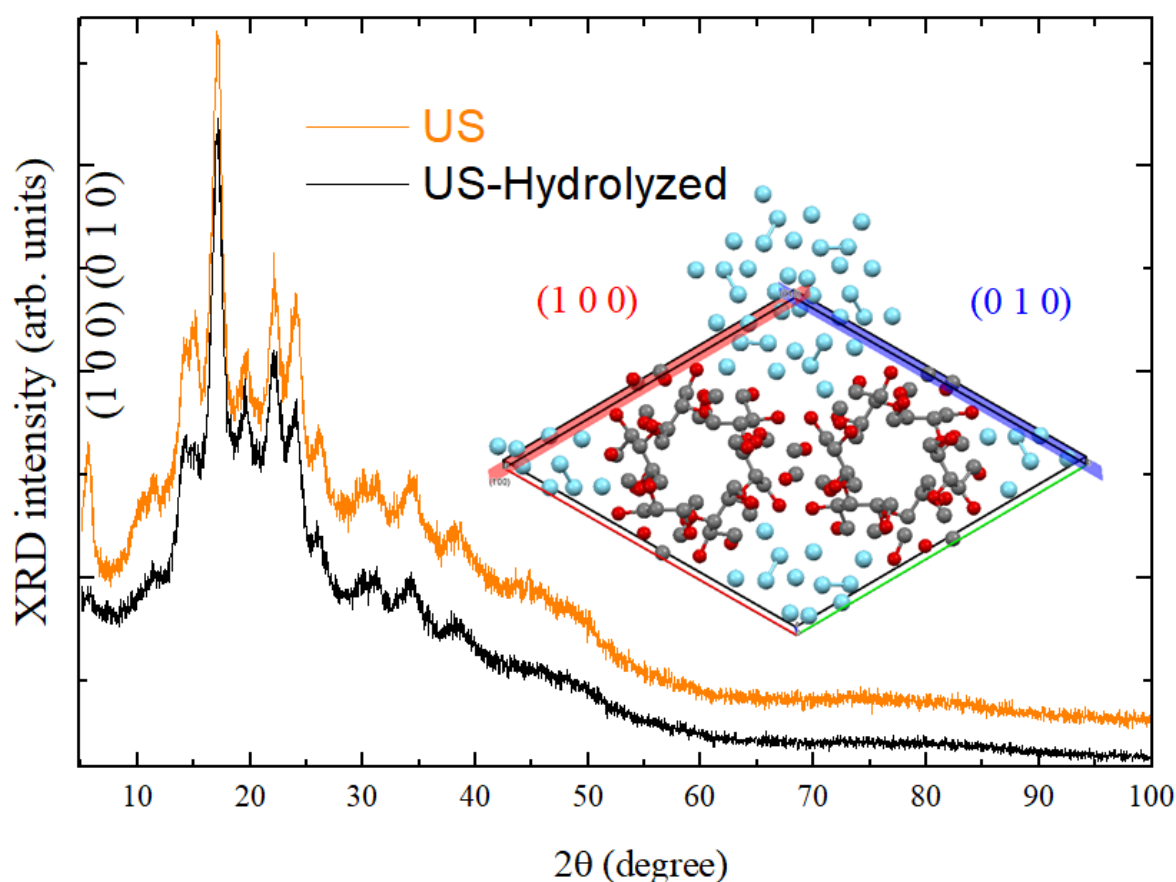


Figure 22 – Overlay comparison of XRD patterns for US and US-Hydrolyzed samples, highlighting interhelix peaks. The inset demonstrates the planes (1 0 0) and (0 1 0). Figure from the author, published in (Pinto; Campelo; Michielon de Souza, 2020)

The observed slight variation in peak positions suggests minor changes in unit cell volume, while the consistent peak widths indicate that crystallite sizes remain unchanged across the samples. The first peak, corresponding to the lamellar (1 0 0) and (0 1 0) planes, traverses regions associated with clusters of water molecules. This peak intensity can be modeled by

reducing the occupancy of water molecules or incorporating preferential orientation (texture) effects (Pecharsky; Zavalij, 2005). The increase in crystallinity observed with hydrolysis is associated with reduced water absorption properties (Halimatul et al., 2019a, 2019b).

Figure 23 illustrates the Rietveld refinement of the US-Hydrolyzed sample. The baseline was modeled using the same 11-term Chebyshev polynomial employed for the Control and US samples. The reduction in the baseline reflects a decrease in the disordered component, consistent with expectations for hydrolysis treatments (Polesi; Sarmiento, 2011).

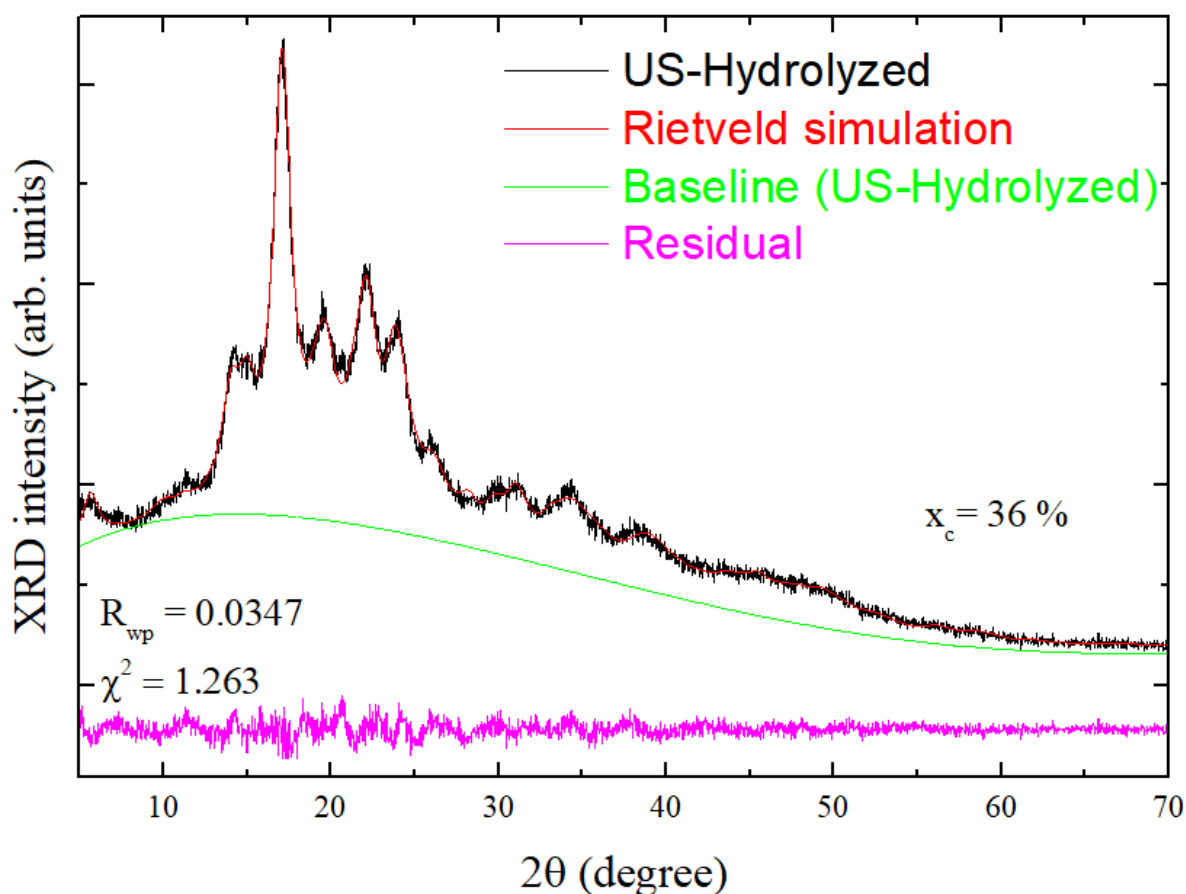


Figure 23 – Rietveld refinement of the US-Hydrolyzed sample. Figure from the author, published in (Pinto; Campelo; Michielon de Souza, 2020)

Table 4 summarizes the crystallinity values across all samples, revealing a 10% increase in crystallinity for hydrolyzed samples compared to their untreated counterparts. This indicates that hydrolysis, as expected, effectively removes a substantial portion of the amorphous component in both the control and ultrasound-pretreated samples.

Table 4 - Microstructural parameters and crystallinity values for B-type starch samples. Published in (Pinto; Campelo; Michielon de Souza, 2020)

Sample	D (Å)	$D_{(hkl)}$ (Å)	ε (%)	$\varepsilon_{(hkl)}$ (%)	x_c (%)
Control	87	44(5)	3	3(1)	26
US	82	63(6)	4	4(5)	26
Hidrolyzed	80	49(8)	2	2.7(7)	36
US-Hidrolyzed	79	52(5)	2	2.5(9)	36

As a future development of the work and for more precise quantification of crystallinity, advanced techniques such as high-resolution synchrotron measurements and humidity-controlled vacuum experiments could be explored in the future. These methods could provide greater accuracy in determining the structural changes induced by hydrolysis and other processing techniques.

ii. Synthesis of Findings

This study represents the first application of the Rietveld refinement method to analyze XRD patterns of B-type starch powder. Additionally, criteria were established for separating the crystalline and amorphous components, thereby minimizing researcher bias in microstructural analysis and crystallinity determination. The crystallite sizes of commercial raw potato starch (Control), US, Hydrolyzed, and US-Hydrolyzed samples were determined to demonstrate the utility of this methodology.

For both Control and ultrasound-treated potato starch, the acid hydrolysis process produced a comparable reduction in crystallinity. Furthermore, the Rietveld refinement method provided detailed insights into the effects of hydrolysis on the B-type crystals, including the spatial distribution of water molecules within the unit cell. Intracrystalline water molecules were identified in discrete pockets that define the lamellar structure characteristic of B-type starch.

Following hydrolysis, the relative intensity of the lamellar peak decreased, suggesting structural disruptions along the C-axis and the breaking of fibrous arrangements. This finding

offers significant advancements in the understanding of the structural properties of B-type starch, emphasizing the value of crystallographic studies in elucidating its complex behavior. The results also provide a robust foundation for further investigations into the relationship between structural features and functional properties in starch-based materials.

3.3 Repercussion of our work:

This work was published as “Rietveld-based quantitative phase analysis of B-type starch crystals subjected to ultrasound and hydrolysis processes” (Pinto; Campelo; Michielon de Souza, 2020), and has gathered some interest of both areas of Condensed Matter Physics and Food Science. Up to this moment, the article has been cited 18 times, and even raised discussions of its implications. Rodriguez-Garcia et al. (2021) described the problem many authors face in trying to separate the elastic and inelastic scattering contributions from the XRD patterns, but that our work described in this chapter “using Rietveld method in B-Type starch powder XRD patterns ... solved that problem” (Rodriguez-Garcia et al., 2021).

This prompted us to expand our investigation to address additional questions and explore related challenges, now focusing on alternative materials. Fortunately, the Amazon Biome provides a wealth of underexplored and intriguing starch sources, offering a unique opportunity to broaden the scope of this research and uncover new insights.

3.4 Other questions remain

Therefore, while the combination of XRD and the Rietveld Refinement Method has demonstrated potential for investigating the microstructure of starches, several questions remain unanswered:

- Can this method be reproduced for other **more complex** starches that underwent **non-conventional processing** techniques?
- Has this method the capacity to unravel and quantify **other interesting information** regarding the starch’s microstructure?
- Might one be able to correlate that microstructure information obtained with structural refinement with **other characterization techniques**?

CHAPTER 4 – RESULTS II

Modifying exotic Amazon starch from Ariá (*Goepertia allouia*) with unconventional processing techniques

*In this chapter, the proposed method for structural refinement will once again be employed to investigate the microstructural changes induced by non-conventional techniques, namely gamma-ray irradiation and cold plasma, on a unique starch called Ariá (*Goepertia allouia*) sourced from the Amazon region. The objective is to decipher its intricate structure by distinguishing its crystalline portions (A and B-type phases) from the noncrystalline regions. To validate the findings, SEM, FTIR, and rheology analyses were utilized in a cross-validation approach.*

In order to obtain a deeper understanding of more complex starch structures such as the one obtained in Amazon root Ariá (*Goepertia allouia*), this work proceeded to further investigate the method of structural refinement to address another yet common but still complicated issue. Specifically, the focus shifted towards the challenge of deconvoluting two semicrystalline phases within the Ariá starch: A and B-type. Notably, this was the first attempt made to tackle this particular problem.

Building upon previous work with potato starch and leveraging structural refinement by Rietveld method, this chapter focuses on distinguishing and analyzing the two distinct semicrystalline phases present in starch samples subjected to non-conventional processing methods. The investigation successfully identified the individual contributions of these phases to overall crystallinity and other structural properties while isolating the non-crystalline fraction of the starch. This work significantly advances the understanding of starch structure by addressing the previously unexplored complexity of C-type starch, which combines A- and B-type polymorphs.

By applying structural refinement, the research revealed that different regions of the starch granule may respond variably to processing techniques. This finding not only enhances

the structural understanding of starch but also allows for the potential tuning of properties in exotic starch sources, such as those derived from Amazonian plants. The ability to manipulate and optimize the properties of starches containing mixed structures, and even monitor the conversion between polymorphs, opens new avenues for expanding the applications of this biomaterial in diverse fields.

This chapter investigates these questions by examining the effects of two non-conventional processing techniques—gamma-ray irradiation and cold plasma—on a C-type starch derived from an Amazonian source, Ariá.

Tuberous roots of *Goepertia allouia* (SisGen – Brazilian National Management System of the Genetic Heritage and Associated Traditional Knowledge – authorization code AF97191) were sourced from local markets in Manaus, Amazonas, Brazil. The tubers were thoroughly washed and sanitized using a 200 mg L⁻¹ sodium hypochlorite solution to eliminate physical contaminants. They were then manually peeled and processed in a knife mill at a 1:2 (roots:water, w/v) ratio. The resulting material was filtered through polyester fabric, and the filtrate was left to rest for 15 hours, allowing the starch to settle by phase separation. The supernatant was carefully removed, and the deposited starch underwent five consecutive washes until a clean, white starch remained at the bottom of the container. The washed starch was dried in an air-circulation oven at 40 °C for 16 hours. The resulting dried starch powder was stored in laminated polypropylene packages under vacuum in a desiccator at room temperature until further analysis. The same starch was then subjected to a number of processing techniques described in this work.

This starch presents a challenging structure due to its combination of A- and B-type crystalline regions. The deconvolution of the crystalline phases and the non-crystalline portion is proposed as a means to better understand the structural complexity of this material.

4.1 γ -radiation of Ariá starch

Gamma (γ) radiation modification of starch is an eco-friendly and cost-effective physical method that has gained attention for its industrial potential (Sudheesh et al., 2019). This technique does not require catalysts, thereby avoiding the generation of effluents and ensuring that the final product remains free from toxic residues (Verma et al., 2018). Previous studies have explored the effects of irradiation on the physical, chemical, and rheological

properties of commercial starches, demonstrating its promise for various industrial applications (Sudheesh et al., 2019). However, the full depth impact of γ -radiation on the crystalline structure of starch remains insufficiently understood.

In this section, we applied the Rietveld refinement method for the first time to analyze the X-ray diffraction (XRD) patterns of type-C starch from Ariá and its irradiated derivatives. This analysis enabled the quantification of A- and B-type polymorphic contents, as well as the crystallinity and amorphous components of the starch and this work was published at (Pinto et al., 2021a). Starch extracted from Ariá was subjected to varying doses of γ -radiation, and the structural effects of irradiation were evaluated through a combination of XRD analysis and pasting property measurements. This approach provides new insights into the structural modifications induced by γ -radiation and their implications for the functional properties of starch.

i. Starch modification process: γ -irradiation

Samples of Ariá starch with a moisture content of 8.45% (w/w) (~100 g per treatment) were placed in a γ -radiation chamber at a calculated distance from the Cobalt-60 source to achieve the intended radiation dose, as specified in **Table 5**. The irradiation process was conducted using a panoramic multi-purpose irradiator (category II, MDS Nordion, Canada, Model IR-214, type GB-127) equipped with a Cobalt-60 source. Following irradiation, the starch samples were stored in plastic bags at room temperature and shielded from light until subsequent analysis.

Table 5 - Experimental design used to modify Ariá starch

Sample	Dose (kGy)	Dose rate (Gy.h ⁻¹)	Distance to cobalt source (cm)
Raw Ariá starch	0	0	-
1 kGy	1	226.43	86.5
5 kGy	5	1131.49	32
20 kGy	20	4527.10	9
50 kGy	50	11614.44	1

ii. XRD characterization and Rietveld Refinement

Figure 24 presents the X-ray diffraction (XRD) patterns of Ariá starch samples measured between $2\theta = 5^\circ$ and 100° , both before and after the γ -radiation treatments described in Table 5.

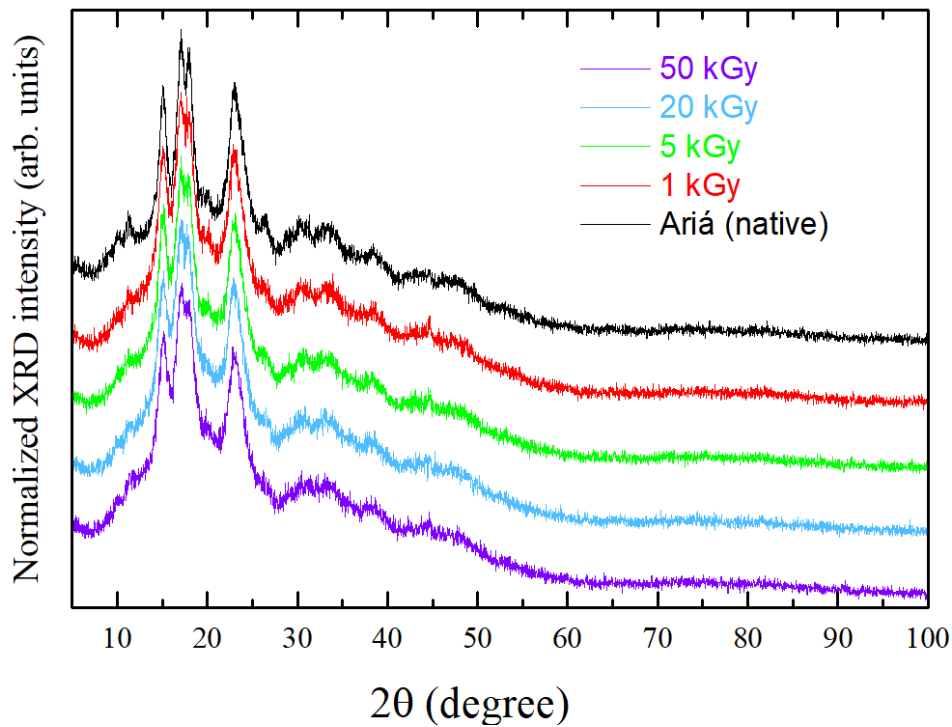


Figure 24 – XRD patterns of Ariá samples before and after 4 doses of radiation.

The freeze-dried raw Ariá starch exhibits, as expected, a XRD pattern indicative of two structural components: a semi-crystalline (ordered) phase and an amorphous (disordered) phase. The semi-crystalline phase is responsible for the distinct Bragg peaks and is composed of two organized arrangements with differing symmetry, namely both starch polymorphs A- and B-type which together can be identified as C-type starch. In contrast, the amorphous phase produces a broad, low-intensity halo due to diffuse X-ray scattering, observable between $2\theta = 5^\circ$ and approximately 65° . Beyond $2\theta = 65^\circ$, the intensity stabilizes, with no significant contributions from either crystalline or amorphous components.

For crystallinity estimation, it is critical that the XRD measurements encompass both low and high 2θ angles to capture the diffuse scattering from the disordered component, ensuring comprehensive data for analysis (Wagner, 1978). To enhance the visualization of these subtle details in the XRD experimental data, a close-up view is presented. In°Figure 25, the

XRD patterns were normalized to the most intense peak at $2\theta \approx 17^\circ$ to enable qualitative comparison of the relative intensities of the semi-crystalline components, observed between $2\theta \approx 10^\circ$ and 25° .

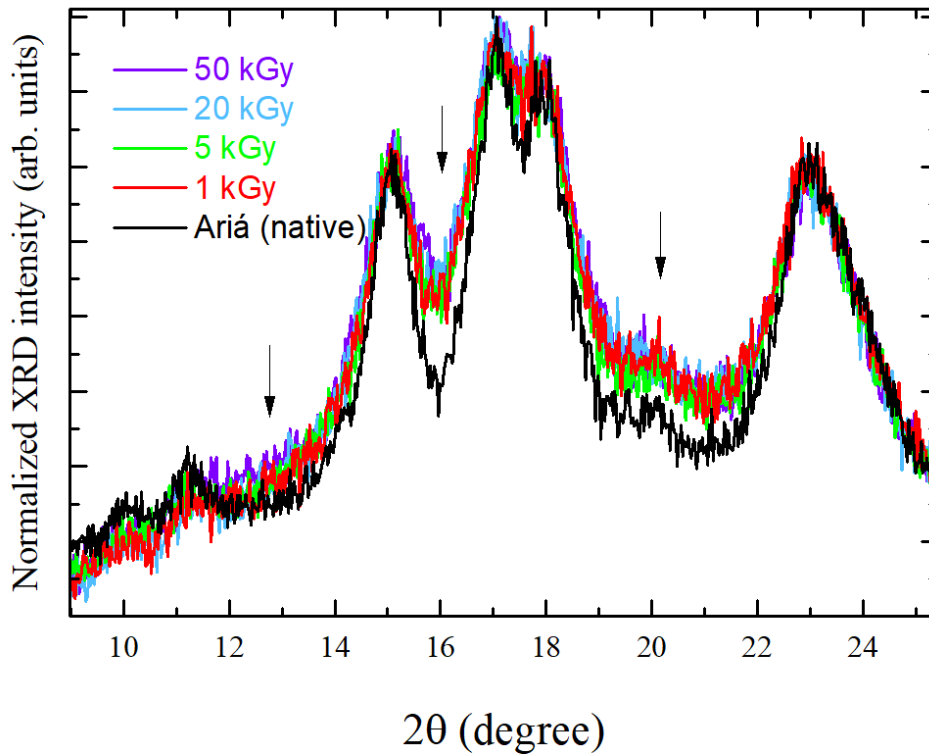


Figure 25 – The details in the XRD patterns shows the structural changes caused by irradiation of Ariá samples.

The results indicate that while the modifications induced by γ -radiation are subtle, distinct changes are evident. All γ -radiation doses caused broadening of the semi-crystalline peaks and an increase in the relative intensities at $2\theta \approx 13^\circ$, 16° , and 20° , as indicated by the arrows in the °Figure 25. As extensively discussed in Chapter 1, the observed peak broadening in all samples can be attributed to three primary factors: (i) a reduction in the average size of the organized domains, (ii) an increase in structural defects within the semi-crystalline phase, or (iii) instrumental effects. It is important to highlight that, as described in Chapter 2, to account for instrumental contributions, measurements were conducted on a LaB_6 standard sample. These effects were further minimized using the Rietveld refinement method, which then mathematically corrected instrumental influences in the diffraction pattern.

The observed increase in the baseline intensity proportional to radiation dose, also indicated by arrows in Figure 25, may result from an increase in the amorphous component,

reflecting a reduction in overall crystallinity. Alternatively, it may stem from a shift in the relative phase proportions of A-type starch compared to B-type starch. These changes provide insights into the structural transformations induced by γ -radiation, underscoring its impact on the semi-crystalline and amorphous components of the starch.

Figure 26 presents the X-ray diffraction (XRD) patterns of Ariá starch (before γ -radiation treatment) across four distinct 2θ ranges.

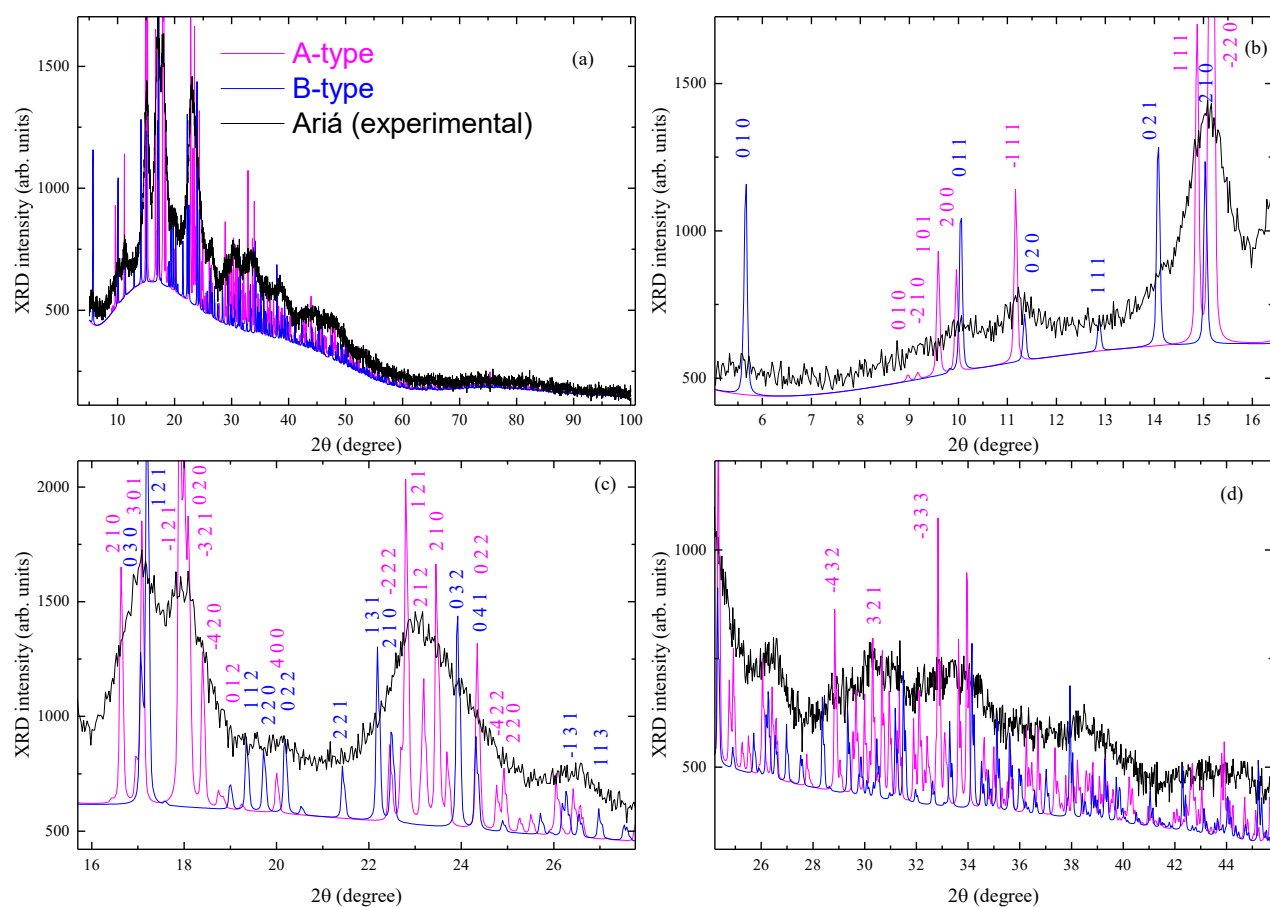


Figure 26 – XRD patterns of Ariá starch overlapped the theoretical patterns of A-type and B-type starch perfect crystals, in different ranges of 2θ .

These figures aim to index the peaks corresponding to A- and B-type semi-crystals and elucidate the structural effects of γ -radiation on the starch. In an ideal scenario, where crystals are defect-free, infinite in size, and devoid of instrumental influences, the diffraction peaks

would appear narrow, intense, and well-defined. Such an idealized pattern can be simulated using crystallographic data combined with software like Mercury (Macrae et al., 2006, 2008), facilitating peak identification for corresponding crystalline planes.

Figure 26 (a) overlays the experimental XRD pattern of Ariá starch ($2\theta = 5^\circ\text{--}100^\circ$) with the idealized patterns for A- and B-type semi-crystals, derived from crystallographic information in the literature and (Popov et al., 2009) and (Pinto; Campelo; Michielon de Souza, 2020), respectively. The first peak, at $2\theta \approx 5^\circ$, corresponds to diffraction in the lamellar planes, a feature characteristic of type B crystals, and is indexed as the (0 1 0) plane. This peak is particularly noteworthy as its intensity is influenced by the random distribution of water molecules between the helices of B-type amylopectin structures (Pinto; Campelo; Michielon de Souza, 2020; Takahashi; Kumano; Nishikawa, 2004). Additionally, the second most intense peak of the B-type phase, observed at $2\theta = 14^\circ$ and indexed as (0 2 1), is distinct from the peaks of the A-type phase.

The peak at $2\theta = 15^\circ$, however, represents the convolution of multiple peaks: (1 1 1) and (-2 2 0) from the A-type phase, and (2 1 0) from the B-type phase, indicating the coexistence of both structural types. This overlapping, compounded by the contributions of the amorphous portion, presents a challenge for direct quantification. The increases in diffracted intensity at $2\theta \approx 13^\circ$, 16° , and 20° observed in Figure 25 (b) can now be attributed. Specifically, the peak at $2\theta = 13^\circ$ belongs to the B-type phase, while the increase at $2\theta = 16^\circ$ does not correspond to any semi-crystalline phase but instead indicates an increase in diffuse scattering from the amorphous component.

Figure 26 (c) highlights the asymmetry in the three most intense experimental peaks at $2\theta \approx 17^\circ$, 18° , and 23° , caused by the overlap of multiple peaks from both A- and B-type phases. In Figure 26 (d), the complexity becomes evident, making peak indexing unfeasible through simple visual inspection or manual mathematical fitting using functions such as Lorentzian, Gaussian, or Voigt. Microstructural characterization of starch nanocrystals is a topic of ongoing research, and this is a typical example of why traditional fitting methods often fail to accurately represent the diffraction patterns of semi-crystalline materials at the nanometric scale (Cheetham; Tao, 1998; Lopez-Rubio et al., 2008; Xie et al., 2014). As extensively defined in this work and is important to highlight once again? as crystallite size decreases, peak broadening intensifies due to microstructural effects, which overlap with the diffuse scattering from the amorphous phase, resulting in a summed pattern that obscures individual peak

contributions. This aspect is particularly significant for naturally nanometric and semi-crystalline materials such as starch. However, unlike potato starch, which is extensively documented in the literature, Ariá starch remains underexplored. Consequently, direct measurements are essential for advancing the understanding of its structural and functional properties.

To address these challenges, then, we used our approach of combining Rietveld refinement method (RM) to all obtained XRD. For the first time in the literature, with this method we were able to make the separation and quantification of the crystalline contributions from A- and B-type starches, as well as the amorphous portion. With RM we also studied microstructural effects, including crystallite size (D) and microstrain (ϵ). Crystallographic data from (Popov et al., 2009) and (Pinto; Campelo; Michielon de Souza, 2020) were used to define the A- and B-type starch crystal structures, providing a robust framework for analysis. This approach allowed for a detailed characterization of the structural transformations in Ariá starch, offering insights into the interplay between its crystalline and amorphous phases.

The unit cell parameters and microstructural values were refined iteratively until the convergence factors reached their minimum values. In all cases, convergence was efficiently achieved by adjusting the lattice parameters, line width components (Gaussian and Lorentzian) (Borges et al., 2018; Scardi; Leoni; Delhez, 2004), and the texture index (Pecharsky; Zavalij, 2005). The texture indices converged at value approximately 3. The quality of the refinement was assessed using the convergence factors χ^2 and R_{wp} , along with the residual curve. Acceptable refinement quality is indicated by χ^2 values approaching 1 and R_{wp} values below 0.1 (Toby, 2006). The convergence factors are detailed in **Table 6** and corresponding refined lattice parameters are presented in **Table 7**.

Table 6 - *Quality factors and weight fraction of Rietveld refinement of the three phases: amorphous (x_a), A-type (W_A), B-type (W_B) and the crystallinity (x_c).*

Sample	χ^2	R_{wp}	$x_a(\text{wt}\%)$	$W_A(\text{wt}\%)$	$W_B(\text{wt}\%)$	$x_c = W_A + W_B(\text{wt}\%)$
Raw Ariá starch	1.111	0.0496	77.824	18.822(3)	3.354(3)	22.176
1 kGy	1.108	0.0403	79.36	17.307(4)	3.333(3)	20.64
5 kGy	1.166	0.0484	78.356	18.578(5)	3.066(4)	21.644
20 kGy	1.211	0.0437	79.081	17.150(6)	3.769(5)	20.919
50 kGy	1.05	0.0379	79.396	17.012(1)	3.592(1)	20.604

Microstructural values as a function of γ -radiation dose are shown in **Table 7**.

Table 7 - Unit cell parameters of the A-type (named "A") and B-type (named "B") structure from the literature and obtained with Rietveld refinement analysis.

Sample	Phase	$a(\text{\AA})$	$b(\text{\AA})$	$c(\text{\AA})$	γ (°)	$V(\text{\AA}^3)$	D (nm)	$\langle \epsilon \rangle$ %
(Popov et al., 2009)	A	20.83(6)	11.45(4)	10.58(3)	122.0(2)	2140(11)	-	-
(Pinto; Campelo; Michielon de Souza, 2020)	B	18.169(5)	-	10.703(8)	120	3059.8(2)	-	-
Raw Ariá starch	A	21.03(8)	11.771(6)	10.623(7)	122.06(3)	2219(1)	124(3)	3.9(3)
	B	18.01(4)	-	10.54(8)	120	2962(16)	75(5)	3.6(2)
1 kGy	A	21.06(2)	11.78(1)	10.6(2)	122.2(5)	2226(2)	120(3)	5.0(4)
	B	17.97(8)	-	11.2(2)	120	3134(48)	57(5)	4.8(3)
5 kGy	A	21.05(1)	11.80(1)	10.63(1)	122.45(5)	2228(2)	109(3)	5.9(3)
	B	17.9(1)	-	11.802(2)	120	3432(68)	51(5)	8.9(4)
20 kGy	A	20.98(1)	11.82(1)	10.60(1)	122.06(4)	2227(2)	115(3)	5.6(4)
	B	18.161(1)	-	11.7(2)	120	3338(25)	60(7)	9.1(5)
50 kGy	A	21.00(2)	11.79(1)	10.58(1)	122.19(5)	2219(2)	102(2)	5.3(4)
	B	17.99(2)	-	12.9(2)	120	3605(58)	36(6)	6.0(5)

The mean crystallite sizes are consistent with literature values for both A- and B-type crystals (Le Corre; Angellier-Coussy, 2014; Le Corre; Bras; Dufresne, 2010) and reveal that A-type crystallites are nearly twice as large as those in the B-type phase. Additionally, lattice strains increased sharply at initial radiation doses. The observed continuous decrease in mean crystallite size and crystallinity, coupled with the increase in microstrain, aligns with the expected structural impacts of γ -radiation on starch (Gani et al., 2014; Kong et al., 2009; Zhu, 2016).

The following figures illustrate the representative XRD patterns of freeze-dried raw Ariá starch before and after γ -radiation treatment, overlaid with their corresponding Rietveld refinement simulations. The residual curve represents the difference between the experimental and simulated patterns, ideally appearing as a straight line.

Figure 27 displays the experimental XRD pattern of freeze-dried raw Ariá starch, overlaid with its respective Rietveld refinement simulation. The residual curve, shown in blue, represents the discrepancy between the experimental data and the simulated pattern.

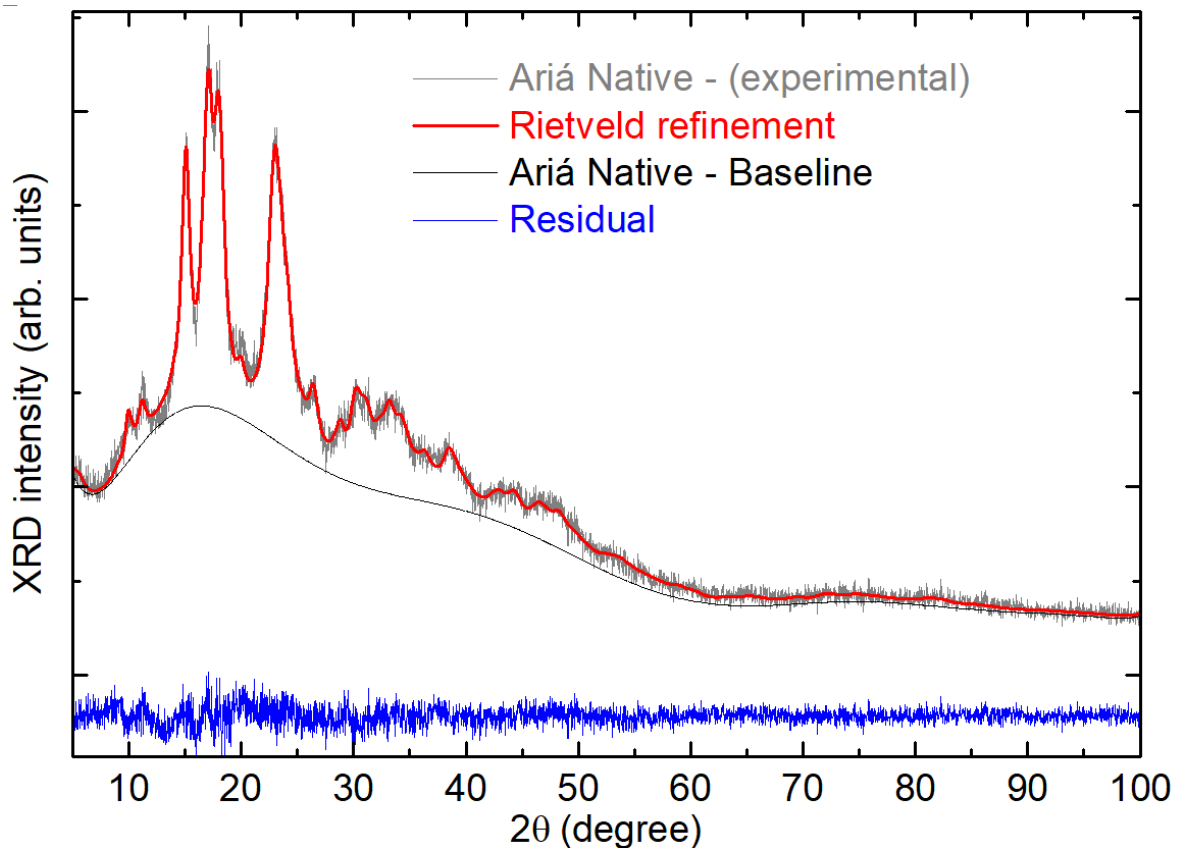


Figure 27 –Refined XRD patterns of freeze-dried raw Ariá starch.

To achieve an accurate Rietveld refinement, particular attention was given to the region around $2\theta = 16^\circ$, which lacks semi-crystalline peaks or tailing effects caused by nanometric crystallites. The refinement approach followed our methodology and the disordered component and inelastic scattering background were modeled using Chebyshev polynomials. The number of terms optimized was based on the smallest convergence factors and a well-defined residual curve. For this study, though, more terms to the Chebyshev polynomials were necessary: in this study we employed 15–20 terms.

Similarly, Figure 28 displays the experimental XRD pattern of Ariá starch that underwent γ -irradiation of namely dose 20kGy, overlaid with its respective Rietveld refinement simulation and residual curve.

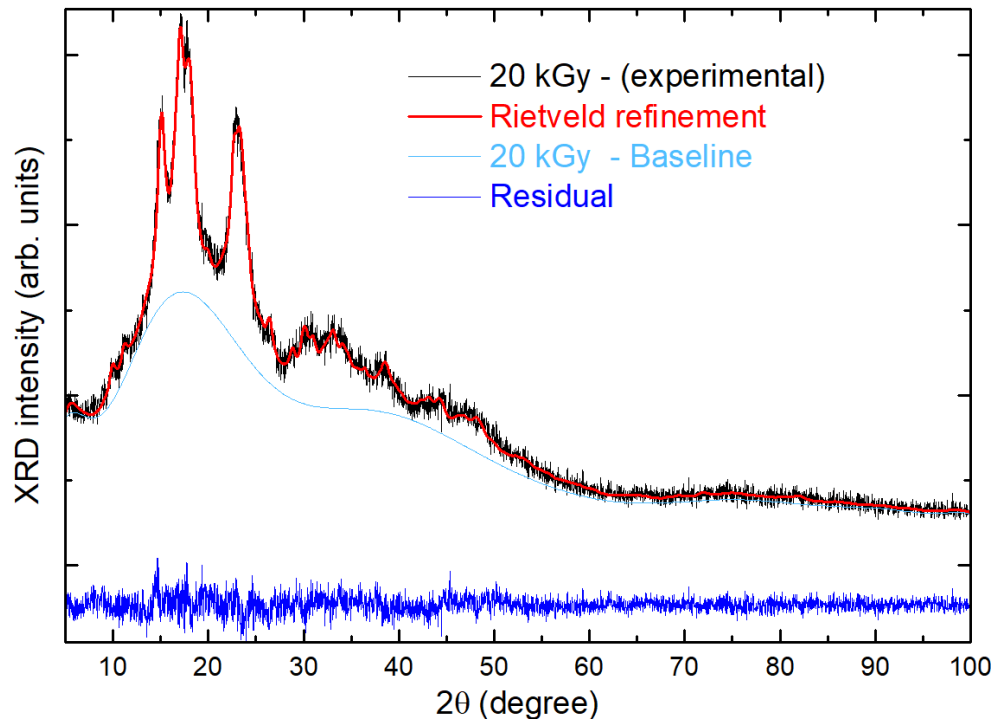


Figure 28 – Refined XRD patterns of Ariá starch sample submitted to 20kGy.

Lastly, Figure 29 presents the experimental XRD pattern of Ariá starch treated with the higher dose of 50kGy γ -radiation, overlaid with its respective Rietveld refinement simulation and residual curve.

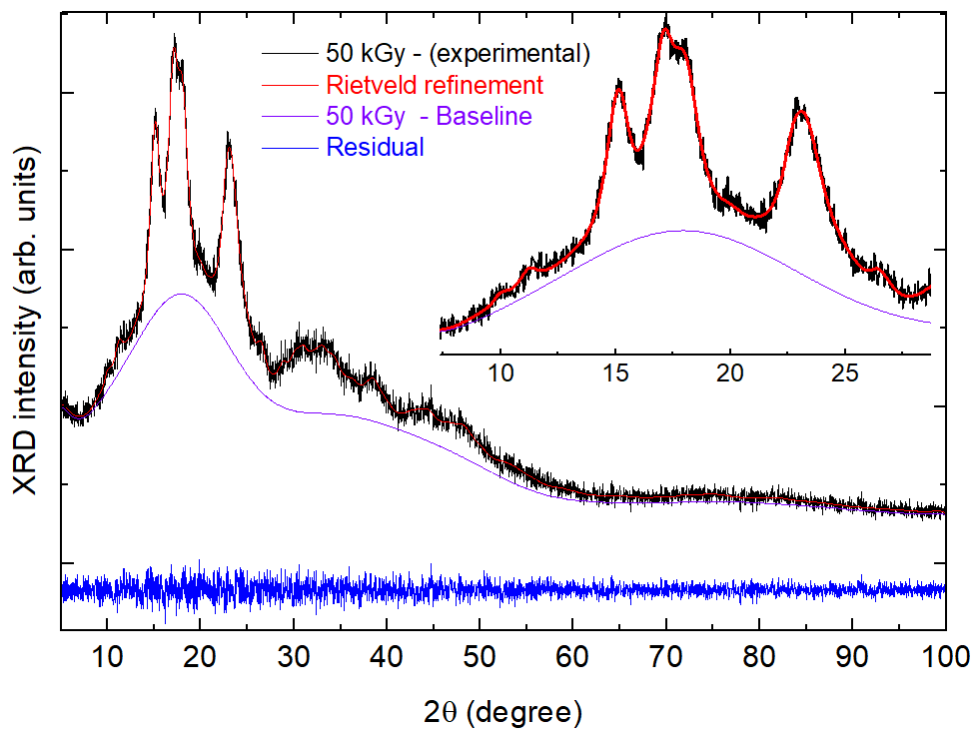


Figure 29 – Refined XRD patterns of Ariá starch sample submitted to 50kGy.

Given that increased γ -radiation doses may exert differential effects on distinct regions within the sample—namely, the crystalline regions of both A- and B-type phases, as well as the disordered (amorphous) regions—we became particularly intrigued by the potential to isolate and study the amorphous component in greater detail. This interest stems from the fact that the amorphous region, often overshadowed by the dominant semi-crystalline contributions, plays a crucial role in determining the functional properties of starch, including its thermal, rheological, and hydration behaviors.

To address this, we focused additional efforts on analyzing and refining the baseline components of the XRD patterns, which are indicative of the amorphous phase contributions. Figure 30 highlights these overlaid baselines, which were modeled and quantified to provide deeper insights into the changes occurring within the disordered regions of the starch as a function of γ -radiation dose. By refining the baselines using Chebyshev polynomials and comparing the results across treatments, we aimed to unravel the complex interplay between the semi-crystalline and amorphous phases, enhancing our understanding of how radiation-induced modifications influence the overall starch structure. This detailed analysis provides a foundation for further exploration of the role of the amorphous region in starch functionality and its response to processing conditions.

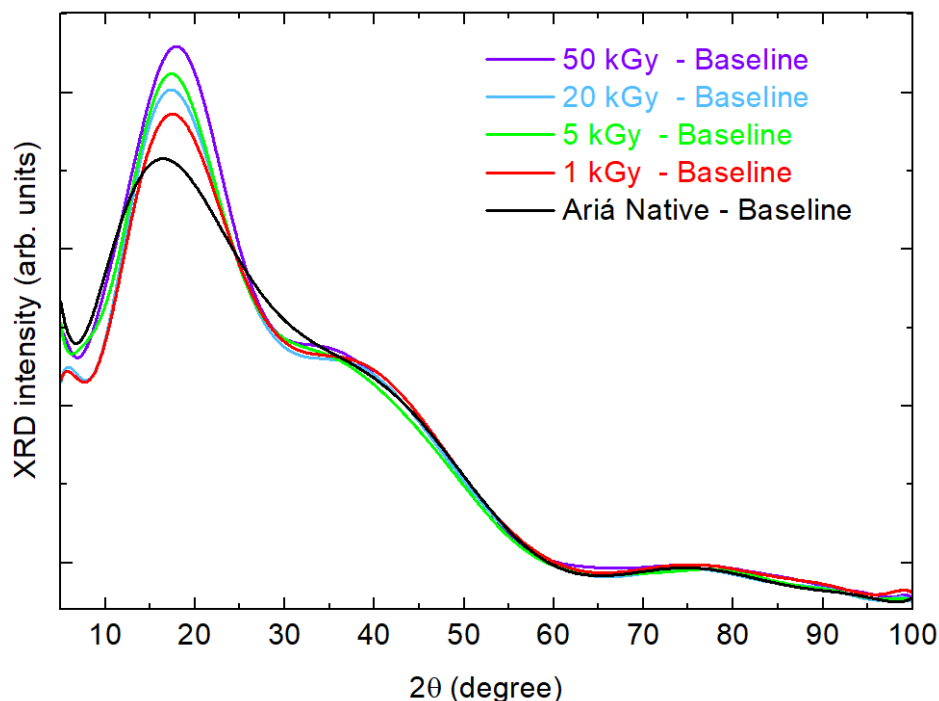


Figure 30 – The XRD baselines obtained from the Rietveld Refinement of freeze-dried raw Ariá and irradiated starch samples.

From the integrated intensity of the baselines in Figure 30, the proportion of the amorphous phase (x_a) and the semi-crystalline content, or crystallinity (x_c), were calculated. From previous literature, the native Ariá starch exhibited a crystallinity of 32% (Barros et al., 2020), consistent with previous publications, while freeze-drying reduced crystallinity to 22%, highlighting the role of moisture in determining starch crystallinity. The semi-crystalline contents of A-type W_A and B-type W_B phases were determined using Rietveld refinement, marking the first time the phase fractions of C-type starch (expressed as A- and B-type components) have been quantified via X-ray diffraction and the Rietveld method. As shown in **Table 6**, the amorphous phase increased slightly with higher γ -radiation doses. By mass conservation, assuming no volatilization of starch molecules, this increase in the amorphous phase occurs at the expense of the A-type phase, which decreases, while the B-type phase remains relatively stable. The superior resistance of B-type starch to γ -radiation may be attributed to its higher water content, with 36 water molecules per unit cell compared to 8 in A-type starch (Okazaki, 2018).

These results were highly encouraging, prompting further exploration of non-conventional modification techniques for Ariá starch, including cold plasma treatments with varying tension and excitation frequencies.

4.1 Cold plasma treatment of Ariá starch

Cold plasma technology has gained considerable attention in the food industry for its diverse applications in food safety, preservation, and the structural and functional modification of food components, particularly starches (Dong et al., 2017; Muhammad et al., 2018). This eco-friendly, non-thermal method employs ionized gas at atmospheric pressure to inactivate microorganisms and modify food materials without compromising their quality (Noriega et al., 2011; Sarangapani et al., 2016). The effectiveness of cold plasma treatment is influenced by several operational parameters, including voltage, excitation frequency, gas composition, and processing time, all of which can be optimized to achieve desired outcomes, particularly in starch modification (Nithya C et al., 2023).

Plasma operates through the interaction of reactive species, such as electrons, ions, and free radicals, with food components (Harikrishna et al., 2023; Sudheesh et al., 2019). When applied to starch, these interactions can lead to three primary modification mechanisms:

crosslinking, depolymerization, and chemical reactions (Thirumdas; Sarangapani; Annapure, 2015).

This study aimed to investigate the impact of cold plasma varying excitation frequencies (0–550 Hz) and generation voltage (7, 10, 14, and 20 kV) on the physicochemical and functional properties of Ariá starch, exploring its potential as an innovative food ingredient. Key aspects analyzed include the morphological structure of Ariá starch and the associated changes in crystallinity type, amylose content, starch digestibility, gel hydration capacity, and pasting and thermal properties. These comprehensive evaluations were both published, highlighting the potential of cold plasma as a transformative tool for enhancing the functional versatility of starches in food applications.

4.1.1 Variation of Cold plasma excitation frequency

i. Starch modification process: cold plasma with varying excitation frequency

Approximately 20 g of Ariá starch powder were evenly distributed in glass Petri dishes ($\varnothing = 90$ mm), forming a layer approximately 3 mm thick. The samples were subjected to atmospheric cold plasma treatment using a parallel plate system (Model PLS 0130, Inergiae, Brazil) at five different excitation frequencies: 50, 100, 200, 350, and 550 Hz. The electrical voltage was maintained at 20 kV, with a processing time of 15 minutes and a 15 mm gap between the electrodes, constant across all treatments. Following the plasma treatment, the starch samples were stored in laminated polypropylene packages at room temperature, protected from moisture, until further analysis.

ii. XRD characterization and Rietveld Refinement

The XRD patterns of native and cold plasma-treated *Ariá* starch samples are presented in Figure 31. The effects of cold plasma on the XRD profiles revealed slight differences, primarily associated with peak broadening. This phenomenon can be attributed to two main factors, as extensively defined in this work: a reduction in crystallite size and/or an increase in defect density within the crystal lattice. Additionally, diffuse scattering from disordered components (e.g., amylose, water, and air) or inelastic scattering phenomena (e.g., Compton

scattering, atomic absorption, fluorescence) could also contribute to this effect. However, since all measurements were conducted under identical conditions, the background contribution, which lacks structural information, remains constant across all samples. Thus, the observed profile changes are likely due to cold plasma-induced modifications in amylopectin and amylose within the starch.

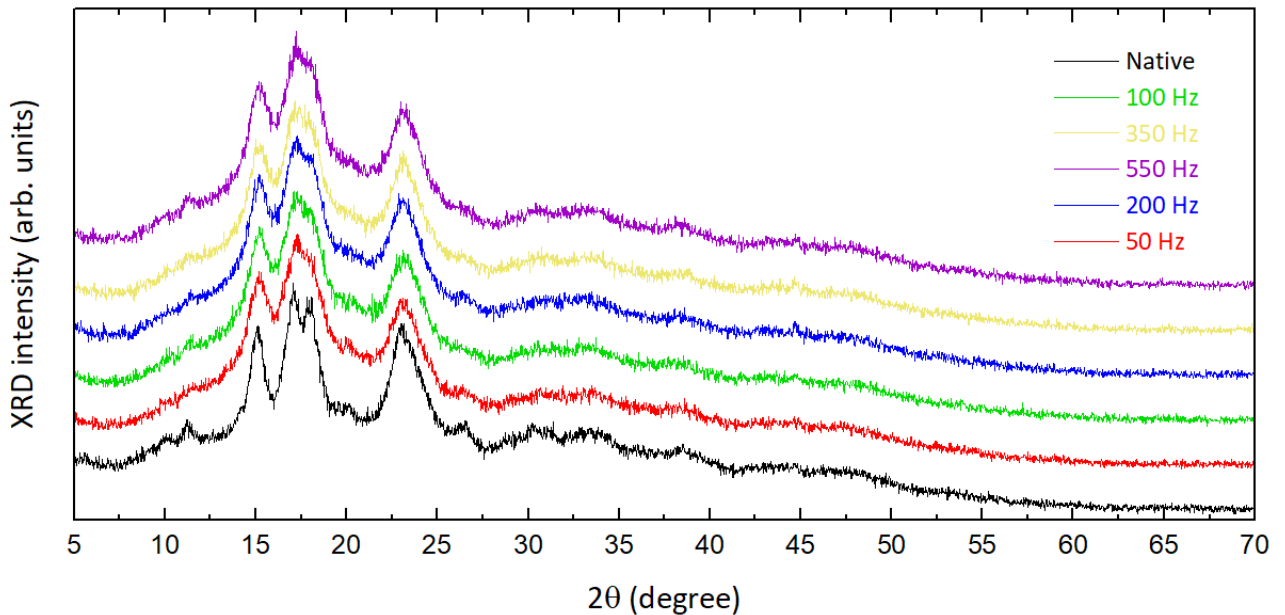


Figure 31 - XRD patterns of native and cold plasma treated starches.

To achieve a comprehensive and accurate characterization of the microstructural changes induced by cold plasma, the Rietveld refinement method was applied to the XRD data. Crystallinity was quantified by the relative integrated areas of the crystalline and amorphous phases. The following figures depict the Rietveld refinement results for cold plasma treatments at frequencies of 50, 100, 200, 350, and 550 Hz. All figures obey the same design: experimental XRD data in grey, refined result in red, background in green and residual line in pink. The close agreement between the calculated curves and experimental patterns confirms the reliability of the refinements, as indicated by the residual curves and low values of quality factors χ^2 and R_{wp} .

Figure 32 depicts the refined XRD data obtained for sample that underwent cold plasma treatment with 50Hz.

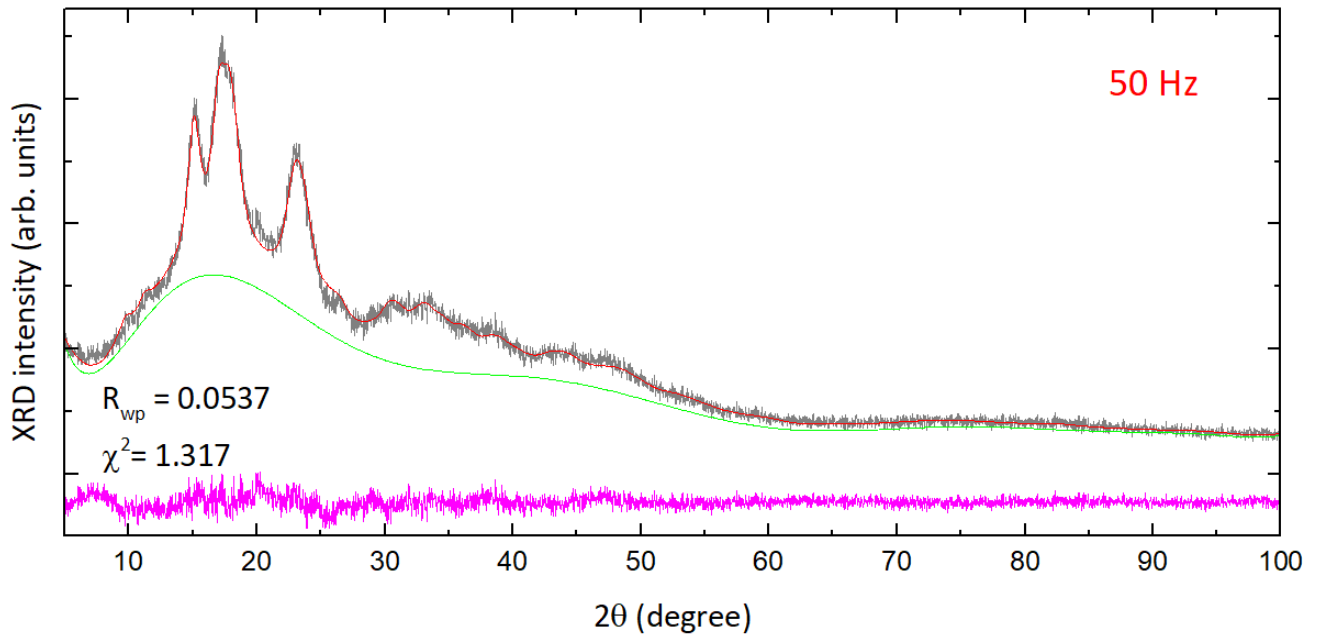


Figure 32 - The XRD data Rietveld refinement method was applied to the starch samples treated with cold plasma at 50 Hz.

In Figure 33 it can be seen the refined XRD data obtained for sample that underwent cold plasma treatment with 100Hz.

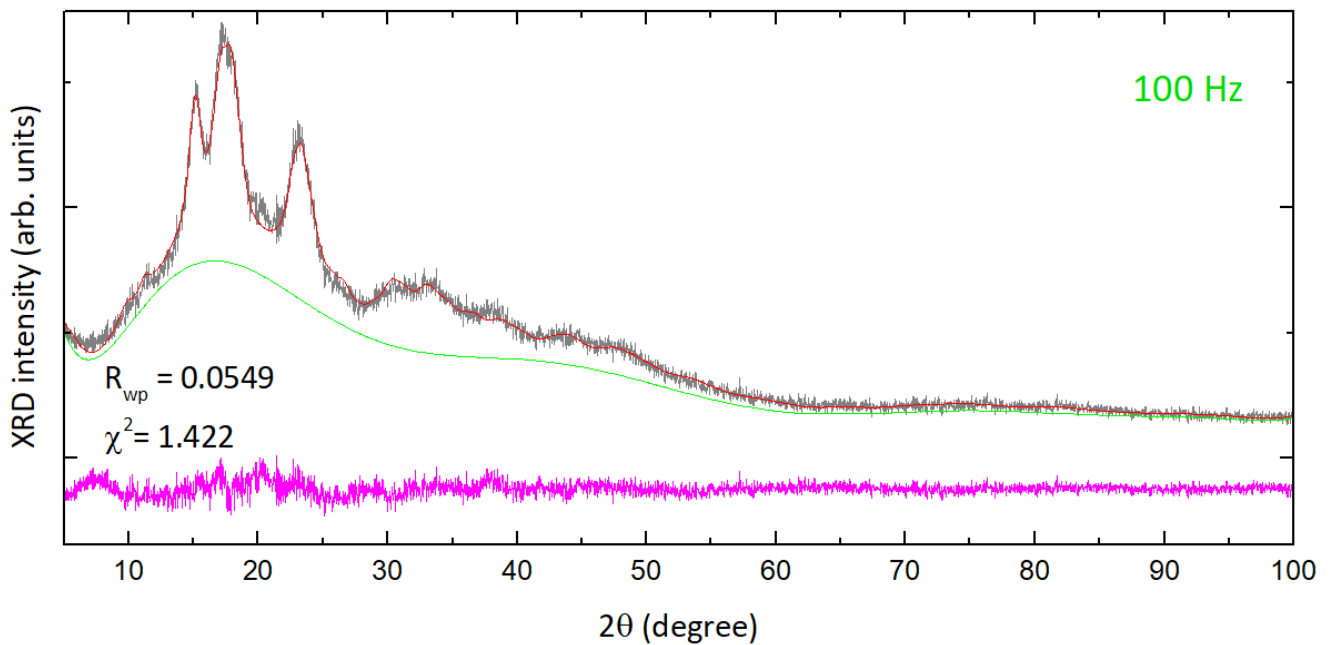


Figure 33 - The XRD data Rietveld refinement method was applied to the starch samples treated with cold plasma at 100 Hz.

XRD data obtained for sample that underwent cold plasma treatment with 200Hz is shown on Figure 34.

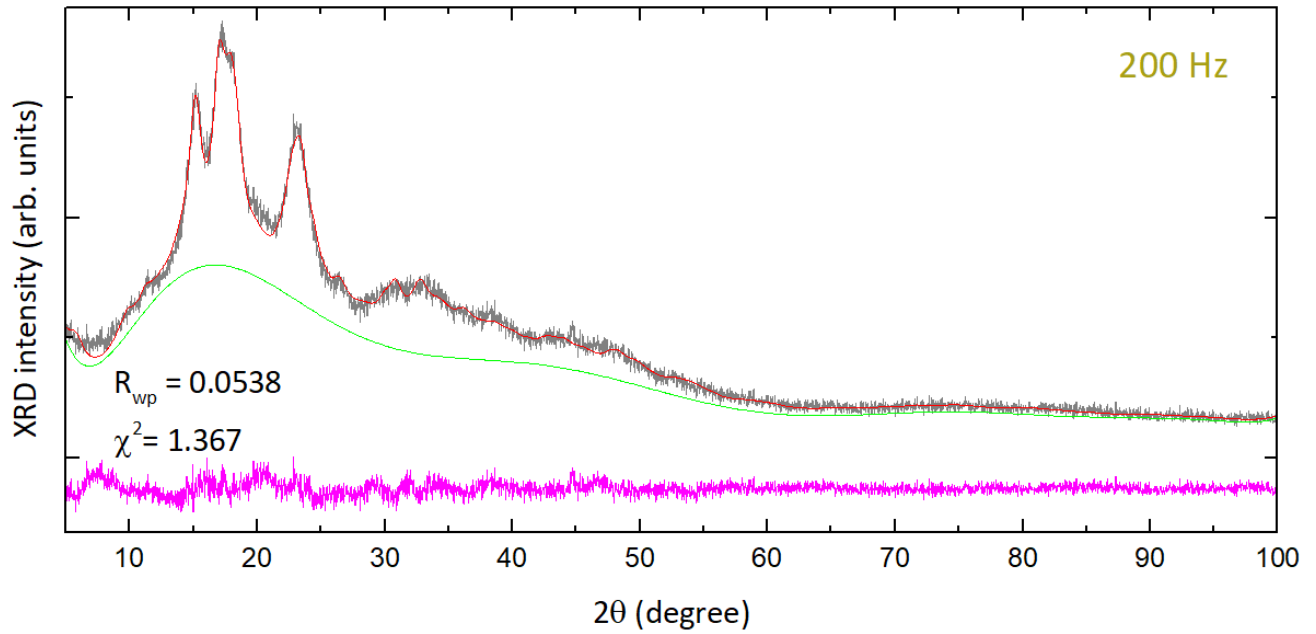


Figure 34 - The XRD data Rietveld refinement method was applied to the starch samples treated with cold plasma at 200 Hz.

The sample treated with 350Hz can be seen at Figure 35.

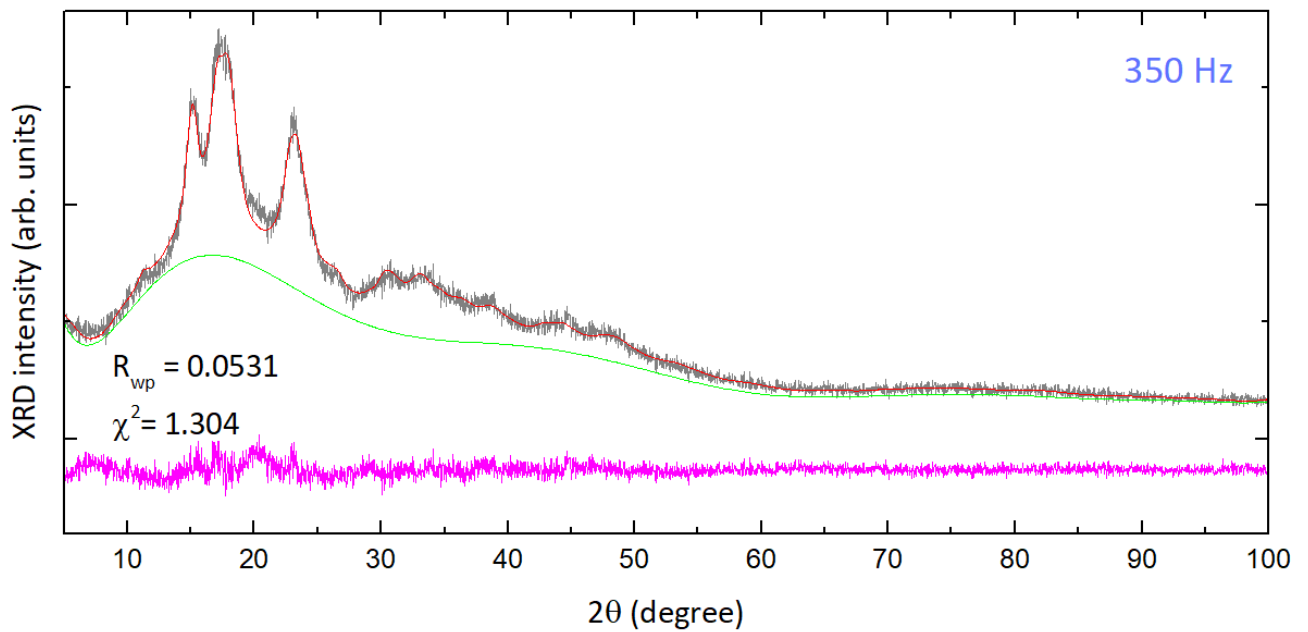


Figure 35 - The XRD data Rietveld refinement method was applied to the starch samples treated with cold plasma at 350 Hz.

Lastly, sample that underwent cold plasma treatment with 550Hz can be seen at Figure 36.

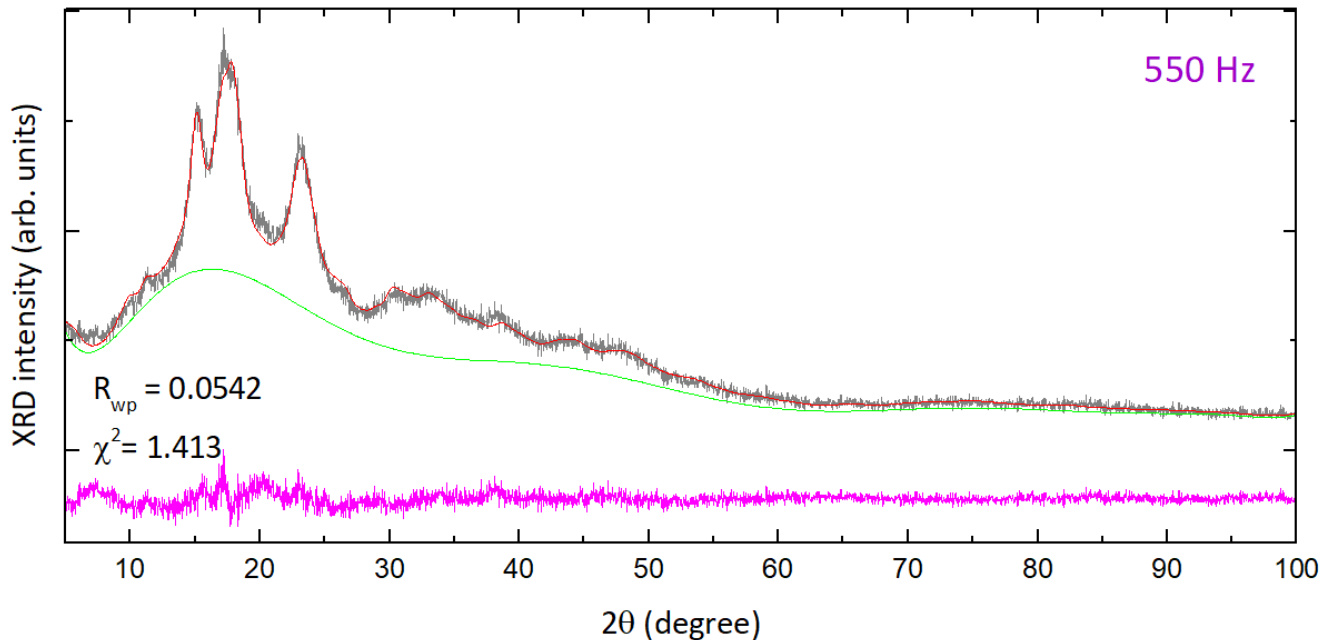


Figure 36 - The XRD data Rietveld refinement method was applied to the starch samples treated with cold plasma at 550 Hz.

Table 8 summarizes the Rietveld refinement results for *Ariá* starch under cold plasma treatments. While no significant changes were observed in unit cell parameters, minor fluctuations were detected, likely due to the overlapping of peaks from A- and B-type phases as we reported earlier in this chapter and in literature (Pinto et al., 2021a). An increase in crystallinity with higher frequencies was noted, suggesting that cold plasma promotes greater organization in amylopectin or reduces the amylose mass fraction. Assuming total mass conservation during processing, it can be inferred that a small fraction of amylose was converted to amylopectin, particularly at 200 Hz, where crystallinity increased by approximately 18% compared to the native sample.

The average crystallite size also reflected the impact of cold plasma. At 200 Hz, crystallite size increased by approximately 14% relative to the native sample, potentially indicating enhanced cross-linking within the organized domains of amylopectin. This finding aligns with Zhu (Zhu, 2016), who reported an increase in molecular size induced by plasma treatments. Similarly, Cheetham and Tao (Cheetham; Tao, 1998) observed that long amylose chains favor the formation of B-type crystallinity, while shorter chains promote A-type crystal formation in maize starches.

Table 8 - Parameters and results of the from the Rietveld refinement method for the cold plasma treatments with different frequency of aria starch.

Samples	x_c (%)	Starch	a (Å)	b (Å)	c (Å)	γ (°)	V (Å ³)	D (Å)	ϵ (%)	W (%)
Native	22.176	A-type	21.026(8)	11.771(6)	10.623(7)	122.06(1)	2218(1)	124(2)	3.9(3)	18.82
		B-type	18.01(4)	--	10.54(8)	--	2962(16)	75(5)	3.6(2)	3.35
50 Hz	24.918	A-type	21.02(2)	11.778(8)	10.59(1)	122.12(7)	2220(3)	96(4)	6.6(3)	17.58
		B-type	17.2(9)	--	12.1(2)	--	31279(38)	30(3)	14(1)	7.34
100 Hz	25.651	A-type	20.84(2)	11.734(9)	10.689(9)	121.95(7)	2218(3)	100(5)	6.0(5)	17.82
		B-type	17.70(8)	--	12.1(1)	--	3279(27)	42(4)	12(2)	7.83
200 Hz	27.02	A-type	20.89(2)	17.767(8)	10.67(2)	121.85(7)	2216(3)	142(10)	7.6(4)	15.66
		B-type	17.77(6)	--	11.57(9)	--	3162(22)	36(2)	10(2)	11.35
350 Hz	25.051	A-type	20.887(2)	11.734(8)	10.61(2)	121.93(6)	2207(3)	104(5)	6.6(5)	17.79
		B-type	17.89(8)	--	11.5(1)	--	3178(31)	35(2)	5(1)	7.25
550 Hz	26.252	A-type	20.863(2)	11.746(9)	10.62(2)	122.029(6)	2206(2)	101(5)	5.7(5)	18.36
		B-type	17.87(6)	--	11.65(7)	--	3221(20)	46(3)	7(2)	7.88

x_c : Crystallinity, a, b, c and γ : lattice parameters, V : volume of unit cell, D : average size of crystallites, ϵ : micro-tension percentage of network, W : phase fraction. Type A (monoclinic) and type B (hexagonal) starches.

The distinct effects observed at 200 Hz remain insufficiently understood and require further confirmatory studies. While temperature variations during plasma treatment (Birania et al., 2022; Mir; Shah; Mir, 2016) may play a role, the applied plasma conditions appear to serve as a valuable tool for achieving controlled polymorphic changes in starch. These findings open avenues for tailoring starch properties using cold plasma as a non-thermal modification technique.

Overall, cold plasma application had minimal impact on the morphology of *Ariá* starch granules, although the treatment at 200 Hz induced some surface damage. This observation aligns with findings reported in the literature for similar polysaccharides and corresponds to an increase in carboxyl and carbonyl group content as we reported in (Pinto et al., 2023). X-ray diffraction analysis provided detailed insights into the microstructure of the starch, revealing that higher crystallinity levels were achieved as the frequency increased, with the most pronounced effects observed at 200 Hz.

Next, the same samples underwent slightly different treatment, now varying generation voltage.

4.1.2 Variation of Cold plasma generation voltage

i. Starch modification process: cold plasma with varying generation voltage

Starch samples (20 g) were evenly distributed on glass Petri dishes ($\varnothing = 90$ mm) to form a uniform 3 mm layer. The samples were treated using a dielectric barrier plasma system (Model PLS 0130, Inergiae, Brazil) at a control voltage (0 kV) and four different high voltages for plasma generation: 7, 10, 14, and 20 kV. The plasma excitation frequency was fixed (200 Hz), treatment duration (15 minutes), and the distance between the aluminum electrodes (15 mm) were maintained constant across all treatments. Processing was conducted at room temperature ($\sim 25^{\circ}\text{C}$) under average atmospheric pressure (1013 MPa) using ambient air as the working gas. Following plasma treatment, the starch samples were stored in plastic containers to prevent moisture exposure and kept at room temperature until further analysis.

ii. XRD characterization and Rietveld Refinement

Figure 37 presents the microstructural effects of various cold plasma generation voltages on *Ariá* starch, as revealed by X-ray diffraction (XRD) analysis. Measurements were conducted over a 2θ range of 5° to 100° , capturing the scattering from amylopectin (semi-crystalline component) and amylose (non-crystalline component) without truncating the XRD pattern.

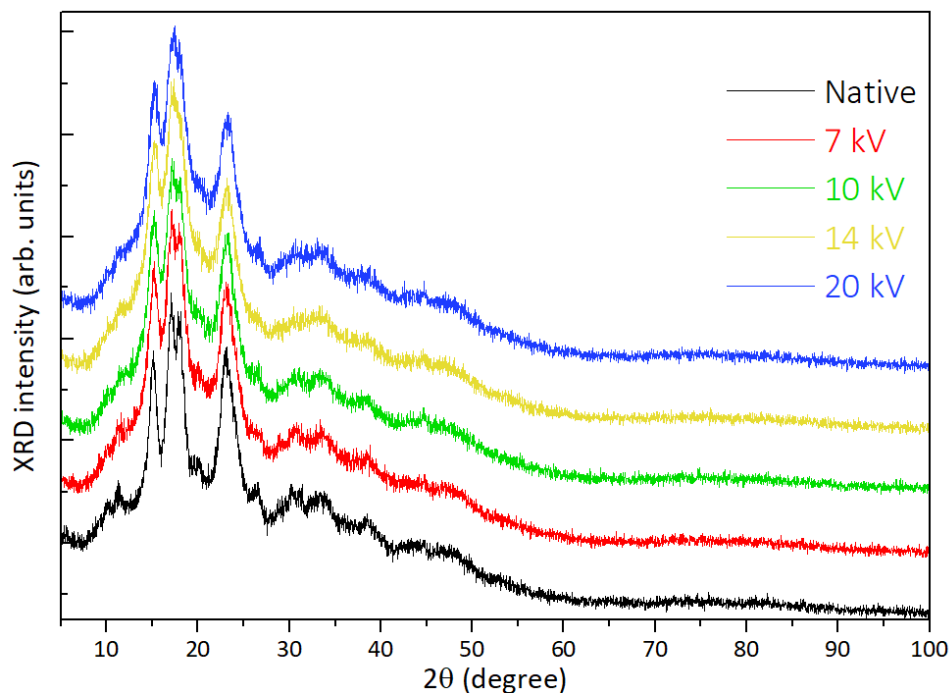


Figure 37 – XRD patterns of *Ariá* samples before and after cold plasma treatment with varying voltage.

Figure 38 displays normalized XRD patterns, emphasizing the effects of plasma voltage on the lyophilized native starch.

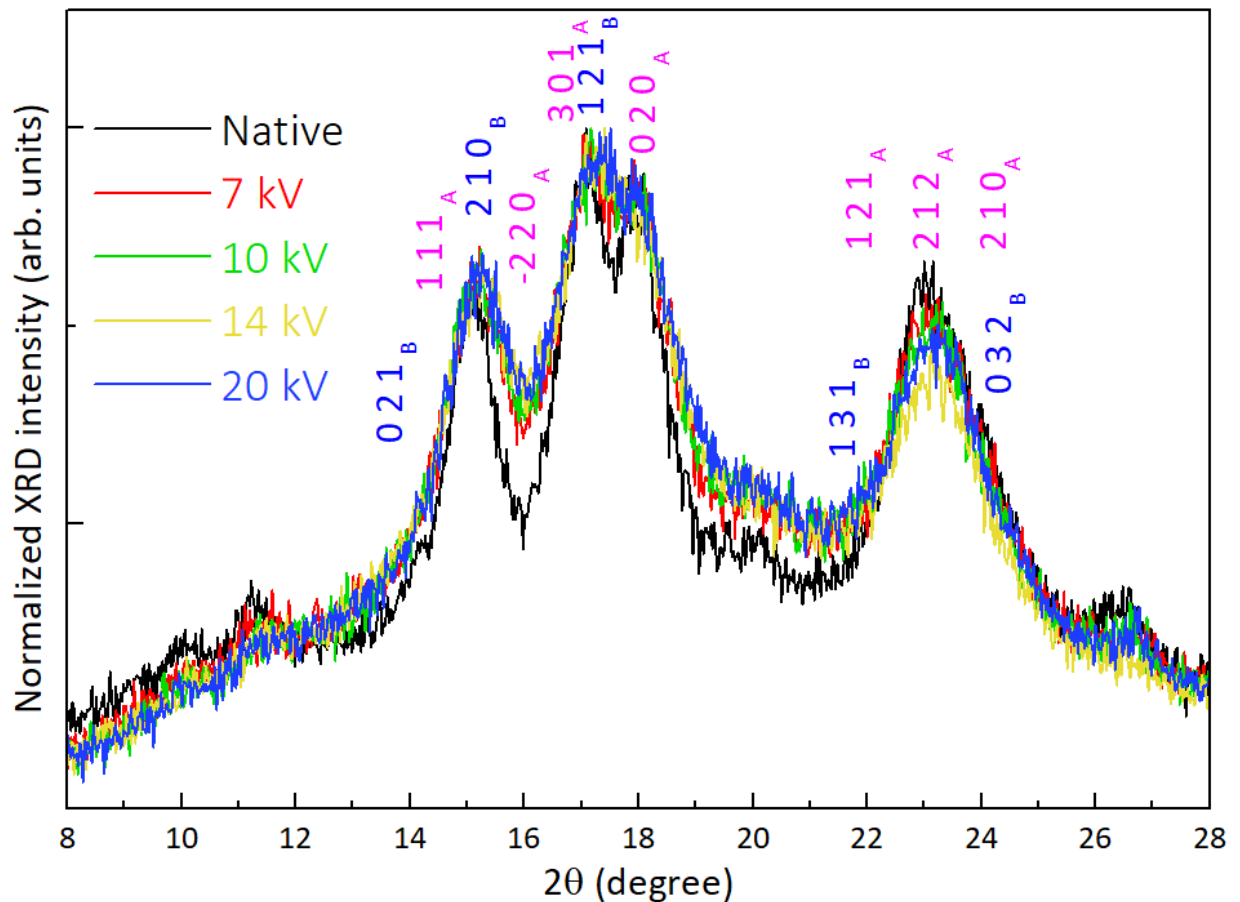


Figure 38 – Normalized XRD patterns of Ariá samples before and after cold plasma treatment with varying voltage.

Most observed peaks result from the overlap of A- and B-type phases, except for the peak near $2\theta \approx 18^\circ$, which is exclusively associated with phase A. Notably, the region around $2\theta \approx 16^\circ$, marked with an asterisk, lacks any defined peaks from the crystalline phases. Again, as we've defined in this work before, the intensity increase in this region can be attributed to two potential factors: (i) peak broadening caused by reduced average crystallite size and increased defect density or microstrain, and/or (ii) an increase in the amorphous component.

To better understand the origin of these changes and quantify the crystallographic parameters, again we applied the Rietveld refinement method. Figure 39 illustrates the Rietveld refinement of the XRD pattern for the sample treated at 14 kV, showing excellent agreement between the experimental data and the simulated curve, as indicated by the residual line and low convergence factors χ^2 and R_{wp} .

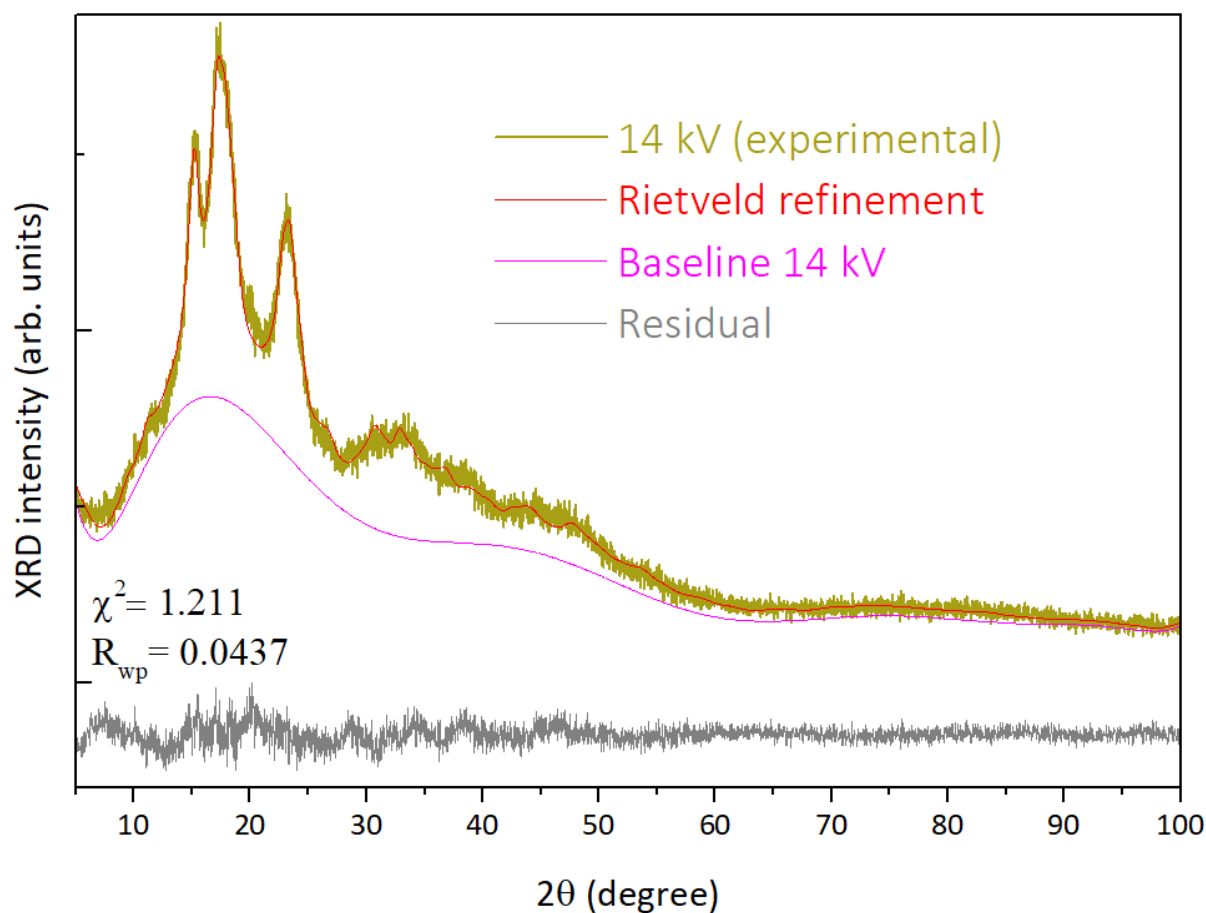


Figure 39 – Refined XRD patterns of the sample treated at 14 kV.

The pink curve corresponds to the baseline maximum, modeled with an 11-term Chebyshev polynomial, further demonstrating the refinement's accuracy. Crystallographic parameters, convergence factors, and microstructural properties are summarized in Table 9.

Table 9 - Unit cell parameters refined using the Rietveld method for A-type starch (monoclinic, $a \neq b \neq c$) and B-type starch (hexagonal, $a = b \neq c$) along with quality factors of aria starch treated with different voltages.

T (kV)	Starch	a (Å)	b (Å)	c (Å)	γ (°)	V (Å ³)	χ^2	R_{wp}
0	A-type	21.026(8)	11.771(6)	10.623(7)	122.06(1)	2218(1)	1.111	0.0496
	B-type	18.01(4)		10.54(8)		2962(16)		
7	A-type	21.12(2)	11.86(2)	10.45(2)	122.31(2)	2211(3)	1.569	0.0576
	B-type	17.97(1)		11.2(2)		3134(48)		
10	A-type	21.11(1)	11.81(1)	10.59(1)	122.26(1)	2232(3)	1.066	0.0484
	B-type	17.75(3)		11.1(1)		3018(17)		
14	A-type	20.88(2)	11.758(9)	10.69(1)	122.06(3)	2224(4)	1.211	0.0437
	B-type	17.72(1)		11.9(3)		3239(27)		
20	A-type	20.91(2)	11.78(1)	10.57(2)	122.00(4)	2206(3)	1.05	0.0379
	B-type	17.98(1)		12.8(2)		3605(58)		

Table 10 summarizes other information extracted from the refinement, such as crystallite size (D), lattice microstrain percentage (ϵ), phase fraction (W), and crystallinity (x_c).

Table 10 - Average crystallite size (D), lattice microstrain percentage (ϵ), phase fraction (W), and crystallinity (x_c) of *aria* starch treated with different voltages

T (kV)	Starch	$D(\text{\AA})$	ϵ (%)	$W(\text{wt}\%)$	$x_c(\text{wt}\%)$
0	A-type	124(2)	3.9(3)	18.822(3)	22.176
	B-type	75(5)	3.6(9)	3.354(3)	
7	A-type	80(2)	3.5(3)	22.699(3)	26.45
	B-type	41(3)	4.1(8)	3.75(5)	
10	A-type	80(4)	2.8(4)	22.752(2)	26.49
	B-type	42(2)	4.9(3)	3.74(3)	
14	A-type	78(2)	3.2(4)	17.487(4)	27.1
	B-type	27(3)	10(3)	9.58(2)	
20	A-type	81(3)	3.2(2)	23.607(2)	28.59
	B-type	25(2)	5(1)	4.98(5)	

Figure 40 overlays the baselines obtained from the Rietveld method for native and plasma-treated *Ariá* samples, illustrating changes in crystallinity x_c and the amorphous phase.

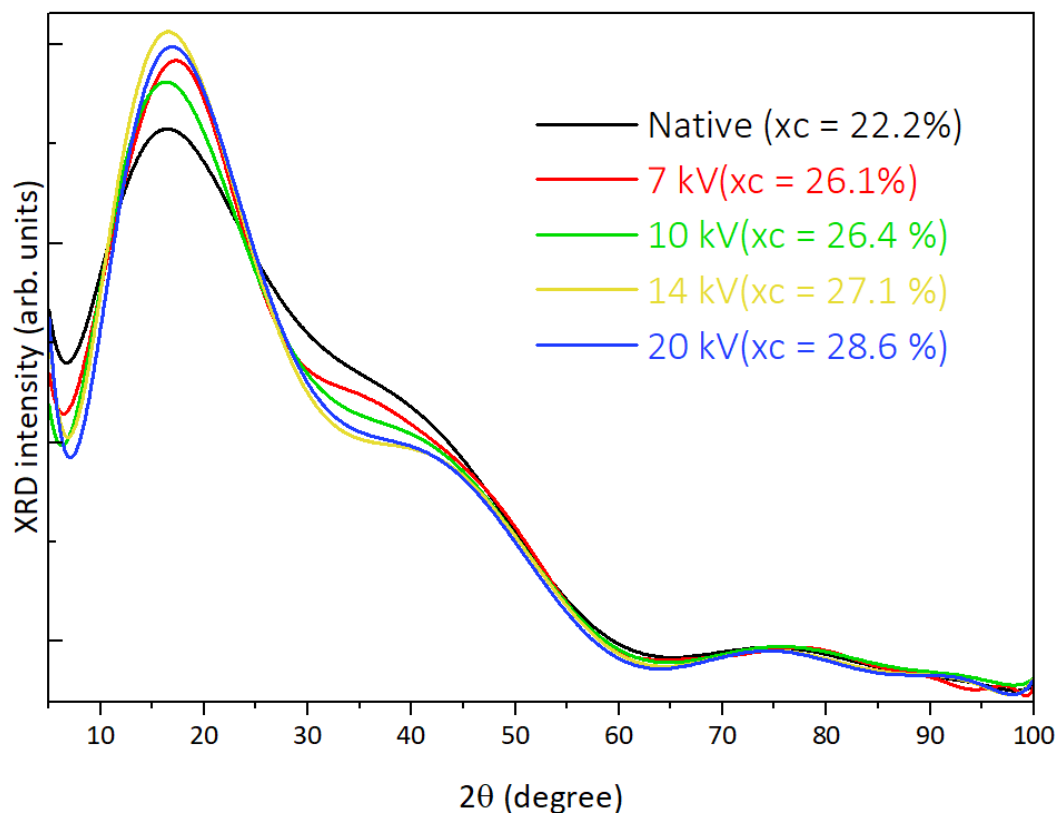


Figure 40 – Baselines of freeze-dried samples before and after plasma treatment.

The unit cell parameters showed slight variations, while average crystallite sizes decreased significantly with increasing plasma voltage. Crystallinity increased, corresponding to a reduction in the amorphous phase, consistent with a decrease in amylose content. This finding aligns with prior studies (Gao et al., 2019) that suggest cold plasma primarily acts on the amorphous phase, breaking it down into smaller molecular sugars and thereby increasing the crystalline phase.

The depolymerization of starch chains by plasma may also involve intrinsic water within the helical structure. Reactive plasma species can excite water molecules, making them active participants in glycosidic bond cleavage (Zhang et al., 2020). This effect appears particularly pronounced at 14 kV, where phase A shows a notable reduction, as evidenced by the diminished intensity of the 2 1 2 peak at $2\theta \approx 23^\circ$. Table 10 further confirms the relative decrease in phase A compared to phase B. This phenomenon may be due to the shorter, closely branched amylopectin chains in A-type crystals, which are more susceptible to degradation by reactive water species within the crystalline structure (Zhang et al., 2020). Concurrently, B-phase content increased, likely due to this preferential degradation of A-type chains.

In summary, cold plasma affects starch structure in two primary ways: (i) reducing the amorphous phase during initial processing due to its higher reactivity with plasma-generated species and (ii) inducing the formation of reactive water species within starch crystals, resulting in internal structural modifications. These findings highlight the potential of cold plasma as a tool for tailoring starch properties by targeting specific structural components.

Cold plasma with varying operational parameters and gamma irradiation were applied to *Ariá* starch samples as non-conventional methods to induce structural modifications. These subtle changes were effectively analyzed using X-ray diffraction (XRD) in combination with the Rietveld refinement method. Furthermore, the potential for studying additional samples using these techniques is demonstrated in the final chapter of this thesis.

CHAPTER 5 – RESULTS III

Science Strengthened Through Collaboration: Investigating alternative Starch Sources from Amazon Biome

Through collaborations, we studied other unconventional starch sources from Amazonian Biome such as Thorny Cará. We also extend the scope of our research beyond national borders to a neighboring country that shares the Amazon rainforest with us: Peru. Focused on Andean beans and corns, we examined their unique structural and compositional characteristics through a close partnership with other accomplished female researchers, emphasizing the power of interdisciplinary and international collaboration. This collaborative effort not only enriches our understanding of these important staples but also underscores the role of cooperative scientific endeavors in advancing knowledge across borders and disciplines.

The study of new starch sources from unconventional origins, such as Amazonian roots and cereals, holds immense potential for advancing food science, materials engineering, and sustainability. These underutilized starches offer unique physicochemical and functional properties that can differ significantly from conventional sources like corn, wheat, and potato, reducing the use of commoditized food sources and monotony in dietary patterns (lack of diversity in food options) (Salvador-Reyes; Clerici, 2020). Additionally, the recovery of ancient habits of consuming native plants aligns with growing consumer interest in deep-rooted regional products that carry designations of origin and distinctive properties (Salvador-Reyes et al., 2021). Amazonian starches, for instance, often exhibit appealing colors, distinct textures, and unique structural characteristics that reflect their adaptation to the region's diverse ecosystems. These attributes not only enhance their value in food applications but also support the preservation of traditional agricultural practices, fostering cultural continuity and sustainability (Salvador-Reyes et al., 2024). By tapping into the potential of these native starches, research can diversify supply chains, meet the demand for innovative and authentic

products, and contribute to the development of renewable materials for food, bioplastics, and pharmaceuticals (Kennedy et al., 2011). To harness unconventional maize as a new starch source, scientists and industries must develop a profound understanding of these starches.

However, this research represents a challenging scientific endeavor that is difficult to pursue in isolation or within the confines of a single graduate program. To address the complexity and scope of this work, this chapter highlights a series of collaborative efforts involving both published and unpublished studies in synergy with Food scientists. These collaborations bring together diverse expertise and resources, expanding and enhancing the application of the methodology that combines X-ray diffraction (XRD) and Rietveld refinement for analyzing the structures of raw and processed starches from various sources. By leveraging the collective knowledge and skills of interdisciplinary teams, this chapter demonstrates the robustness and versatility of this analytical approach, providing critical insights into the structural transformations of starches across a range of treatments and origins.

Last but not least, these collaborations held profound significance for the author, emphasizing the critical need to address dietary monotony perpetuated by the commoditization of food supplies. They underscore the importance of fostering food security through the diversification of food resources, highlighting the value of Amazonian biodiversity for solving our own concerns as society. Moreover, this work serves as a testament to the importance of scientific protagonism by Amazonians in the study and sustainable utilization of Amazonian resources. By actively contributing to the research and knowledge production surrounding our region's natural wealth, we Amazonians assert our role as stewards and innovators in science, bridging cultural heritage with global scientific advancements.

5.1 Andean Fava beans

Peruvian fava beans (PFB) are a rich source of protein, fiber, vitamins, and minerals, widely cultivated across Peru's coastal and highland regions. These beans thrive in high altitudes, withstand cold temperatures, and contribute to soil enrichment through nitrogen fixation (Salvador-Reyes et al., 2024). Historically considered marginal food, their popularity has surged recently due to the rise of Peruvian gastronomy, increasing their production and commercial value. PFB are used in various food products, including bread, cookies, pasta, snacks, and gluten-free items, with significant industrial potential. However, despite their

diverse applications, gaps remain in understanding their physical, nutritional, and techno-functional properties, which are essential for optimizing their use in innovative and high-quality food products (Salvador-Reyes et al., 2024).

To achieve a more comprehensive understanding of the molecular organization of these starches and accurately quantify their crystalline content, X-ray diffraction (XRD) combined with the Rietveld refinement method proved to be a highly effective analytical approach.

i. Starch extraction

Following the method for isolating the starch described in (Ferrari Felisberto et al., 2020), the Peruvian fava beans was extracted from imported fava beans from Peru, and ground with water (1: 3 w / w) in an industrial blender. This pulp was then filtered on polyester fabrics and the starch was decanted for 24 h under refrigeration ($\sim 7\text{ }^{\circ}\text{C}$), with the supernatant being removed later. After the first decantation, the starch was resuspended and washed with distilled water. This process was repeated twice. After final decantation, the starch was freeze-dried ($-18\text{ }^{\circ}\text{C}$; 0.998 mbar; 3 days; equipment: Edwards High Vacuum, L4KR, SP, Brazil), and packed in laminated bags for further analysis. The total starch yield was 11% w/w.

ii. XRD characterization and Rietveld Refinement

The X-ray diffractograms of starch samples extracted from Peruanita (AFP), Quelco (AFQ), and Fava Verde (AFV) beans are presented in Figure 41 (A). The XRD patterns of the AFP and AFQ samples exhibit notable similarities, while the AFV sample displays differences in the intensities of the most prominent peaks, as well as variations in the intensity and shape of the background. All three samples were identified as having C-type starch semi-crystals. C-type starches are characterized by a combination of type A (monoclinic symmetry, space group B2 (Imberty; Chanzy; Perez, 1988)) and type B (hexagonal symmetry, space group P6₁ (Imberty; Perez, 1988)) polymorphs, along with an intrinsic amorphous component.

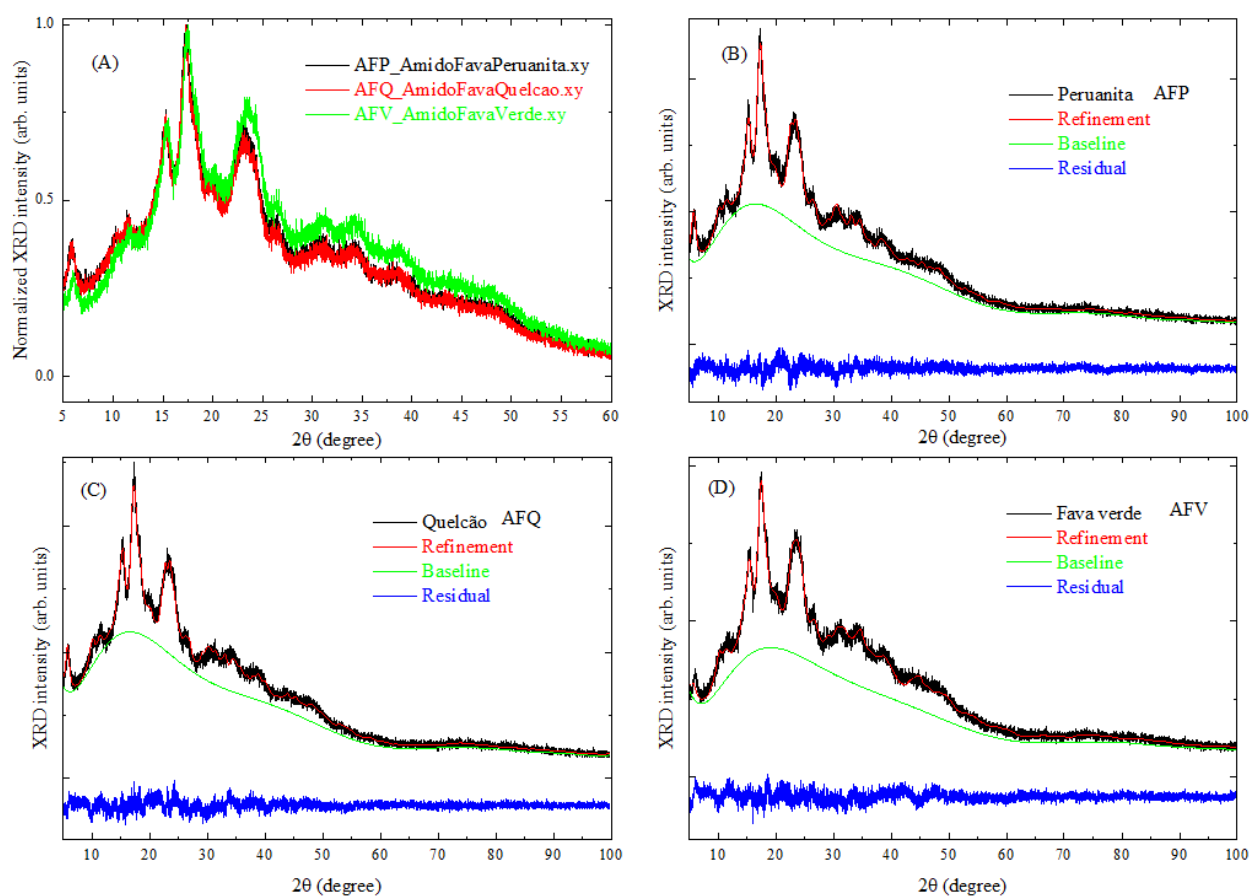


Figure 41 – (A) superposition of the normalized X-ray Diffraction Patterns of the starch samples extracted from peruvian beans, peruanite (AFP), quelcão (AFQ) and fava verde (AFV); (B), (C) and (D) correspond to refinements by Rietveld method considering crystallographic information of type A starch and type B starch.

The disordered phase and inelastic scattering background were modeled using a Chebyshev polynomial, with the number of terms varied to optimize the fit. The selection criterion prioritized the smallest number of polynomial terms that minimized convergence factors and residuals, and this was achieved using an 11-term Chebyshev polynomial.

Table 11 lists the refined unit cell parameters obtained by Rietveld refinement, for both A-type and B-type phases, for all three samples: starch extracted from peruvian beans, peruanite (AFP), quelcão (AFQ) and fava verde (AFV).

Table 11 - Unit cell parameters of the A-type (named "A") and B-type (named "B") structure obtained by using the Rietveld refinement analysis.

Sample	Phase	$a(\text{Å})$	$b(\text{Å})$	$c(\text{Å})$	$\gamma (^{\circ})$	$V(\text{Å}^3)$
AFP	A	20.07(2)	11.836(7)	10.408(6)	120.00(3)	2208(1)
	B	17.56(1)	-	10.53(1)	120	2813(4)
AFQ	A	20.72(1)	11.89(8)	10.402(7)	120.03(3)	2220(1)
	B	17.536(7)	-	11.48(1)	120	2790(3)
AFV	A	20.75(1)	11.60(1)	10.503(6)	120.9(4)	2168(2)
	B	17.62(2)	-	10.49(2)	120	2822(6)

Table 12 summarizes the crystallinity data for the samples. The AFQ sample exhibited the highest fraction of the amorphous phase (~80 wt%), corresponding to a lower crystallinity of approximately 20 wt%. Within this crystalline fraction, 16 wt% was identified as A-type starch and 4 wt% as B-type starch. Conversely, the AFV sample displayed the highest crystallinity among the three, with an estimated X_c of approximately 30 wt%. These findings highlight the compositional and structural differences between the starches extracted from these bean varieties.

Table 12 - Quality factors and weight fraction of Rietveld refinement of the three phases: amorphous (x_a), A-type (W_A), B-type (W_B) and the crystallinity (x_c).

Sample	χ^2	R_{wp}	$x_a(\text{wt}\%)$	$W_A(\text{wt}\%)$	$W_B(\text{wt}\%)$	$x_c = W_A + W_B(\text{wt}\%)$
AFP	1.419	0.0481	77.189	17.291(3)	5.519(3)	22.811(6)
AFQ	1.481	0.0482	79.507	16.188(3)	4.304(4)	20.493(7)
AFV	1.483	0.0511	71.838	19.896(5)	8.2916(4)	28.162(9)

X-ray diffraction (XRD) analysis identified the semi-crystals of starches extracted from three Peruvian bean varieties as C-type. The diffractograms were quantified using the Rietveld

refinement method, enabling the estimation of crystallinity through integration of the experimental diffraction areas and the modeled background. Additionally, the proportions of A- and B-type structures within the starches were determined, providing a comprehensive understanding of their microstructural composition.

5.2 Peruvian Andean Maize

Peruvian Andean Maize represents a diverse group of maize varieties renowned for their extensive genetic, cytogenetic, and morphological variability, which enhances their adaptability to diverse environmental conditions. These varieties offer unique starch types with distinct structural characteristics, making them of particular interest for scientific and industrial applications. In this study, we focus on five PAM varieties: *Chullpi*, *Piscorunto*, *Sacsá*, *Giant Cuzco*, and *Purple*, which have been extensively characterized in prior research by the same female researchers now studying its starch (Salvador-Reyes et al., 2021; Salvador-Reyes; Clerici, 2020).

Those studies have demonstrated that these varieties are rich in unsaturated fatty acids, particularly oleic and linoleic acids, as well as proteins. Notably, *Chullpi* maize exhibits a higher concentration of these components, potentially contributing to its unique bioactive properties, including anti-inflammatory potential. These fatty acids and proteins are presumed to exist primarily in a non-crystalline state within the starch matrix (Salvador-Reyes; Clerici, 2020).

To gain a deeper understanding of the molecular organization of these starches and to accurately quantify their crystalline content, X-ray diffraction (XRD) combined with the Rietveld refinement method made a huge contribution as a robust analytical approach. We then determined the crystalline and amorphous components, offering critical insights into the structural properties and potential functional applications of these unique starches.

i. Starch extraction

Following the method for isolating the starch described in the last section for Peruvian Fava Beans described also by (Ferrari Felisberto et al., 2020), the Peruvian Andean maize was extracted from imported corn from Peru.

ii. XRD characterization and Rietveld Refinement

Figure 42 displays the X-ray diffraction (XRD) patterns of starch samples extracted from five Peruvian Andean maize (PAM) varieties: *Chullpi*, *Cuzco*, *Piscorunto*, *Purple*, and *Sacsa*. In Figure 42 (A) the diffractograms, spanning the 2θ range of 5° to 100° , reveal a high degree of similarity in diffraction patterns across the samples. Each sample exhibits a composite structure with at least two distinct components: (1) a semi-crystalline phase, evidenced by well-defined peaks, and (2) a non-crystalline phase, represented by a broad halo extending from approximately 7° to 65° , characteristic of semi-crystalline materials.

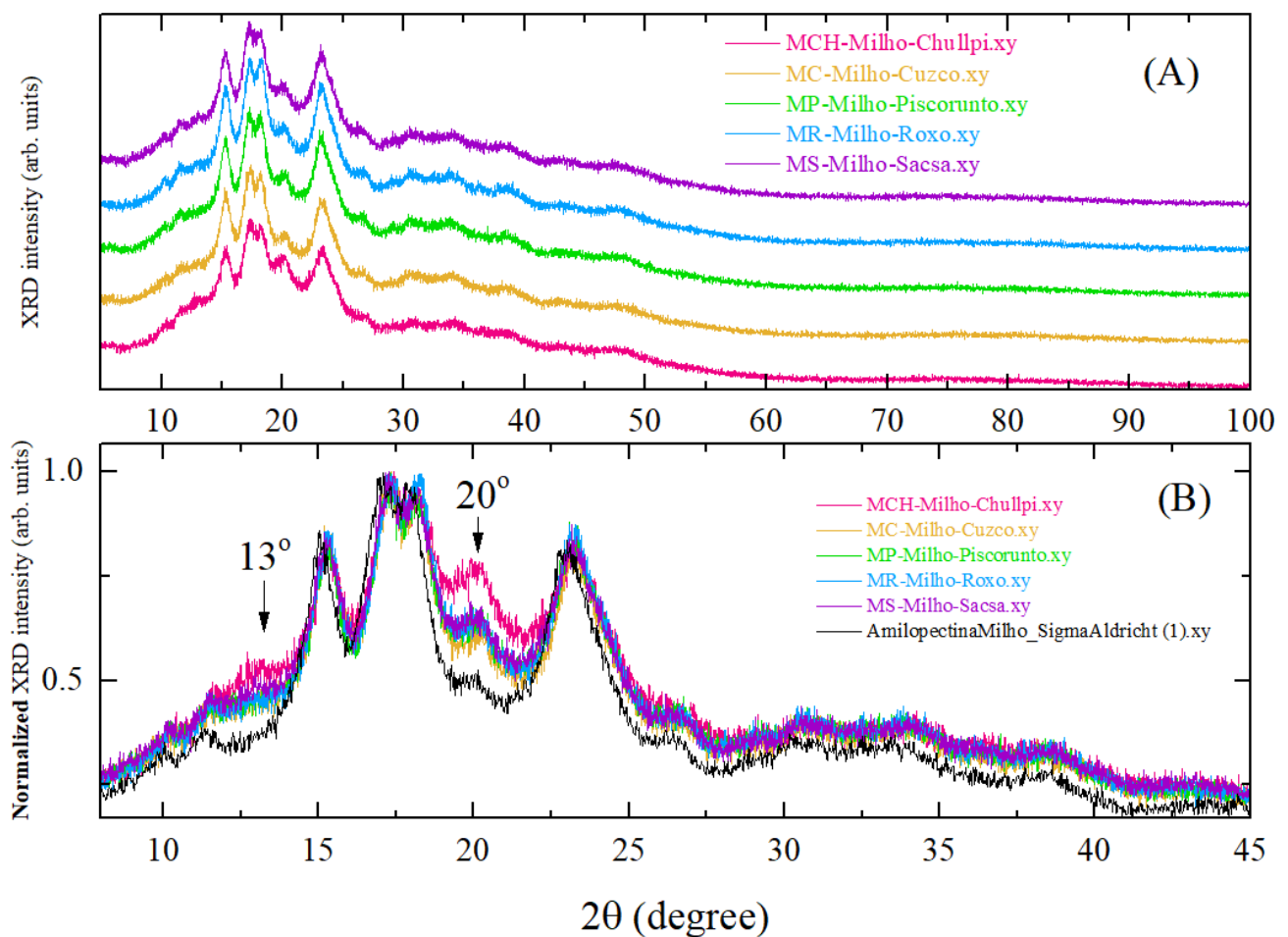


Figure 42 – Experimental XRD patterns of (A) raw starch samples extracted from *Chullpi*, *Cuzco*, *Piscorunto*, *Purple*, and *Sacsa* corn varieties; (B) normalized starch samples extracted from *Chullpi*, *Cuzco*, *Piscorunto*, *Purple*, *Sacsa*, and standard Sigma Aldrich maize corn starch.

For comparative purposes, the normalized XRD pattern of a standard maize starch sample from Sigma Aldrich was overlaid onto the experimental diffractograms in Figure 42 (A), using the most prominent peak at $2\theta = 17^\circ$ as a reference. Figure 42 (B) highlights

differences in peak intensities at $2\theta \sim 13^\circ$ and $2\theta \sim 20^\circ$ among the samples. Notably, *Chullpi* starch exhibits a unique diffraction pattern, with the $2\theta \sim 20^\circ$ peak showing greater intensity compared to the standard maize starch, which has a less pronounced peak. This discrepancy could be attributed to variations in the helical arrangements within the semi-crystalline structures. Additionally, all samples display a peak at $2\theta \sim 13^\circ$, absent in the standard maize starch, indicating the presence of an additional semi-crystalline phase within these varieties.

The peaks in the standard maize starch correspond exclusively to type A semi-crystals, characterized by monoclinic symmetry and belonging to space group B2 (Imberty; Chanzy; Perez, 1988). However, the peaks at $2\theta = 13^\circ$ and 20° in the experimental patterns closely resemble those observed in type V starch (Kong et al., 2014; Le et al., 2018, 2021; Shi et al., 2019). Type V starch, a polymorphic structure, matches well with orthorhombic semi-crystals in space group $P 2_1 2_1 2_1$ space group, with unit cell parameters as follows: $a = 13.65 \text{ \AA}$, $b = 23.70 \text{ \AA}$, $c = 8.05 \text{ \AA}$, $\alpha = \beta = \gamma = 90^\circ$, and $V = 2604 \text{ \AA}^3$ (Le et al., 2018). These findings suggest the coexistence of both A-type and V-type semi-crystalline phases in the Peruvian Andean Maize starch samples.

Figure 43 (A) overlays the normalized experimental diffractograms of the five samples with calculated patterns for type A and type V starches, derived from crystallographic information files (CIFs) CCDC#1019243 (Popov et al., 2009) and CCDC#830463 (Rappenecker; Zugenmaier, 1981), respectively. The analysis confirms that the majority of the observed peaks correspond to A-type semi-crystals, except for the peak at $2\theta \sim 13^\circ$, which is attributable to V-type starch. The peak at $2\theta \sim 20^\circ$ results from the overlap of contributions from both A- and V-type phases.

The refined structural results are shown in Figure 43 (B) *Chullpi*, (C) Purple, (D) *Piscorunto* (E) *Sacsa*, (F) *Cuzco*, with convergence factors provided in **Table 13**. The inability to fit the $2\theta \sim 30^\circ$ peak further supports the coexistence of a secondary semi-crystalline phase.

The Rietveld refinement method was applied to investigate the V-type starch structure using CIF CCDC#830463. However, acceptable convergence factors were not achieved, likely due to the limited structural information in the diffractograms, characterized by only two broad peaks. Conversely, satisfactory refinements were obtained for A-type starch semi-crystals using CIF CCDC#1019243.

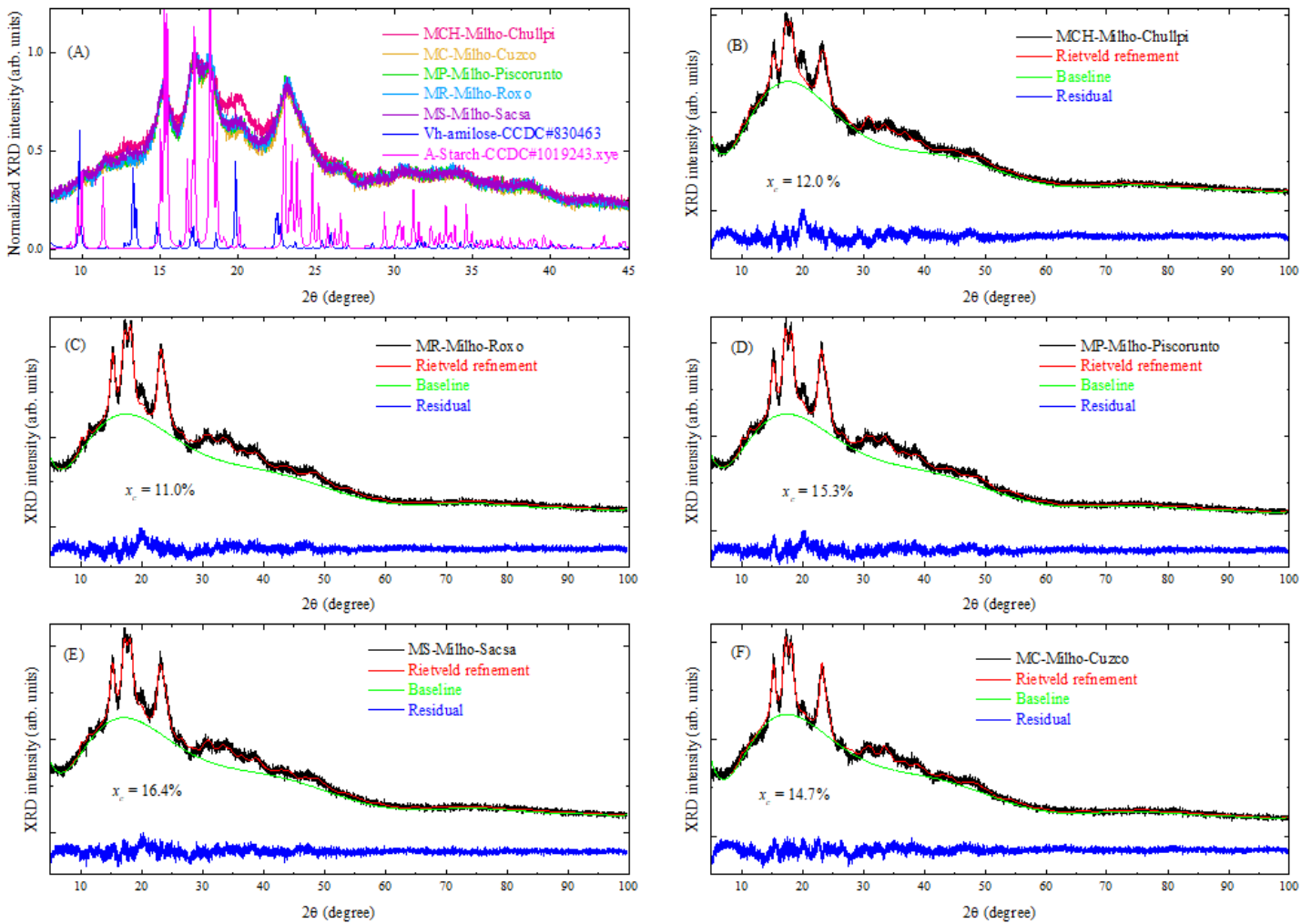


Figure 43 – XRD patterns of (A) starch samples extracted from Chullpi, Cuzco, Piscorunto, Purple, and Sacsca corn varieties overlapped with idealized XRD patterns obtained from the CIF information for A and V-type; Refined X-ray diffraction patterns of starch samples extracted from (B) Chullpi, (C) Purple, (D) Piscorunto (E) Sacsca, (F) Cuzco.

The calculated crystallinity values for the starch samples were 12.0% for Chullpi, 11.0% for Cuzco, 15.3% for Piscorunto, 16.4% for Purple, and 14.7% for Sacsca. **Table 13** presents the refined unit cell parameters for the A-type starch, and the mean crystallite size $D_{(hkl)}$ and microstrain $\varepsilon_{(hkl)}$ were calculated using the Scherrer's equation (Langford; Wilson, 1978), using Equation 9 and Equation 10 presented in Chapter 2.

Table 13 - Crystallographic and microstructural parameters obtained by the Rietveld method and their corresponding convergence parameters.

	Sigma Aldrich	<i>Chullpi</i>	<i>Giant Cuzco</i>	<i>Piscorunto</i>	Purple	<i>Sacsá</i>
a(Å)	21.07192	21.56(1)	20.98(1)	20.93(1)	20.813(9)	20.90(1)
b(Å)	11.69833	11.698(6)	11.619(8)	11.503(7)	11.630(5)	11.777(6)
c(Å)	10.34973	10.49(1)	10.59(1)	10.476(7)	10.540(7)	10.567(9)
γ (o)	122.557	124.98(4)	123.3(4)	122.29(3)	122.38(3)	122.00(3)
V(Å³)	2150.36	2168(2)	2159(3)	2132(2)	2154(1)	2206(1)
D (nm)	180.9	122	148	128	147	131
<ϵ>%	1.2	6	4.1	6.2	5.6	6.5
χ^2	1.581	2.054	1.699	1.577	1.693	1.518
Rwp	0.062	0.0587	0.0541	0.0501	0.0516	0.0495

The disordered component and inelastic scattering background were modeled using a Chebyshev polynomial, with the optimal number of terms determined to achieve the lowest convergence factors and residual line. In this study, a 12-term Chebyshev polynomial was found to provide the best fit, as shown in **Table 13**.

Type V starch is typically associated with heat, moisture treatments, retrogradation, or molecular interactions (Le et al., 2021; Rappenecker; Zugenmaier, 1981). Its presence in native corn starch is unexpected, as it usually nucleates under specific conditions. Previous studies (Wei et al., 2020) noted the occurrence of a $2\theta \sim 20^\circ$ peak in native corn starch XRD patterns but did not report the $2\theta \sim 13^\circ$ peak. The higher fatty acid content in *Chullpi* maize (Salvador-Reyes et al., 2024) could explain its pronounced V-phase peak and distinct pasting properties, including increased viscosity and enhanced retrogradation tendencies during heating.

This study demonstrates the coexistence of type A and type V starches in all five analyzed samples, with *Chullpi* starch exhibiting a higher proportion of V-type starch. Using the Rietveld refinement method, key structural parameters such as crystallinity, average crystallite size, and lattice microstrain were quantified, providing valuable insights into the microstructural characteristics of these starches. The findings are consistent with previous studies and validate the utility of Rietveld refinement for starch analysis, offering a robust approach for exploring their structural and functional properties.

5.3 Thorny Cará or Thorn-yam (*Dioscorea chondrocarpa* Griseb.)

Yams of the genus *Dioscorea* are vital tubers consumed extensively across Latin America, Asia, and Africa, where they are regarded as a staple food source (Barros et al., 2020; Bueno; Weigel, 1981). The Amazon region in northern Brazil is home to a wide variety of *carás* (yams), which grow in symbiosis with the forest trees, using them as natural supports for their climbing growth. This unique relationship enriches not only the forest ecosystem but also the soil, creating a diverse array of edible tubers, some of which can reach remarkable sizes of up to 200 kg per plant. These tubers are an essential source of food and income for local communities, but also could be an important source of starch of industrial interest (Inkinen et al., 2011).

Among these is the *cará de espinho*, thorny cará or thorn-yam, which is particularly noteworthy but faces the threat of extinction due to extensive deforestation, climate change, and unregulated extractive activities that jeopardize the delicate balance of the Amazon ecosystem. Such environmental pressures underscore the urgency of sustainable management practices and conservation efforts to protect these vital resources, which are integral to the livelihoods and food security of Amazonian populations.

i. Methods

The thorn yam (*Dioscorea* sp.), naturally available in the region, was cultivated at the Federal Institute of Education, Science, and Technology of Amazonas (IFAM-CMZL, 3°4'45" S, 59°55'59" W, Manaus, AM, Brazil). Its tubers were harvested, cut into pieces/seeds, and cultivated using a permaculture system. The cultivation involved 4x4x4 pits, irrigation, and sunlight, following the methodology outlined by (Barros et al., 2020). After harvest, the tubers, still with soil, were transported for further evaluation and starch extraction. These analyses were carried out at the Laboratory of Cereals, Roots, and Tubers (School of Food Engineering, Unicamp, SP, Brazil), where the physical and chemical characteristics of the tuber and its starch were examined, as depicted in Figure 1.

The research complied with regulations governing genetic resources, and the studied tuber was registered in the National System for the Management of Genetic Heritage and Associated Traditional Knowledge (SISGEN).

ii. Starch extraction

The thorn yam tubers underwent processing after being thoroughly washed, sanitized, peeled, and cut. The tubers were blended with distilled water at a ratio of 1:3 (tuber:water). The resulting mixture was filtered and transferred to a container with distilled water at ten times the initial volume, allowing for sedimentation under refrigeration for 12 hours. After sedimentation, the supernatant was carefully removed, and the sediment underwent multiple washing and sedimentation cycles to eliminate residual mucilage, continuing until the supernatant appeared clear. The final sediment was dried in a forced-air oven at 50°C until the moisture content was reduced to below 10%.

iii. XRD characterization and Rietveld Refinement

The diffraction patterns of type A and type B starches, which together form the structure known as type C starch, are distinct, and this allows for the potential attribution and estimation of crystallinity in type C starches. However, within the context of type C starches, the overlap of X-ray diffraction patterns from type A and type B structures presents a momentous challenge in determining their individual proportions, as both structures contribute to the formation of XRD patterns.

In the current study, we combined XRD and Rietveld refinement method to analyze thorn yam starch. The unit cell parameters we reported for Ariá studies (Carvalho et al., 2021; Pinto et al., 2021a, 2023) for A- and B-type phases were used as input data. Atomic coordinates and displacement factors were kept fixed during the refinement process. Figure 44 presents the overlay of the experimental diffractogram of thorn yam starch with the calculated diffractogram obtained through Rietveld refinement for type A and type B starches.

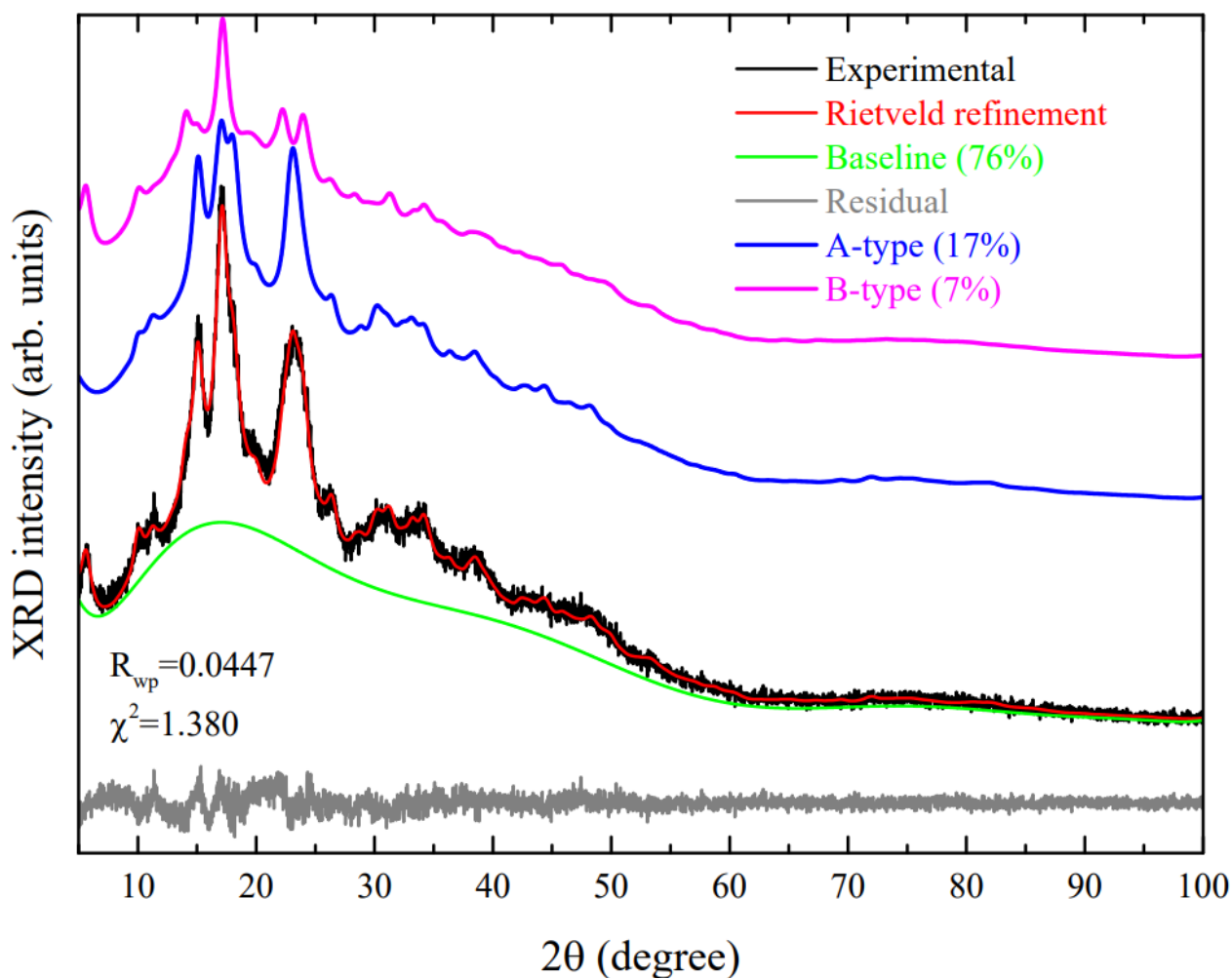


Figure 44 - Experimental diffractogram of yam starch (highlighted in black). In red, there is the diffractogram calculated using the Rietveld method, derived from the structural refinements of type A (represented in blue) and type B (indicated in magenta) starches. The difference between the experimental and calculated diffractogram is represented in gray.

The residual curve analysis and evaluation of convergence factors (R_{wp} and χ^2) (Toby, 2006) demonstrated excellent agreement between the experimental and calculated data, confirming the accuracy of the refinement. The baseline was described using an 11-term Chebyshev polynomial, selected based on the criterion of achieving the best (R_{wp} and χ^2) values with the fewest terms, depicting a similar baseline to Ariá.

After Rietveld Refinement, both phase contributions were separated and the lattice parameters derived from the analysis were summarized in **Table 14**. The weight fractions of A-type used Equation 14 and B-type used Equation 15.

Table 14 Unit cell parameters for type A and type B crystals obtained by the Rietveld method.

Type	<i>a</i> (Å)	<i>b</i> (Å)	<i>c</i> (Å)	γ (°)	<i>V</i> (Å ³)
A	21.07(1)	11.77(1)	10.61(1)	122.54(1)	2217(1)
B	18.00(2)	18.00(2)	10.65(2)	120	2989(4)

From the total area of the experimental diffractogram and the baseline area, as described in this work, the crystallinity *X_c* of thorn yam starch was calculated to be 24%, indicating a non-crystalline component of 76%. The phase percentages derived from Rietveld refinement further revealed that 17% of the crystalline component corresponded to type A crystals, while 7% was attributed to type B crystals.

The refined parameters for each phase were detailed individually. Depicts peak indexing and interplanar distances, calculated using Bragg's law $\lambda = 1.54059$ Å for A-Type crystals and B-Type crystals, respectively.

Table 15 - Miller indices, diffraction angles and interplanar distances for the thorn-yam type A (monoclinic) phase.

h	k	l	2θ	d(Å)
0	1	0	8.8	9.9
-2	1	0	9	9.7
1	0	1	9.6	9.1
2	0	0	9.9	8.9
-1	1	1	11	7.8
1	1	1	15	5.9
-3	1	1	15	5.8
-2	2	0	15	5.8
2	1	0	17	5.3
-4	1	0	17	5.2
3	0	1	17	5.1
-1	2	1	18	4.9
-3	2	1	18	4.9
0	2	0	18	4.9
-4	2	0	18	4.8
0	1	2	19	4.6

Table 16 - Miller indices, diffraction angles, and interplanar distances for the B-type phase (hexagonal) of thorn yam (*cará-de-espinho*).

h	k	l	2θ	d(Å)
0	1	0	5.6	16
1	1	0	9.7	9
0	1	1	10	8.8
0	2	0	11	7.8
0	2	1	14	6.2
1	2	0	15	5.8
0	3	0	17	5.2
1	2	1	17	5.1
2	2	0	20	4.5
1	1	2	19	4.5
1	3	1	22	4
0	4	0	23	3.8
0	3	2	24	3.7
0	1	3	26	3.4
1	2	3	29	3
1	4	2	31	2.8
0	6	0	34	2.5
1	2	4	37	2.4
1	6	1	39	2.3
4	4	1	41	2.2
4	5	2	49	1.8

For the first time in the literature, this study deconvolutes the individual contributions of A- and B-type phases to the X-ray diffraction pattern of a starch, using thorn-yam starch as proof of concept, using the Rietveld method. The results highlight a notable similarity between thorn yam and Ariá starches, both of which exhibit type C structures. Ariá starch, as previously reported, contains approximately 19% of phase A and 3% of phase B, with an overall crystallinity of 22%. This comparison underscores the consistency of type C starch structures across different sources, providing valuable insights into the shared characteristics and potential applications of different starch sources in Amazon region, which in turn might be important for future industrial applications.

CONCLUSIONS

This research demonstrates the effectiveness of combining X-ray diffraction (XRD) and the Rietveld refinement method for the detailed characterization of starch structures, particularly in response to non-conventional processing techniques. For the first time in the literature, Rietveld refinement was used for discussing microstructure of starches. Through this approach, the study successfully deconvoluted the A- and B-type crystalline phases within C-type starches derived from Amazonian sources, such as *Ariá* and thorn yam, representing a substantial advancement in the understanding of starch polymorphism. Key findings include the quantification of phase fractions, where the B-phase demonstrated greater structural resilience to gamma irradiation, likely due to its higher water content.

Gamma irradiation resulted in a reduction of the amorphous phase and an increase in crystallinity, with crystallinity levels rising by approximately 10% depending on the applied dose. Similarly, cold plasma treatment was shown to significantly influence the structural properties of starch, with a notable 18% increase in crystallinity observed at 200 Hz. The reduction in amylose content and the increase in cross-linking within amylopectin domains under plasma treatment were supported by microstructural data derived from the Rietveld refinement. These findings underscore the ability of cold plasma and gamma irradiation to tune starch properties for specific industrial applications.

Future developments in this field are centered on fostering national and international collaborations and advancing large-scale multidisciplinary projects. These initiatives aim to expand the current understanding of starch structures by integrating complementary characterization techniques. Such approaches are expected to provide deeper insights into the structural transformations that raw starch undergoes when subjected to diverse chemical and mechanical processing methods. These efforts not only aspire to enhance the fundamental knowledge of starch biopolymers but also aim to contribute to the development of innovative applications in food science, materials engineering, and sustainable bioplastics. Through collaborative and interdisciplinary approaches, this research has the potential to address both scientific challenges and industrial needs, paving the way for future advancements in the field.

As an Amazonian, the author identified another profound implication of this work: assuming a leadership role in the comprehensive study of regional resources, thereby contributing to the recognition and valorization of those with significant potential for

agroforestry development. This responsibility extends beyond scientific inquiry, reflecting a commitment to sustainable resource management and the empowerment of local communities. As a scientist in training, this realization profoundly shaped the author's perspective, instilling a sense of purpose and dedication to a research trajectory that embraces these values. It highlights a future focused on advancing knowledge while fostering the sustainable development of Amazonian biodiversity.

Challenges and Opportunities for Future Investigations

While this thesis has made significant strides in elucidating the structural intricacies of starches, numerous opportunities for further research remain. Key challenges include enhancing the precision of crystallinity measurements and expanding the application of structural refinement techniques to more complex starch matrices. Investigating the synergy of XRD with advanced characterization tools, such as synchrotron-based methods and computational modeling, could deepen insights into starch polymorphism and processing effects.

Another critical area of investigation lies in unraveling the role of intrinsic water within starch molecules and its contribution to the efficiency and outcomes of various processing techniques. Intrinsic water, often localized within the crystalline lattice or associated with the amorphous regions of starch, may actively participate in structural transformations during treatments such as cold plasma, gamma irradiation, and thermal or enzymatic modifications. Understanding how this water interacts with reactive species, glycosidic bonds, or crystalline domains could provide valuable insights into the mechanisms underlying these processes. Such knowledge could elucidate its role in determining the yield, efficiency, and structural outcomes of these techniques, offering pathways to optimize processing parameters for desired results.

In addition to examining the influence of intrinsic water, further exploration is needed to establish direct correlations between structural modifications and the functional properties of processed starch. These properties, which include gelatinization behavior, solubility, swelling capacity, rheological performance, and digestibility, are pivotal for tailoring starch for specific applications in food, packaging, pharmaceuticals, and bioplastics. A deeper understanding of how processing-induced changes at the molecular and crystalline levels affect these functional attributes would enable more precise predictions and control over starch behavior. This approach could facilitate the design of starch-based materials with customized properties, enhancing their applicability across diverse industries and advancing sustainable innovations.

Future investigations should also prioritize the integration of Amazonian starches into value-added bioplastic and pharmaceutical products, leveraging their unique properties to address sustainability goals. By fostering interdisciplinary and international collaborations, these endeavors can bridge scientific knowledge with technological innovation, ultimately benefiting global biopolymer research and application.

REFERENCES

ABRAL, H. *et al.* A simple method for improving the properties of the sago starch films prepared by using ultrasonication treatment. **Food Hydrocolloids**, v. 93, n. February, p. 276–283, 2019.

ADAMSKI, P.; ALBRECHT, A.; MOSZYŃSKI, D. Synthesis and crystal structure of layered molybdate $\text{NH}_4\text{Co}_2\text{OH}(\text{MoO}_4)_2 \cdot \text{H}_2\text{O}$. **Powder Diffraction**, v. 38, n. 4, p. 240–243, 28 dez. 2023.

ADAMU, B. O. A. Resistant starch derived from extruded corn starch and guar gum as affected by acid and surfactants: Structural characterization. **Starch/Staerke**, v. 53, n. 11, p. 582–591, nov. 2001.

AGARWAL, U. P.; REINER, R. S.; RALPH, S. A. Cellulose I crystallinity determination using FT–Raman spectroscopy: univariate and multivariate methods. **Cellulose**, v. 17, n. 4, p. 721–733, 15 ago. 2010.

AHVENAINEN, P.; KONTRO, I.; SVEDSTRÖM, K. Comparison of sample crystallinity determination methods by X-ray diffraction for challenging cellulose I materials. **Cellulose**, v. 23, n. 2, p. 1073–1086, 2016.

ALONSO-GOMEZ, L. *et al.* Physicochemical transformation of cassava starch during fermentation for production of sour starch in Colombia. **Starch/Staerke**, v. 68, n. 11–12, p. 1139–1147, 2016.

ANAND, K. *et al.* Effect of Starch Nanocrystals on Natural Rubber Latex Vulcanizate Properties. **Progress in Rubber, Plastics and Recycling Technology**, v. 34, n. 2, p. 75–87, 4 maio 2018.

ANDRÉA BERTOLINI. **Starches Characterization, Properties, and Applications**. Boca Raton: CRC Press, 2010.

ANGELLIER, H. *et al.* Optimization of the Preparation of Aqueous Suspensions of Waxy Maize Starch Nanocrystals Using a Response Surface Methodology. **Biomacromolecules**, v. 5, n. 4, p. 1545–1551, jul. 2004.

ASHCROFT, NEIL W, MERMIN, D. N.-. **Solid State Physics**. Orlando, FL: Harcourt College Publishers, 1976.

ASIRI, S. A.; ULBRICH, M.; FLÖTER, E. Partial Hydrolysis of Granular Potato Starch Using α -Amylase - Effect on Physicochemical, Molecular, and Functional Properties. **Starch - Stärke**, p. 1800253, 20 nov. 2018.

ATIQAHA, A. *et al.* Physical and thermal properties of treated sugar palm/glass fibre reinforced thermoplastic polyurethane hybrid composites. **Journal of Materials Research and Technology**, v. 8, n. 5, p. 3726–3732, 2019.

BAERLOCHER, C. Restraints and constraints in Rietveld refinement. Em: **The Rietveld Method**. [s.l.] Oxford University PressOxford, 1993. p. 186–196.

BANURA, S. *et al.* Modification of starch using low pressure radio frequency air plasma. **LWT**, v. 89, p. 719–724, mar. 2018.

BAO, J.; AO, Z.; JANE, J. Characterization of Physical Properties of Flour and Starch Obtained from Gamma-Irradiated White Rice. **Starch - Stärke**, v. 57, n. 10, p. 480–487, out. 2005.

BARROS, D. R. *et al.* Ariá (*Goeppertia allouia*) Brazilian Amazon tuber as a non-conventional starch source for foods. **International Journal of Biological Macromolecules**, nov. 2020.

BARUAH, K. N.; SINGHA, S.; UPPALURI, R. V. S. Preparation of Potato Starch Nanoparticles Using Acid Hydrolysis and Ultrasonic Post-treatment. **ACS Food Science & Technology**, v. 3, n. 4, p. 626–634, 21 abr. 2023.

B.E. WARREN. **X-Ray Diffraction**. 2. ed. New York: Dover Publications, 1990.

BEL HAAJ, S. *et al.* Starch nanoparticles formation via high power ultrasonication. **Carbohydrate Polymers**, v. 92, n. 2, p. 1625–1632, 2013.

BEMILLER, J.; WHISTLER, R. **Starch: Chemistry and Technology**. 3. ed. London: Elsevier, 2009.

BERA, S. *et al.* Potential effect of ultrasound on carbohydrates. **Carbohydrate Research**, v. 410, p. 15–35, jun. 2015.

BERTOFT, E. Understanding Starch Structure: Recent Progress. **Agronomy**, v. 7, n. 3, p. 56, 25 ago. 2017.

BIE, P. *et al.* Structural characteristics and rheological properties of plasma-treated starch. **Innovative Food Science & Emerging Technologies**, v. 34, p. 196–204, abr. 2016.

BIOMY, M. Effect of Gamma Irradiation on Some Rice Varieties Properties. **Annals of Agricultural Science, Moshtohor**, v. 59, n. 3, p. 485–494, 1 jun. 2021.

BIRANIA, S. *et al.* Cold plasma in food processing and preservation: A review. **Journal of Food Process Engineering**, v. 45, n. 9, 22 set. 2022.

BISMARCK, O. *et al.* Dextrose Equivalent Analysis of Acid Hydrolysed Corn and Cassava Starch Sourced from Ghana. **Science Journal of Chemistry**, v. 9, n. 2, p. 45, 2021.

BLAZEK, J.; GILBERT, E. P. Effect of enzymatic hydrolysis on native starch granule structure. **Biomacromolecules**, v. 11, n. 12, p. 3275–3289, 2010.

BLEICHER, L.; SASAKI, J. M.; PAIVA SANTOS, C. O. Development of a graphical interface for the Rietveld refinement program DBWS. **Journal of Applied Crystallography**, v. 33, n. 4, p. 1189–1189, 1 ago. 2000.

BORGES, Z. V. *et al.* Structural, thermal, optical, and photoacoustic study of mechanically alloyed nanocrystalline SnTe. **Materials Research**, v. 21, n. 4, 2018.

BORO, U.; KASHYAP, N.; MOHOLKAR, V. S. Sonochemical Synthesis of Poly(lactic acid) Nanocomposites with ZnO Nanoflowers: Effect of Nanofiller Morphology on Physical Properties. **ACS Engineering Au**, v. 2, n. 1, p. 46–60, 16 fev. 2022.

BRANDON, D.; KAPLAN, W. D. **Microstructural Characterization of Materials**. 2. ed. Wiltshire: John Wiley & Sons, 2008.

BROWN, I. D.; MCMAHON, B. The Crystallographic Information File (CIF). **Data Science Journal**, v. 5, p. 174–177, 2006.

BUENO, C. R.; WEIGEL, P. Brotação e desenvolvimento inicial de rizomas de Ariá (*Calathea allouia* (Aubl.) Lindl.). **Acta Amazonica**, v. 11, n. 2, p. 407–410, jun. 1981.

BULÉON, A. *et al.* **Mini review Starch granules: structure and biosynthesis** **International Journal of Biological Macromolecules**. [s.l.: s.n.].

CARVALHO, A. P. M. G. *et al.* Dielectric barrier atmospheric cold plasma applied to the modification of Ariá (*Goeppertia allouia*) starch: Effect of plasma generation voltage. **International Journal of Biological Macromolecules**, v. 182, p. 1618–1627, 2021.

CASTILLO, L. A. *et al.* Crystalline morphology of thermoplastic starch/talc nanocomposites induced by thermal processing. **Heliyon**, v. 5, n. 6, 2019.

CHANG, Y. *et al.* High efficiency and low cost preparation of size controlled starch nanoparticles through ultrasonic treatment and precipitation. **Food Chemistry**, v. 227, p. 369–375, 2017.

CHEETHAM, N. W. H.; TAO, L. Variation in crystalline type with amylose content in maize starch granules: An X-ray powder diffraction study. **Carbohydrate Polymers**, v. 36, n. 4, p. 277–284, 1998.

CHEMAT, F.; ZILL-E-HUMA; KHAN, M. K. Applications of ultrasound in food technology: Processing, preservation and extraction. **Ultrasonics Sonochemistry**, v. 18, n. 4, p. 813–835, jul. 2011.

CHISENGA, S. M. *et al.* Characterization of physicochemical properties of starches from improved cassava varieties grown in Zambia. **AIMS Agriculture and Food**, v. 4, n. 4, p. 939–966, 2019.

CULLITY, B. D.; STOCK, S. R. **Elements of X-Ray Diffraction**. 3 ed ed. [s.l.] Pearson Education, 2014.

DA COSTA PINTO, C. *et al.* X-ray diffraction and Rietveld characterization of radiation-induced physicochemical changes in Ariá (*Goeppertia allouia*) C-type starch. **Food Hydrocolloids**, v. 117, n. December 2020, 2021.

DA COSTA PINTO, C. *et al.* Modulation of the Physicochemical Properties of Aria (*Goepertia allouia*) Starch by Cold Plasma: Effect of Excitation Frequency. **Food and Bioprocess Technology**, v. 16, n. 4, p. 768–784, 2023.

DA SILVA, L. S. *et al.* Semiconducting nanocomposite based on the incorporation of polyaniline on the cellulose extracted from *Bambusa vulgaris*: structural, thermal and electrical properties. **Chemical Papers**, 2021.

DAI, L. *et al.* Preparation and characterization of starch nanocrystals combining ball milling with acid hydrolysis. **Carbohydrate Polymers**, v. 180, n. September 2017, p. 122–127, 2018.

DAVE, V. S. *et al.* Correlation of Structural and Macroscopic Properties of Starches with Their Tableability Using the SM2 Approach. **Journal of Pharmaceutical Sciences**, v. 104, n. 11, p. 3870–3882, 2015.

DE FIGUEIREDO, L. P.; FERREIRA, F. F. The Rietveld Method as a Tool to Quantify the Amorphous Amount of Microcrystalline Cellulose. **Journal of Pharmaceutical Sciences**, v. 103, n. 5, p. 1394–1399, 2014.

DE KEIJSER, TH. H. *et al.* Use of the Voigt function in a single-line method for the analysis of X-ray diffraction line broadening. **Journal of Applied Crystallography**, v. 15, n. 3, p. 308–314, 1982.

DE SOUZA, P. M.; E MAGALHÃES, P. DE O. Application of microbial α -amylase in industry - a review. **Brazilian Journal of Microbiology**, v. 41, n. 4, p. 850–861, 2010.

DELHEZ, R.; DE KEIJSER, T. H.; MITTEMEIJER, E. J. **Determination of Crystallite Size and Lattice Distortions through X-Ray Diffraction Line Profile Analysis Recipes, Methods and Comments** *Fresenius Z Anal Chem.* [s.l: s.n.].

DINNEBIER, R. E.; BILLINGE, S. J. L. **Powder Diffraction**. Cambridge: Royal Society of Chemistry, 2008.

DINNEBIER, R. E.; LEINWEBER, A.; EVANS, J. S. O. **Rietveld Refinement - Practical powder diffraction pattern analysis using TOPAS**. Berlin/Boston: [s.n.].

DOMENE-LÓPEZ, D. *et al.* Influence of starch composition and molecular weight on physicochemical properties of biodegradable films. **Polymers**, v. 11, n. 7, p. 1–17, 2019.

DONG, S. *et al.* Effects of Dielectric Barrier Discharges (DBD) Cold Plasma Treatment on Physicochemical and Structural Properties of Zein Powders. **Food and Bioprocess Technology**, v. 10, n. 3, p. 434–444, 22 mar. 2017.

DRIEMEIER, C.; CALLIGARIS, G. A. Theoretical and experimental developments for accurate determination of crystallinity of cellulose i materials. **Journal of Applied Crystallography**, v. 44, n. 1, p. 184–192, 2011.

DUFRESNE, A. Current Opinion in Colloid & Interface Science Crystalline starch based nanoparticles. **Current Opinion in Colloid & Interface Science**, v. 19, n. 5, p. 397–408, 2014.

ELTON K KAUFMANN. **CHARACTERIZATION OF MATERIALS**. New Jersey: Wiley Interscience, 2003.

ERIC LIFSHIN. **X-ray Characterization of Materials**. 1. ed. New York: Wiley-VCH, 1999.

ESCLAPEZ, M. D. *et al.* Ultrasound-Assisted Extraction of Natural Products. **Food Engineering Reviews**, v. 3, n. 2, p. 108–120, 3 jun. 2011.

EVANS, J. S. O.; EVANS, I. R. Structure Analysis from Powder Diffraction Data: Rietveld Refinement in Excel. **Journal of Chemical Education**, v. 98, n. 2, p. 495–505, 9 fev. 2021.

FARRÁN, A. *et al.* Green Solvents in Carbohydrate Chemistry: From Raw Materials to Fine Chemicals. **Chemical Reviews**, v. 115, n. 14, p. 6811–6853, 2015.

FAWCETT, T. G. *et al.* Reference materials for the study of polymorphism and crystallinity in cellulose. **Powder Diffraction**, v. 28, n. 1, p. 18–31, 2013.

FERRARI FELISBERTO, M. H. *et al.* Characterization and technological properties of peach palm (*Bactris gasipaes* var. *gasipaes*) fruit starch. **Food Research International**, v. 136, n. July, p. 109569, 2020.

FLORES CANO, D. A. *et al.* Fifty years of Rietveld refinement: Methodology and guidelines in superconductors and functional magnetic nanoadsorbents. **Revista de Investigación de Física**, v. 24, n. 3, p. 39–48, 7 dez. 2021.

FRAZIER, R. A. Química de alimentos. Em: CAMPBELL-PLATT, GEOFFREY. (Ed.). **Ciência e Tecnologia de Alimentos**. [s.l.] Blücher, 2015. p. 5–30.

FRENCH, A. D. Idealized powder diffraction patterns for cellulose polymorphs. **Cellulose**, v. 21, n. 2, p. 885–896, 2014.

FRENCH, A. D.; SANTIAGO CINTRÓN, M. Cellulose polymorphy, crystallite size, and the Segal Crystallinity Index. **Cellulose**, v. 20, n. 1, p. 583–588, 2013.

GALLYAMOV, E. M. *et al.* Mn²⁺ Luminescence in Ca₉Zn_{1-x}Mn_xNa(PO₄)₇ Solid Solution, 0 ≤ x ≤ 1. **Materials**, v. 16, n. 12, p. 4392, 14 jun. 2023.

GANESAN, A. R. *et al.* Application of cold plasma on food matrices: A review on current and future prospects. **Journal of Food Processing and Preservation**, v. 45, n. 1, jan. 2021.

GANI, A. *et al.* Effect of γ -irradiation on granule structure and physicochemical properties of starch extracted from two types of potatoes grown in Jammu & Kashmir, India. **LWT - Food Science and Technology**, v. 58, n. 1, p. 239–246, set. 2014.

GAO, S. *et al.* The effects of dielectric barrier discharge plasma on physicochemical and digestion properties of starch. **International Journal of Biological Macromolecules**, v. 138, p. 819–830, out. 2019.

GERNAT, C. *et al.* Supramolecular Structure of Legume Starches Revealed by X-Ray Scattering. **Starch - Stärke**, v. 42, n. 5, p. 175–178, 1990.

GHALAMBOR, P. *et al.* Investigation of dual modification on physicochemical, morphological, thermal, pasting, and retrogradation characteristics of sago starch. **Food Science & Nutrition**, v. 10, n. 7, p. 2285–2299, 24 jul. 2022.

GUINIER, A. *et al.* **Diffraction In Crystals, Imperfect Crystals, and Amorphous Bodies**. [s.l: s.n.].

HAFEZI, K. Hydrocolloids: Structure, preparation method, and application in food and pharmaceutical industries. p. 1–32, 2022.

HALIMATUL, M. J. *et al.* Effect of sago starch and plasticizer content on the properties of thermoplastic films: Mechanical testing and cyclic soaking-drying. **Polimery/Polymers**, v. 64, n. 6, p. 422–431, 2019a.

HALIMATUL, M. J. *et al.* Water absorption and water solubility properties of sago starch biopolymer composite films filled with sugar palm particles. **Polimery/Polymers**, v. 64, n. 9, p. 596–604, 2019b.

HAMAKER, B. R. **Current and future challenges in starch research. Current Opinion in Food Science** Elsevier Ltd, , 1 ago. 2021.

HARIKRISHNA, S. *et al.* Cold plasma as an emerging nonthermal technology for food processing: A comprehensive review. **Journal of Agriculture and Food Research**, v. 14, p. 100747, dez. 2023.

HAROLD P KLUG; LEROY E ALEXANDER. **X-Ray Diffraction Procedures For Polycrystalline and amorphous materials**. 2. ed. London: Wiley-Interscience, 1974.

HE, B. B. **Two-Dimensional X-Ray Diffraction**. Hoboken, NJ, USA: John Wiley & Sons, Inc., 2009.

HELLENBRANDT, M. The Inorganic Crystal Structure Database (ICSD)—Present and Future. **Crystallography Reviews**, v. 10, n. 1, p. 17–22, 22 jan. 2004.

HORSTMANN, S. W.; LYNCH, K. M.; ARENDT, E. K. Starch characteristics linked to gluten-free products. **Foods**, v. 6, n. 4, p. 1–21, 2017.

HUANG, V. T.; PERDON, A. A. Major changes in cereal biopolymers during ready-to-eat cereal processing. Em: **Breakfast Cereals and How They Are Made: Raw Materials, Processing, and Production**. [s.l.] Elsevier, 2020. p. 109–140.

ILYAS, R. A. *et al.* Development and characterization of sugar palm nanocrystalline cellulose reinforced sugar palm starch bionanocomposites. **Carbohydrate Polymers**, v. 202, n. September, p. 186–202, 2018a.

ILYAS, R. A. *et al.* Development and characterization of sugar palm nanocrystalline cellulose reinforced sugar palm starch bionanocomposites. **Carbohydrate Polymers**, v. 202, n. September, p. 186–202, 2018b.

ILYAS, R. A. *et al.* Sugar palm (*Arenga pinnata* (Wurmb.) Merr) cellulosic fibre hierarchy: A comprehensive approach from macro to nano scale. **Journal of Materials Research and Technology**, v. 8, n. 3, p. 2753–2766, 2019a.

ILYAS, R. A. *et al.* Effect of sugar palm nanofibrillated cellulose concentrations on morphological, mechanical and physical properties of biodegradable films based on agro-waste sugar palm (*Arenga pinnata* (Wurmb.) Merr) starch. **Journal of Materials Research and Technology**, v. 8, n. 5, p. 4819–4830, 2019b.

ILYAS, R. A. *et al.* Sugar palm nanofibrillated cellulose (*Arenga pinnata* (Wurmb.) Merr): Effect of cycles on their yield, physico-chemical, morphological and thermal behavior. **International Journal of Biological Macromolecules**, v. 123, p. 379–388, 2019c.

ILYAS, R. A. *et al.* Sugar palm (*Arenga pinnata* [Wurmb.] Merr) starch films containing sugar palm nanofibrillated cellulose as reinforcement: Water barrier properties. **Polymer Composites**, v. 41, n. 2, p. 459–467, 2020.

ILYAS, R. A.; SAPUAN, S. M.; ISHAK, M. R. Isolation and characterization of nanocrystalline cellulose from sugar palm fibres (*Arenga Pinnata*). **Carbohydrate Polymers**, v. 181, n. June 2017, p. 1038–1051, 2018.

ILYAS RUSHDANA, A. *et al.* Nanocrystalline Cellulose As Reinforcement For Polymeric Matrix Nanocomposites And Its Potential Applications: A Review. **Current Analytical Chemistry**, v. 13, p. 203–225, 2017.

IMBERTY, A. *et al.* Recent Advances in Knowledge of Starch Structure. **Starch - Stärke**, v. 43, n. 10, p. 375–384, 1991.

IMBERTY, A.; CHANZY, H.; PEREZ, S. The Double-helical Nature of the Crystalline Part of A-starch. p. 365–378, 1988.

IMBERTY, A.; PEREZ, S. A revisit to the three-dimensional structure of B-type starch. **Biopolymers**, v. 27, n. 8, p. 1205–1221, 1988.

INKINEN, S. *et al.* **From lactic acid to poly(lactic acid) (PLA): Characterization and analysis of PLA and Its precursors.** *Biomacromolecules*, 14 mar. 2011.

ISLAM, MD. N.; ZHANG, M.; ADHIKARI, B. The Inactivation of Enzymes by Ultrasound—A Review of Potential Mechanisms. *Food Reviews International*, v. 30, n. 1, p. 1–21, 2 jan. 2014.

JANE, J. Current Understanding on Starch Granule Structures. *Journal of Applied Glycoscience*, v. 53, n. 3, p. 205–213, 2006.

JIANG, X. *et al.* Effect of ultrasonic treatment on the physicochemical properties and oxidative stability of phospholipids in emulsion system. *Journal of Food Process Engineering*, v. 44, n. 1, 30 jan. 2021.

JUSTINO, H. DE F. M. *et al.* Exploring ultrasound-assisted technique for enhancing techno-functional properties of plant proteins: a comprehensive review. *International Journal of Food Science & Technology*, v. 59, n. 1, p. 498–511, 8 jan. 2024.

KARKHANIS, R. P.; SINGH, S. P. A Review: Application of Cold Plasma in Food Processing Industry. *Journal of Scientific Research and Reports*, v. 30, n. 3, p. 243–258, 19 fev. 2024.

KENNEDY, J. F. *et al.* **Starch and its derived products: Biotechnological and biomedical applications.** [s.l: s.n.].

KERNOU, O. *et al.* Effect of sonication on microwave inactivation of *Escherichia coli* in an orange juice beverage. *Journal of Food Process Engineering*, v. 44, n. 5, 28 maio 2021.

KHALIL, M. I.; HASHEM, A.; HEBEISH, A. Carboxymethylation of Maize Starch. *Starch - Stärke*, v. 42, n. 2, p. 60–63, 1990.

KIRAN, B. S. Shelf-life extension of wheat flour by irradiation technique. *The Pharma Innovation*, v. 12, n. 7S, p. 727–735, 1 jan. 2023.

KONG, L. *et al.* Characterization of Starch Polymorphic Structures Using Vibrational Sum Frequency Generation Spectroscopy. *The Journal of Physical Chemistry B*, v. 118, n. 7, p. 1775–1783, fev. 2014.

KONG, X. *et al.* Effect of gamma irradiation on the thermal and rheological properties of grain amaranth starch. **Radiation Physics and Chemistry**, v. 78, n. 11, p. 954–960, nov. 2009.

KROUMOVA, E. *et al.* Bilbao Crystallographic Server : Useful Databases and Tools for Phase-Transition Studies. **Phase Transitions**, v. 76, n. 1–2, p. 155–170, jan. 2003.

LANGFORD, J. I.; WILSON, A. J. C. Scherrer after sixty years: A survey and some new results in the determination of crystallite size. **Journal of Applied Crystallography**, v. 11, n. 2, p. 102–113, abr. 1978.

LAVEN, P. Separating diffraction from scattering: the million-dollar challenge. **Journal of Nanophotonics**, v. 4, n. 1, p. 041593, 2010.

LE BAIL, P. *et al.* Monitoring the crystallization of amylose-lipid complexes during maize starch melting by synchrotron X-ray diffraction. **Biopolymers**, v. 50, n. 1, p. 99–110, 1999.

LE, C. A. K. *et al.* Polymorphism of crystalline complexes of V-amylose with fatty acids. **International Journal of Biological Macromolecules**, v. 119, p. 555–564, 2018.

LE, C. A. K. *et al.* Polymorphism of V-amylose cocrystallized with aliphatic diols. **Polymer**, v. 213, n. September 2020, p. 123302, 2021.

LE CORRE, D.; ANGELLIER-COUSSY, H. Preparation and application of starch nanoparticles for nanocomposites: A review. **Reactive and Functional Polymers**, v. 85, p. 97–120, 2014.

LE CORRE, D.; BRAS, J.; DUFRESNE, A. Starch Nanoparticles: A Review. **Biomacromolecules**, v. 11, n. 5, p. 1139–1153, maio 2010.

LEINEWEBER, A. Anisotropic microstrain broadening due to field-tensor distributions. **Journal of Applied Crystallography**, v. 40, n. 2, p. 362–370, 2007.

LEINEWEBER, A. Understanding anisotropic microstrain broadening in Rietveld refinement. **Zeitschrift fur Kristallographie**, v. 226, n. 12, p. 905–923, dez. 2011.

LEINEWEBER, A.; MITTEMEIJER, E. J. Diffraction line broadening due to lattice-parameter variations caused by a spatially varying scalar variable: Its orientation dependence caused by locally varying nitrogen content in ϵ -FeN_{0.433}. **Journal of Applied Crystallography**, v. 37, n. 1, p. 123–135, 2004.

LEONARSKI, E. *et al.* Bacterial cellulose production from acerola industrial waste using isolated kombucha strain. **Cellulose**, v. 29, n. 14, p. 7613–7627, 2022.

LI, B. *et al.* Insights into Cold Plasma Treatment on the Cereal and Legume Proteins Modification: Principle, Mechanism, and Application. **Foods**, v. 13, n. 10, p. 1522, 14 maio 2024.

LI, J. *et al.* Freeze-Thawing Assisted Preparation of Acid-Hydrolyzed Starch: Microstructure and Physicochemical Properties. **Starch - Stärke**, v. 74, n. 9–10, 9 set. 2022.

LIU, X. *et al.* Spotlight on the Multiscale Structural and Physicochemical Properties of Red Adzuki Bean Starch through Partial Amylose Removal Combined with Hydrochloric Acid. **Foods**, v. 12, n. 18, p. 3366, 7 set. 2023.

LOPEZ-RUBIO, A. *et al.* A novel approach for calculating starch crystallinity and its correlation with double helix content: A combined XRD and NMR study. **Biopolymers**, v. 89, n. 9, p. 761–768, 2008.

LUTTEROTTI, L. *et al.* Combined texture and structure analysis of deformed limestone from time-of-flight neutron diffraction spectra. **Journal of Applied Physics**, v. 81, n. 2, p. 594–600, 15 jan. 1997.

MACRAE, C. F. *et al.* Mercury: visualization and analysis of crystal structures. **Journal of Applied Crystallography**, v. 39, n. 3, p. 453–457, 1 jun. 2006.

MACRAE, C. F. *et al.* Mercury CSD 2.0 – new features for the visualization and investigation of crystal structures. **Journal of Applied Crystallography**, v. 41, n. 2, p. 466–470, 1 abr. 2008.

MADSEN, I. C.; SCARLETT, N. V. Y. Chapter 11. Quantitative Phase Analysis. Em: **Powder Diffraction**. Cambridge: Royal Society of Chemistry, 2008. p. 298–331.

MALIN SJÖÖ; LARS NILSSON. **Starch in Food - Structure, Function and Applications**. 2. ed. Cambridge: Elsevier, 2009.

MANZATO, L. *et al.* New approach for extraction of cellulose from tucumã's endocarp and its structural characterization. **Journal of Molecular Structure**, v. 1143, p. 229–234, 2017.

MARCO-AURELIO DE PAOLI. **DEGRADAÇÃO E ESTABILIZAÇÃO DE POLÍMEROS**. 2. ed. [s.l.] Chemkeys, 2008.

MARTINS, P. C.; GUTKOSKI, L. C.; MARTINS, V. G. Impact of acid hydrolysis and esterification process in rice and potato starch properties. **International Journal of Biological Macromolecules**, v. 120, p. 959–965, 2018.

MCCUSKER, L. B. *et al.* Rietveld refinement guidelines. **Journal of Applied Crystallography**, v. 32, n. 1, p. 36–50, fev. 1999.

MELQUIÁDES, M. O. *et al.* Structural and optical properties of a mechanically alloyed thermoelectric lamellar SnSeS solid solution. **Journal of Applied Physics**, v. 126, n. 13, 2019.

MERKYS, A. *et al.* COD::CIF::Parser: an error-correcting CIF parser for the Perl language. **Journal of Applied Crystallography**, v. 49, n. 1, p. 292–301, 1 fev. 2016.

MIR, S. A.; SHAH, M. A.; MIR, M. M. Understanding the Role of Plasma Technology in Food Industry. **Food and Bioprocess Technology**, v. 9, n. 5, p. 734–750, 22 maio 2016.

MITTEMEIJER, E. J. **Analysis of the Microstructure; Analysis of Lattice Imperfections: Light and Electron Microscopical and X-Ray Diffraction Methods**. [s.l.: s.n.].

MITTEMEIJER, E. J.; WELZEL, U. The “state of the art” of the diffraction analysis of crystallite size and lattice strain. **Zeitschrift für Kristallographie**, v. 223, n. 9, p. 552–560, jan. 2008.

MOHAMMAD AMINI, A.; RAZAVI, S. M. A. A fast and efficient approach to prepare starch nanocrystals from normal corn starch. **Food Hydrocolloids**, v. 57, p. 132–138, 2016.

MOLAVI, H. *et al.* a Review on Biodegradable Starch Based Film. **Journal of microbiology, biotechnology and food sciences**, v. 4, n. 5, p. 456–461, 2015.

MUHAMMAD, A. I. *et al.* Understanding the Impact of Nonthermal Plasma on Food Constituents and Microstructure—A Review. **Food and Bioprocess Technology**, v. 11, n. 3, p. 463–486, 18 mar. 2018.

MUSIELAK, G.; MIERZWA, D.; KROEHNKE, J. Food drying enhancement by ultrasound – A review. **Trends in Food Science & Technology**, v. 56, p. 126–141, out. 2016.

NAM, S. *et al.* Segal crystallinity index revisited by the simulation of X-ray diffraction patterns of cotton cellulose I β and cellulose II. **Carbohydrate Polymers**, v. 135, p. 1–9, 2016.

NASCIMENTO, G. R. DO *et al.* INFLUÊNCIA NAS PROPRIEDADES FUNCIONAIS DA PELÍCULA DA FARINHA DA AMÊNDOA DO COCO BABAÇU (ORBIGNYA SP) / INFLUENCE ON THE FUNCTIONAL PROPERTIES OF BABASSU COCONUT ALMOND FLOUR (ORBIGNYA SP) FILM. **Brazilian Journal of Development**, v. 7, n. 1, p. 4196–4205, 2021.

NIEMIRA, B. A.; BOYD, G.; SITES, J. Cold Plasma Rapid Decontamination of Food Contact Surfaces Contaminated with *Salmonella* Biofilms. **Journal of Food Science**, v. 79, n. 5, 17 maio 2014.

NIEMIRA, B. A.; BOYD, G.; SITES, J. Cold Plasma Inactivation of *Escherichia coli* O157:H7 Biofilms. **Frontiers in Sustainable Food Systems**, v. 2, 14 ago. 2018.

NING, G.; FLEMMING, R. L. Rietveld Refinement of LaB₆: Data From MXRD. **Journal of Applied Crystallography**, 2005.

NORIEGA, E. *et al.* Cold atmospheric gas plasma disinfection of chicken meat and chicken skin contaminated with *Listeria innocua*. **Food Microbiology**, v. 28, n. 7, p. 1293–1300, out. 2011.

NWABOR, O. F. *et al.* A Cold Plasma Technology for Ensuring the Microbiological Safety and Quality of Foods. **Food Engineering Reviews**, v. 14, n. 4, p. 535–554, 24 dez. 2022.

ODEKU, O. A. Potentials of tropical starches as pharmaceutical excipients: A review. **Starch - Stärke**, v. 65, n. 1–2, p. 89–106, jan. 2013.

OKAZAKI, M. The structure and characteristics of sago starch. **Sago Palm: Multiple Contributions to Food Security and Sustainable Livelihoods**, p. 247–259, 2018.

OSSI, P. M. **Disordered Materials: An Introduction**. 2. ed. Milano: Advanced Texts in Physics, 2006.

PARK, S. *et al.* Cellulose crystallinity index: measurement techniques and their impact on interpreting cellulase performance. **Biotechnology for Biofuels**, v. 3, n. 1, p. 10, 24 dez. 2010.

PECHARSKY, V. K.; ZAVALIJ, P. Y. **Fundamentals of powder diffraction and structural characterization of materials**. [s.l.] Springer US, 2005.

PINTO, C. C.; CAMPELO, P. H.; MICHIELON DE SOUZA, S. Rietveld-based quantitative phase analysis of B-type starch crystals subjected to ultrasound and hydrolysis processes. **Journal of Applied Polymer Science**, p. 49529, jun. 2020.

PINTO, C. DA C. *et al.* X-ray diffraction and Rietveld characterization of radiation-induced physicochemical changes in Ariá (*Goepertia allouia*) C-type starch. **Food Hydrocolloids**, v. 117, n. December 2020, 2021a.

PINTO, C. DA C. *et al.* Mechanical alloying synthesis of Sm₃NbO₇ defect fluorite and structural characterization by X-ray diffraction, Raman spectroscopy and DFT calculation. **Ceramics International**, v. 47, n. 7, p. 8936–8943, 2021b.

PINTO, C. DA C. *et al.* Modulation of the Physicochemical Properties of Aria (*Goepertia allouia*) Starch by Cold Plasma: Effect of Excitation Frequency. **Food and Bioprocess Technology**, v. 16, n. 4, p. 768–784, 2023.

PINTO, V. Z. *et al.* Physical Pretreatment on Common Bean Starch at Acid Hydrolyzed Nanocrystals Structure and Properties. **Starch/Staerke**, v. 76, n. 5–6, 1 maio 2024.

PIYASENA, P.; MOHAREB, E.; MCKELLAR, R. C. Inactivation of microbes using ultrasound: a review. **International Journal of Food Microbiology**, v. 87, n. 3, p. 207–216, nov. 2003.

POLESI, L. F.; SARMENTO, S. B. S. Structural and physicochemical characterization of RS prepared using hydrolysis and heat treatments of chickpea starch. **Starch/Staerke**, v. 63, n. 4, p. 226–235, 2011.

POPOV, D. *et al.* Crystal structure of A-amylose: A revisit from synchrotron microdiffraction analysis of single crystals. **Macromolecules**, v. 42, n. 4, p. 1167–1174, 2009.

POPOVIĆ, B. M. *et al.* Enhancement of Antioxidant and Isoflavones Concentration in Gamma Irradiated Soybean. **The Scientific World Journal**, v. 2013, n. 1, 5 jan. 2013.

PRABHU, M. *et al.* Starch from the sea: The green macroalga *Ulva ohnoi* as a potential source for sustainable starch production in the marine biorefinery. **Algal Research**, v. 37, n. October 2018, p. 215–227, 2019.

PUNIA BANGAR, S. *et al.* Cold plasma for microbial safety: Principle, mechanism, and factors responsible. **Journal of Food Processing and Preservation**, v. 46, n. 12, 4 dez. 2022.

QUIRÓS, M. *et al.* Using SMILES strings for the description of chemical connectivity in the Crystallography Open Database. **Journal of Cheminformatics**, v. 10, n. 1, p. 23, 18 dez. 2018.

R E DINNEBIER; S J L BILLINGE. **Powder Diffraction Theory and Practice**. Cambridge: RSC Publishing, 2008.

RADOSTA, S. *et al.* Molecular composition of surface sizing starch prepared using oxidation, enzymatic hydrolysis and ultrasonic treatment methods. **Starch - Stärke**, v. 68, n. 5–6, p. 541–548, maio 2016.

RAO, W. *et al.* The Application of Cold Plasma Technology in Low-Moisture Foods. **Food Engineering Reviews**, v. 15, n. 1, p. 86–112, 3 mar. 2023.

RAPPENECKER, G.; ZUGENMAIER, P. Detailed refinement of the crystal structure of Vh-amylose. **Carbohydrate Research**, v. 89, n. 1, p. 11–19, 1981.

RIETVELD, H. M. Line profiles of neutron powder-diffraction peaks for structure refinement. **Acta Crystallographica**, v. 22, n. 1, p. 151–152, 1 jan. 1967.

RIETVELD, H. M. The Rietveld method. **Physica Scripta**, v. 89, n. 9, 2014.

RODRÍGUEZ-CARVAJAL, J. Recent advances in magnetic structure determination by neutron powder diffraction. **Physica B: Condensed Matter**, v. 192, n. 1–2, p. 55–69, out. 1993.

RODRIGUEZ-GARCIA, M. E. *et al.* Crystalline structures of the main components of starch. **Current Opinion in Food Science**, v. 37, n. October 2020, p. 107–111, 2021.

RUS, A. Z. M.; SULONG, N. Fundamental Technique of Pre-Blending of Bio-Matrix with Commercial HDPE. **Applied Mechanics and Materials**, v. 393, p. 121–125, set. 2013.

SALVADOR-REYES, R. *et al.* Kernel characterization and starch morphology in five varieties of Peruvian Andean maize. **Food Research International**, v. 140, n. December 2020, 2021.

SALVADOR-REYES, R. *et al.* Peruvian fava beans for health and food innovation: physicochemical, morphological, nutritional, and techno-functional characterization. **Food Research International**, v. 192, 1 set. 2024.

SALVADOR-REYES, R.; CLERICI, M. T. P. S. Peruvian Andean maize: General characteristics, nutritional properties, bioactive compounds, and culinary uses. **Food Research International**, v. 130, n. April 2019, p. 108934, 2020.

SANCHES, E. A. *et al.* Structural characterization of Chloride Salt of conducting polyaniline obtained by XRD, SAXD, SAXS and SEM. **Journal of Molecular Structure**, v. 1036, p. 121–126, mar. 2013.

SANTOS, C. O. P. **Aplicações do Método de Rietveld**. São Paulo: [s.n.].

SARANGAPANI, C. *et al.* Effect of low-pressure plasma on physico-chemical and functional properties of parboiled rice flour. **LWT - Food Science and Technology**, v. 69, p. 482–489, jun. 2016.

SCARDI, P.; LEONI, M.; DELHEZ, R. Line broadening analysis using integral breadth methods: A critical review. **Journal of Applied Crystallography**, v. 37, n. 3, p. 381–390, 2004.

SCHMITZ, C. S. *et al.* Cassava starch functional properties by etherification - Hydroxypropylation. **International Journal of Food Science and Technology**, v. 41, n. 6, p. 681–687, 2006.

SCHWALL, G. P. *et al.* Production of very-high-amylose potato starch by inhibition of SBE A and B. **Nature Biotechnology**, v. 18, n. 5, p. 551–554, 2000.

SCIENCE, F.; BONINGTON, S. The Relationship of the Crystal Structure of Amylose Polymorphs to the Structure of the Starch Granule. **Carbohydrate Polymers**, v. 6, p. 121–143, 1986.

SEGAL, L. *et al.* An Empirical Method for Estimating the Degree of Crystallinity of Native Cellulose Using the X-Ray Diffractometer. **Textile Research Journal**, v. 29, n. 10, p. 786–794, 1959.

SHAMAI, K.; BIANCO-PELED, H.; SHIMONI, E. Polymorphism of resistant starch type III. **Carbohydrate Polymers**, v. 54, n. 3, p. 363–369, 2003.

SHI, L. *et al.* Starch-menthol inclusion complex: Structure and release kinetics. **Food Hydrocolloids**, v. 97, p. 105183, dez. 2019.

SHU, X. *et al.* Starch structure and digestibility of rice high in resistant starch. **Starch/Staerke**, v. 58, n. 8, p. 411–417, ago. 2006.

SILVA, A. D. S. *et al.* Structural and morphological characterization of Poly(o-ethoxyaniline) Emeraldine-salt form using FTIR, XRD, LeBail Method and SEM. **Journal of Molecular Structure**, v. 1071, n. 1, p. 1–5, 2014.

SOEDIONO, B. General Structure Analysis System. **Journal of Chemical Information and Modeling**, v. 53, p. 160, 1989.

SREENIVASULU, N. **Rice Grain Quality**. New York, NY: Springer New York, 2019. v. 1892

STEPHENS, P. W. Phenomenological model of anisotropic peak broadening in powder diffraction. **Journal of Applied Crystallography**, v. 32, n. 2, p. 281–289, abr. 1999.

STRAMARE, S.; WEPPNER, W. Structural and conductivity investigations of doped Li-titanates. **Ionics**, v. 5, n. 5–6, p. 405–409, set. 1999.

SU, J.; CAVACO-PAULO, A. **Effect of ultrasound on protein functionality**. **Ultrasonics Sonochemistry** Elsevier B.V., , 1 ago. 2021.

SUDHEESH, C. *et al.* Impact of γ - irradiation on the physico-chemical, rheological properties and in vitro digestibility of kithul (*Caryota urens*) starch; a new source of

nonconventional stem starch. **Radiation Physics and Chemistry**, v. 162, n. April, p. 54–65, 2019.

SUMARDIONO, S. *et al.* Effect of chemical modification, drying method, and drying temperature on baking expansion and the physicochemical properties of cassava starch. **Journal of Food Processing and Preservation**, v. 46, n. 1, 3 jan. 2022.

SUN, C. *et al.* Multiscale Structural Evolutions and Deformation Mechanisms of Stereocomplexed and Homocrystalline Poly(lactic acid)s during Stretching: Correlating Thermomechanical Properties with Polymorphic Structures. **Macromolecules**, v. 56, n. 13, p. 5068–5079, 11 jul. 2023.

SUN, Y.; WANG, C. Application of Cold Plasma in Fruits and Vegetables. Em: **Applications of Cold Plasma in Food Safety**. Singapore: Springer Singapore, 2022. p. 183–195.

SUNDER, M.; MUMBREKAR, K. D.; MAZUMDER, N. Gamma radiation as a modifier of starch – Physicochemical perspective. **Current Research in Food Science**, v. 5, p. 141–149, 2022.

SUWANMANEE, U.; LEEJARKPAI, T.; MUNGCHAROEN, T. **Assessment of greenhouse gas (GHG) emissions of Polylactic acid (PLA)/ starch and Polyethylene terephthalate (PET) trays**. Advanced Materials Research. **Anais...**2012.

TAHERI, S. *et al.* Antioxidant Capacities and Total Phenolic Contents Enhancement with Acute Gamma Irradiation in *Curcuma alismatifolia* (Zingiberaceae) Leaves. **International Journal of Molecular Sciences**, v. 15, n. 7, p. 13077–13090, 23 jul. 2014.

TAKAHASHI, Y.; KUMANO, T. Crystal structure of natural rubber. **Macromolecules**, v. 37, n. 13, p. 4860–4864, 2004.

TAKAHASHI, Y.; KUMANO, T.; NISHIKAWA, S. Crystal structure of B-amylose. **Macromolecules**, v. 37, n. 18, p. 6827–6832, 2004.

TESTER, R. F.; KARKALAS, J.; QI, X. Starch - Composition, fine structure and architecture. **Journal of Cereal Science**, v. 39, n. 2, p. 151–165, 2004.

TETLOW, I. J. Starch biosynthesis in developing seeds. **Seed Science Research**, v. 21, n. 1, p. 5–32, 2011.

THIRUMDAS, R. *et al.* Functional and rheological properties of cold plasma treated rice starch. **Carbohydrate Polymers**, v. 157, p. 1723–1731, fev. 2017.

THIRUMDAS, R.; SARANGAPANI, C.; ANNAPURE, U. S. Cold Plasma: A novel Non-Thermal Technology for Food Processing. **Food Biophysics**, v. 10, n. 1, p. 1–11, 27 mar. 2015.

THYGESEN, A. *et al.* On the determination of crystallinity and cellulose content in plant fibres. **Cellulose**, v. 12, n. 6, p. 563–576, 20 dez. 2005.

T.L. BARSBY; A.M. DONALD; P.J. FRAZIER. **Starch Advances in Structure and Function**. 1. ed. Cambridge: The Royal Society of Chemistry, 2001.

TOBY, B. H. EXPGUI , a graphical user interface for GSAS. **Journal of Applied Crystallography**, v. 34, n. 2, p. 210–213, 1 abr. 2001.

TOBY, B. H. R factors in Rietveld analysis: How good is good enough? . **Powder Diffraction**, v. 21, n. 1, p. 67–70, 2006.

TOMASIK, P.; HORTON, D. **Enzymatic conversions of starch**. 1. ed. [s.l.] Elsevier Inc., 2012. v. 68

TORAYA, H. A new method for quantitative phase analysis using X-ray powder diffraction: direct derivation of weight fractions from observed integrated intensities and chemical compositions of individual phases. **Journal of Applied Crystallography**, v. 49, n. 5, p. 1508–1516, 1 out. 2016.

TORAYA-AVILÉS, R. *et al.* Effects of pyroconversion and enzymatic hydrolysis on indigestible starch content and physicochemical properties of cassava (*Manihot esculenta*) starch. **Starch/Staerke**, v. 69, n. 5–6, p. 1–9, 2017.

TRAN, M. Q.; NGUYEN, V. B.; TRAN, X. A. Gamma radiation modification of cassava starch and its characterization. **Polymer Engineering & Science**, v. 62, n. 4, p. 1197–1204, 16 abr. 2022.

VAMADEVAN, V.; BERTOFT, E. Structure-function relationships of starch components. **Starch/Staerke**, v. 67, n. 1–2, p. 55–68, 2015.

VARILLA, C.; MARCONE, M.; ANNOR, G. A. Potential of Cold Plasma Technology in Ensuring the Safety of Foods and Agricultural Produce: A Review. **Foods**, v. 9, n. 10, p. 1435, 11 out. 2020.

VERMA, R. *et al.* Physicochemical and functional properties of gamma irradiated buckwheat and potato starch. **Radiation Physics and Chemistry**, v. 144, p. 37–42, mar. 2018.

VERSINO, F. *et al.* Starch-based films and food coatings: An overview. **Starch/Staerke**, v. 68, n. 11–12, p. 1026–1037, 2016.

VERTUCCIO, L. *et al.* Nano clay reinforced PCL/starch blends obtained by high energy ball milling. **Carbohydrate Polymers**, v. 75, n. 1, p. 172–179, 2009.

VITALIJ K. PECHARSKY; ZAVALIJ, P. Y. **Fundamentals of Powder Diffraction and Structural Characterization of Materials**. Boston, MA: Springer US, 2009.

VON DREELE, R. B.; LARSON, A. C. General Structure Analysis System (GSAS). **Los Alamos National Lab**, v. LAUR, p. 86–748, 1994.

WAGNER, C. N. J. Direct methods for the determination of atomic-scale structure of amorphous solids (X-ray, electron, and neutron scattering). **Journal of Non-Crystalline Solids**, v. 31, n. 1–2, p. 1–40, dez. 1978.

WANG, S. **Starch Structure, Functionality and Application in Foods**. [s.l.] Springer Singapore, 2020.

WANG, X. B. *et al.* Effects of gamma radiation on microbial, physicochemical, and structural properties of whey protein model system. **Journal of Dairy Science**, v. 101, n. 6, p. 4879–4890, jun. 2018.

WEI, B. *et al.* The ex-situ and in-situ ultrasonic assisted oxidation of corn starch: A comparative study. **Ultrasonics Sonochemistry**, v. 61, p. 104854, mar. 2020.

WILD, D. L.; BLANSHARD, J. M. V. The relationship of the crystal structure of amylose polymorphs to the structure of the starch granule. **Carbohydrate Polymers**, v. 6, n. 2, p. 121–143, 1986.

WU, X. *et al.* Crystal Structure Determination of Three Polycyclic Compounds and Comparative Rietveld Refinement Between MS and GSAS Programs. **Chinese Science Bulletin**, 2013.

XIE, Y.-Y. *et al.* Effect of temperature-cycled retrogradation on in vitro digestibility and structural characteristics of waxy potato starch. **International Journal of Biological Macromolecules**, v. 67, n. 9, p. 79–84, jun. 2014.

XU, J. *et al.* Gelatinization dynamics of starch in dependence of its lamellar structure, crystalline polymorphs and amylose content. **Carbohydrate Polymers**, v. 229, n. October, p. 115481, 2020.

YAN, S. *et al.* Improved solubility of banana starch by dielectric barrier discharge plasma treatment. **International Journal of Food Science & Technology**, v. 55, n. 2, p. 641–648, 23 fev. 2020.

YANG, Q.-Y. *et al.* Fine structure, crystalline and physicochemical properties of waxy corn starch treated by ultrasound irradiation. **Ultrasonics Sonochemistry**, v. 51, p. 350–358, mar. 2019.

YOUNG, R. A. **The Rietveld method**. New York: Oxford University Press, 1993.

ZHANG, S. *et al.* Pea protein microgel particles as Pickering stabilisers of oil-in-water emulsions: Responsiveness to pH and ionic strength. **Food Hydrocolloids**, v. 102, p. 105583, maio 2020.

ZHAO, P. *et al.* Error Analysis and Correction for Quantitative Phase Analysis Based on Rietveld-Internal Standard Method: Whether the Minor Phases Can Be Ignored? **Crystals**, v. 8, n. 3, p. 110, 27 fev. 2018.

ZHU, B. *et al.* Ultrasonic Degradation of Konjac Glucomannan and the Effect of Freezing Combined with Alkali Treatment on Their Rheological Profiles. **Molecules**, v. 24, n. 10, p. 1860, 14 maio 2019.

ZHU, F. Impact of γ -irradiation on structure, physicochemical properties, and applications of starch. **Food Hydrocolloids**, v. 52, p. 201–212, jan. 2016.